Investigation of electrospun nano-fibrous polymeric actuators : Fabrication and Properties

DISSERTATION

zur Erlangung des akademischen Grades einer Doktorin/eines
Doktors der Naturwissenschaften (Dr. rer. nat.)
in der Bayreuther Graduiertenschule für Mathematik und Naturwissenschaften
(BayNAT)
der Universität Bayreuth

vorgelegt von

Li LIU
aus Hunan (V. R. China)
Bayreuth, 2018

This doctoral thesis was prepared at the department of *Macromolecular Chemistry II* at the University of Bayreuth from *September/2014* until *May/2018* and was supervised by Prof. Dr. *Seema Agarwal.*

This is a full reprint of the dissertation submitted to obtain the academic degree of Doctor of Natural Sciences (Dr. rer. nat.) and approved by the Bayreuth Graduate School of Mathematical and Natural Sciences (BayNAT) of the University of Bayreuth.

Date of submission: 09. 05. 2018

Date of defence: 25. 07. 2018

Acting director: Prof. Dr. Dirk Schüler

Doctoral committee:

Prof. Dr. Seema Agarwal	(reviewer)
Prof. Dr. Stephan Gekle	(reviewer)
Prof. Dr. Peter Strohriegl	(chairman)
Prof. Dr. Anna Schenk	

Table of Contents

Table of Contents 1

List of Figures 3

List of symbols and abbreviations 8

Summary/Zusammenfassung 10

Summary 10

Zusammenfassung 13

1. Introduction.....16

1.1 Motivation.....16

1.2 The mechanism of polymeric/soft actuator 18

1.3 General polymeric/soft actuators.....19

1.4 Porous polymeric/soft actuators 26

1.5 Electrospinning.....29

1.5.1 Large aspect ratio.....31

1.5.2 Large specific area and high porosity.....32

1.5.3 Electrospun polymeric/soft actuators 34

1.6 Directionally controlled polymeric/soft actuators 34

1.7 Fabrication of polymeric/soft actuators by electrospinning 36

1.8 References.....38

2. Thesis Overview 63

2.1 Giving direction to motion and surface with ultra-fast speed using oriented hydrogel fibers 66

2.2 One-component dual actuation: Only Poly(NIPAM) can actuate to stable 3D forms with reversible size change 71

2.3 Composite Polymeric Membranes with Directionally Embedded Fibers for Controlled Dual Actuation 75

2.4 Individual Contribution to Joint Publications.....80

3. Outlook.....82

4. Acknowledgement 84

5. Appendix 86

5.1 Publication 1: Giving direction to motion and surface with ultra-fast speed using oriented hydrogel fibers 87

5.2 Publication 2: One-component dual actuation: Only Poly(NIPAM) can actuate to stable 3D forms with reversible size change 100

5.3 Publication 3: Composite Polymeric Membranes with Directionally Embedded Fibers for Controlled Dual Actuation 114

6. List of publications.....128

List of Figures

Figure 1. Growth of research of polymeric actuators The increasing number of scientific papers containing results of both the keyword "polymeric actuator" and "soft actuator" from SciFinder indicates the upward increasing trend of polymeric actuators.....19

Figure 2. The temperature-composition diagram of thermoresponsive polymers aqueous solution. Reprinted from ref [21], copyright (2017) Royal Society of Chemistry, license number: 4342511322624. 21

Figure 3. Mechanism of UV crosslinking. When the free radicals are produced from benzophenone fragment by UV irradiation, the "C-C" or "C-N" are built between the activated benzophenone and the NIPAM part from another polymer chain, thus resulting in crosslinking. 23

Figure 4. Schematic of bilayer polymeric actuator. 24

Figure 5. Images of reversible bending behavior of 1) photos, 2) schematics and 3) the corresponding polymer chains. The golden one is the passible layer and the active layer is made of poly(NIPAm-AA) in the presence of poly(diallyldimethylammonium chloride) PDADMAC. Reprinted from ref [49], copyright (2017) Royal Society of Chemistry, license number: 4342521000764. 25

Figure 6. The mechanism of bending behavior of UCST-LCST bilayer

structure actuator. At low temperature (15°C), the PNIPAM layer is swollen by water. Increasing temperature to 40°C leads to a shrinking of the PNIPAM layer, a directional water transfer to the P(AAc-co-AAm) layer that consequently swells and in result lets the bilayer hydrogel bends. Reprinted from,[74] copyright (2017), Royal Society of Chemistry, license number: 4342521434124. 26

Figure 7. The concept, gradient structure characterization, and actuation of the polymeric actuator . (a) A scheme fabricating the actuator (b, scale bar (black), 30 mm); top surface (c, scale bar, 3 mm); and cross-section (d, scale bar: 1 mm); (e) the DEC gradient along the thickness direction (from top to down). (f) fast actuation response to acetone vapor. Reproduced from [81], copyright (2014) Springer Nature, license number: 4342530538058. 28

Figure 8. Growth of research of electrospinning. The increasing number of scientific papers containing the keyword “electrospinning” from SciFinder indicates the upward trend of electrospinning. 31

Figure 9. The set-up of electrospinning 31

Figure 10. Schematic illustrating the relationship of the diameter of fibers and its specific area. Reproduced from [145], copyright (2001) Elsevier Science B.V., license number: 4342531220951. 33

Figure 11. The schematic of actuation of the composite, in which, parallel glass fibers embedded within the agarose, in response to humidity.

Reprinted from [177] copyright (2015) John Wiley and Sons, license number: 4342540024870. 36

Figure 12. Schematic showing the formation of bilayer actuators by sequential electrospinning of TPU and P(NIPAM-ABP) followed by UV cross-linking (steps 1 and 2). The samples were cut at different angles to get varied orientations of thermoresponsive P(NIPAM-ABP) fibers (steps 3 and 4). The TPU and P(NIPAM-ABP) solutions were mixed with rhodamine B (RB) and methylene blue, respectively to observe the actuation phenomenon optically better. Copyright (2015), John Wiley and Sons, license number: 4342540732801. 67

Figure 13. SEM images of a) P(NIPAM-ABP) side – as spun bilayer membrane, b) P(NIPAM-ABP) side - after treatment with hot water, c) TPU side- as spun bilayer membrane and d) the cross-section of the bilayer sample in water at 40 ^{o}C after drying shows a strong interface between TPU (left side) and P(NIPAM-ABP) (right side). Scale bar = 10 µm. Copyright (2015), John Wiley and Sons, license number: 4342540732801. 68

Figure 14. Fiber orientation-dependent actuation behaviour of bilayer TPU (pink)/P(NIPAM-ABP) (blue) fibrous membranes (length: 2.0 cm, width: 0.5 cm) in water at different temperatures. Black arrows show the fibre orientation direction, 0, 45 and 90^{o} are angles between the fibre direction and the long axis of the sample, as indicated by a black dotted line on the sample. Scale bar = 0.5 cm. The TPU and P(NIPAM-ABP) were dyed to

get a better contrast but in real photos and movies the contrast might not be visible as P(NIPAM-ABP) becomes transparent in contact with water. Copyright (2015), John Wiley and Sons, license number: 4342540732801. 69

Figure 15. a) Schematic of formation of Bi-PNIPAM-0^{o}, 45^{o}, 90^{o} actuator by electrospinning of aligned layer and random layer, respectively (step 1), followed by pressing and cross-linking (steps 2 and 3). At last, the samples were cut into pieces at different angles (step 4); b) One component PNIPAM directionally controlled actuation: movement of Bi-PNIPAM-0o, 45o, 90o mat (aligned (blue)/random (pink) (length: 2.0 cm, width: 0.5 cm) with the thickness ratio (aligned / bilayer) of 0.65) in water at different temperatures. Fiber alignment direction was indicated by a black dotted line on the sample. The good color contrast by dying the aligned and random mats might be invisible due to the transparency of P(NIPAM-ABP) in water; c) Equilibrium shapes of bilayer mats obtained from finite-element simulations in 40° water. From left to right are 0°, 45°, and 90° fiber orientations. By using anisotropic expansion coefficients in combination with an anisotropic elastic modulus, good agreement with the experimental shapes in Fig. 1b is obtained. Copyright (2016), John Wiley and Sons, license number: 4342541040242. 73

Figure 16. The effect of temperature of water on the curvature of Bi-PNIPAM-0^{o} mat with the thickness ratio (aligned / bilayer) of 0.65.

Curvature=1/r. Copyright (2016), John Wiley and Sons, license number: 4342541040242. 74

Figure 17. (a) Schematic fabrication of the composite membrane. (b-d) Raman-AFM imaging of the composite membrane; (b) optical microscope image with position of Raman cross-section (red line), (c) Raman cross-section with domains rich in TPU colored in yellow and those rich in poly(NIPAm-AA) in green and (d) Raman spectra of neat components, i.e., TPU and poly(NIPAm-AA). (e-h) SEM images of the composite membrane; (e) poly(NIPAm-AA) aligned fibrous mat side, (f) TPU side, (g) cross-section and (h) interface between aligned poly(NIPAm-AA) fibers and TPU. 77

Figure 18. (a) Actuation of the composite membrane in buffer solution with different pH at 40 ^{o}C. (b) The corresponding schematics for the actuation of composite membrane at 40 ^{o}C. Poly(NIPAm-AA) is colored in green and TPU in yellow.....78

List of symbols and abbreviations

2D	Two-dimensional
3D	Three-dimensional
ABP	4-acryloylbenzophenone
AA	Acrylic acid
^{o}C	Centigrade degree
DSC	Differential scanning calorimetry
DMF	N,N-dimethylformide
Dioxane	1,4-Dioxacyclohexane
E	E-modulus
FTIR	Fourier transform infrared spectroscopy
g	Gram
Gpa	Giga pascal
h	Hour
L	Length along long axis
LCST	Lower critical solution temperature
Mpa	Mega pascal
Micro-DSC	Micro differential scanning calorimetry
mN	Millinewton
mg	Milligram

min	Minute
mm	Millimeter
N	Newton
nm	Nanometer
NIPAM	N-isopropylacrylamide
P(NIPAM)	Poly(N-isopropylacrylamide)
PAA	Poly(Acrylic acid)
P(NIPAM-ABP)	Poly(N-isopropylacrylamide-co-4-acryloylbenzophenone)
P(NIPAM-AA-ABP)	Poly(N-isopropylacrylamide-co-acrylic acid-co-4- acryloylbenzophenone)
SEM	Scanning electron microscopy
TGA	Thermogravimetric analysis
TPU	Thermoplastic Polyurethane
THF	Tetrahydrofuran
UV	Ultraviolet
UCST	Upper critical solution temperature
Wt%	Weight percent
W	Width along short axis
µm	Micrometer

Summary/Zusammenfassung

Summary

Bioinspired polymeric actuators are very well-known in the literature. They are mostly based on a bilayer structure with asymmetrical swelling/shrinkage. The existing problems are: speed of the actuation, direction control of the movements and multi-responsive ability. The aim of my work is to have detailed studies related to responsive polymeric actuators with high sensitivity (fast actuation), directionally controlled and multi-responsive ability. For enhancing the speed of actuation, porous fibrous mats were used in this work with a hypothesis of increasing the mass transport and thus resulting in high speed of actuation. Electrospinning was used as a tool for making porous fibrous mats.

Firstly, through combining the passive layer of aligned thermoplastic polyurethane (TPU) fibrous mat and the active layer of poly(n-isopropylarylamide) P(NIPAM), a bilayer thermoresponsive polymeric actuator is obtained. It demonstrates the following highlights: 1) ultra-fast actuation between 0.6 – 5 s; 2) reversible directionally controlled movement (rolls, tubes, helices); 3) there was not only shape changes but also surface changes triggered by temperature.

Secondly, a stable one-component polymeric actuator was created by

electrospinning a random P(NIPAM) fibrous mat and an aligned P(NIPAM) fibrous mat. The combined bilayer thermoresponsive actuator consists of only one component of P(NIPAM) and the actuation of this actuator is irreversible. In addition, the temperature-triggered formed size could be controlled by temperature. Moreover, the actuation is directionally controlled depending on the angles between fiber alignment and long axis and it is demonstrated that by numerical simulations the observed behaviour is the unique combination of anisotropic thermal expansion with an equally anisotropic elastic modulus of the employed material as well.

Thirdly, a dual-responsive composite actuator composed of thermo- and pH-responsive poly(N-isopropylacrylamide-co-acrylic acid) (poly(NIPAm-AA)) fibers (average diameter ~ 905 nm) embedded within a passive thermoplastic polyurethane (TPU) matrix at different angles with degree of alignment as high as 98% was presented. The actuation direction were dependent on the angles between fiber alignment and long axis. The actuation and the actuated tube was is independent of temperature at pH 7 and above. However, temperature could be used to control the size of the actuated tubes at lower pH. Although the polymeric actuator is only 5.8 mg, it was able to reversibly lift and release ~426 times weight of its own mass (2.47 g metal ring).

In summary, it is worth noting that our strategy, through which it is very convenient to obtain porous structure and directionally controlled actuation,

is not only applicable to P(NIPAM) and P(NIPAM-AA), but also to other "smart" polymers, which therefore enriches the designs of versatile polymeric actuators with high sensitivity.

Zusammenfassung

Von der Natur inspirierte, synthetische Aktuatoren sind in der Literatur ausgiebig bekannt. In den meisten Fällen sind diese aus zwei unterschiedlichen Schichten, welche unterschiedliche Quell-bzw. Schrumpfungseigenschaften, besitzen. Allerdings existieren hierbei folgende Probleme: Die Geschwindigkeit der Aktuatoren, die nicht kontrollierbare Richtung der Faltungsbewegung und die fehlende Multiresponsivität. Ziel meiner Arbeit ist die detaillierte Untersuchung von Aktuatoren welche sehr sensitiv, also sehr schnell, richtungskontrollierbar und auch auf mehrere Umgebungsbedingungen wie Temperatur oder pH reagieren, also multiresponsive Eigenschaften besitzen. Um einen schnellen Faltungsvorgang zu erreichen, wurden in dieser Arbeit poröse Fasermatten verwendet, da die Hypothese war, dass mit steigendem Stofftransport der Faltungsvorgang sehr schnell abläuft. Um poröse Fasern herzustellen, wurde die Methode des Elektro Spinning verwendet. Im ersten Fall wurde durch Kombination einer passiven Schicht(Fassermatte) welche aus einem thermoplastischen Polyurethanfasern hergestellt wurde und einer aktiven Schicht (Fassermatte) aus thermoresponsiven Poly(N-isopropyl acrylamid) P(NIPAM) ein zweischichtiger, thermoresponsiver Aktuator erhalten, welcher folgende Eigenschaften besitzt: 1) Ultra schneller Faltungsvorgang in 0,6- 5 Sekunden, 2) reproduzierbare richtungskontrollierte Bewegung (Rollen, Röhren und Helices, 3)

Veränderung der Oberflächenbeschaffenheit mit der Temperatur.

Im zweiten Fall wurde ein Aktuator aus nur einer Komponente hergestellt, welcher aus einer Schicht (Fasermatte) elektrogesponnener P(NIPAM)Fasern mit zufällig verteilter Ausrichtung und einer weiteren Schicht (Fasermatte) von P(NIPAM), mit allen in der gleichen Orientierung befindlichen Fasern, besteht. Der Bewegungsvorgang dieses Aktuators ist durch die Temperatur als auch durch die Ausrichtung der zwei Schichten zueinander abhängig, allerdings nicht reversibel. Mithilfe mathematischer Simulationen wurde die seltene Kombination einer anistropisch thermischen Expansion und gleich großer elastischem anisotropen Modul dargestellt.

Im dritten Teil meiner Arbeit, wurde durch Kombination einer Schicht (Fasermatte) elektrogesponnener P(NIPAM-AA) Fasern (~ 905nm Durchmesser), welche thermo- und pH responsives Verhalten zeigen, in eine passive Matrix aus thermoplastischem Polyurethan eingebettet. Die Ausrichtung der P(NIPAM-AA)Fasern zeigt einen deutlichen Einfluss auf den Faltvorgang, weshalb die Fasern bis zu einem Anteil von maximal 98 % in der PU Matrix ausgerichtet wurden. Die so hergestellten Aktuatoren zeigten ein thermoresponsives Verhalten bei kleiner pH =7, allerdings nicht bei pH >7. Nichtsdestotrotz konnte bei pH<7 zeigt werden, dass bereits ein Aktuator mit einer Masse von 5,8 mg die Masse von 2,47 g (425-fache) durch Änderung der Temperatur anheben und wieder absenken kann.

Zusammenfassend ist festzuhalten, dass unsere Strategie der Herstellung von porösen Fasern um eine Richtungsorientierte Faltung zu erreichen nicht nur für die Beispiele von P(NIPAM) and P(NIPAM-AA) funktioniert, sondern auch auf weitere „smarte“ Polymere angewendet werden kann um die Vielseitigkeit von Polymeraktuatoren weiter zu erhöhen.

1. Introduction

1.1 Motivation

Polymeric actuators, also called soft actuators, are made of stimuli-responsive polymers, which are capable of performing shape changes, and/or adaptive motion in response to external stimuli and thus result in macro-, micro-, and nanoscales mechanical motions.[1, 2] Nowadays, polymeric actuators have attracted scientists' interest and have been employed in various applications in sensors, switches, artificial muscles, and other items.[3-5] These synthetic actuators are inspired mostly from natural process. For example, pine cone is a well-known plant that can exhibit opening and closing behavior upon changes in environmental humidity allowing the release of seeds from pine cone inside. The mechanism of this behavior is the anisotropic swelling in each scale. Pine cone consists of many pieces of scales that are similar to bilayer structure, in which, one layer is composed of aligned cellulose fibrils along the length of the scale and the other one is made up of perpendicular fibrils. Upon drying/wetting, the swelling/shrinkage behavior in each layer is constrained by the alignment of the cellulose fibrils, thus resulting in the opening and closing behavior of pine cone.[6-8] In addition, a similar example to this type of bilayer structure can also be observed in chiral

pod.[9] Regarding Bauhinia variegate, the opening of the chiral pod is induced by uniaxial swelling/shrinkage between the two fibrous layers, in which, the fibrils are oriented at roughly $\pm 45^{o}$ with respect to the pod's long axis. Therefore, during the opening process, two flat pod valves cured into helical strips of opposite handedness upon changes in air humidity. The synthetic actuators inspired from these nature plants are based on polymeric bilayer structure, in which, asymmetry is generated either by having one layer capable of changing size by absorbing water (active layer) and the other hydrophobic layer (passive layer) or gradient structure. This leads into bending, rolling movements depending upon the bilayer divergence and layer thickness. For reversible actuation, stimuli-responsive polymers are used to make active layers, such as thermo-responsive polymers, pH- responsive polymers. When these active layer are combined with the passive layer, the formed polymeric actuator can exhibit reversible temperature or pH-triggered actuation. The existing challenge in the field of polymeric actuators are: 1) slow actuation; 2) directional controlled actuation is waiting; 3) multi-responsive ability. In my research, I take these challenges and carry out the work with an aim to provide bilayer polymeric actuators with very fast response, directional controlled and multi-responsive actuation.

1.2 The mechanism of polymeric/soft actuator

Polymeric/soft actuators composed of stimuli responsive polymers capable of changing their shape or properties in response to environmental stimuli have attracted much interest for various applications such as sensors, switches, artificial muscles, optical and microfluidic devices, walkers and encapsulating/releasing systems.[3-5, 10, 11](**Figure 1**) Why are they able to perform shape changes in response to external stimuli and thus result in macro-, micro-, and nanoscale mechanical motion? The key of the mechanism is anisotropy.[12-17]

An interesting phenomenon could be easily observed when a piece of tracing paper is gently placed on the surface of calm water. At first, the paper rolls up and then gradually unrolls with time. This occurs because of the water diffusion anisotropy between the two sides of the paper. Paper as a fibrous structure is made from cellulose fibers which swell after absorbing water.[18, 19] When a piece of tracing paper is gently placed on the surface of calm water, it starts rolling up from one edge, owing to the swelling face that is in contact with water. Then it gradually unrolls and becomes a piece of flat paper again, because the water has arrived at the other face of the paper, which removes the swelling anisotropy between the two sides of the paper.[20] When this kind of anisotropy is applied in the polymeric actuators, it is always presented in the form of layer structure. Based on it, various kinds of polymeric/soft actuators have been built.

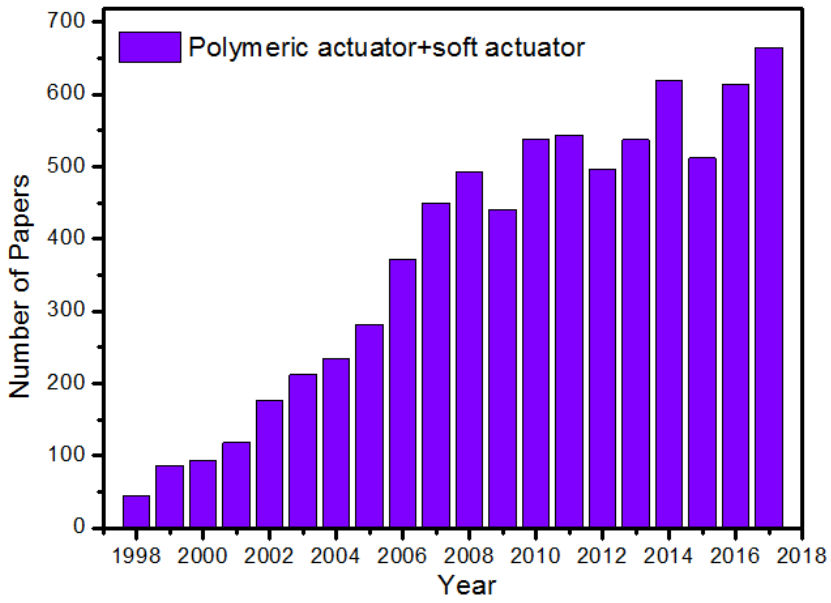

Figure 1. Growth of research of polymeric actuators The increasing number of scientific papers containing results of both the keyword "polymeric actuator" and "soft actuator" from SciFinder indicates the upward increasing trend of polymeric actuators.

1.3 General polymeric/soft actuators

Among polymeric/soft actuators, the bilayer structure is the most common one. The bilayer structure is more easily realized and widely employed. Similar to the paper-curling mechanism, the bilayer polymeric/soft actuators are designed through combing one active layer with the other passive layer creating vertical anisotropy in thickness direction. For example, thermoresponsive polymers are used as active layer in combination with other passive, hydrophobic polymers. The thermoresponsive polymers are the most widely applied one among intelligent materials which exhibit self-alterable dynamic properties due to

their ability to respond to small changes around their environments.[21-29] Thermoresponsive polymers are also called as temperature-responsive polymers having temperature-triggered volume transition property that is caused by the transition between two thermodynamically stable states of coil and globule in solution.[28, 30, 31] When at coil state, the polymer chains are at an expanded hydrophilic coil conformation which exhibits phenomenon of dissolving or swelling. Conversely, they are at a collapsed hydrophobic globule state which indicates precipitation or shrinkage. These kind of temperature-triggered polymers can be divided into two types of Lower Critical Solution Temperature (LCST) and Upper Critical Solution Temperature (UCST). They are capable of displaying a miscibility gap at high temperatures and/or low temperatures in their temperature-composition diagram, respectively. In this kind of temperature-composition diagram, the minimum and maximum temperatures are determined as LCST and UCST, respectively.[21, 27, 29] (**Figure 2**) Regarding the LCST polymers, when the temperature is below the LCST, the polymers are soluble or swelling in solution, otherwise they will be precipitated or shrunk, and vice versa for a UCST polymer.

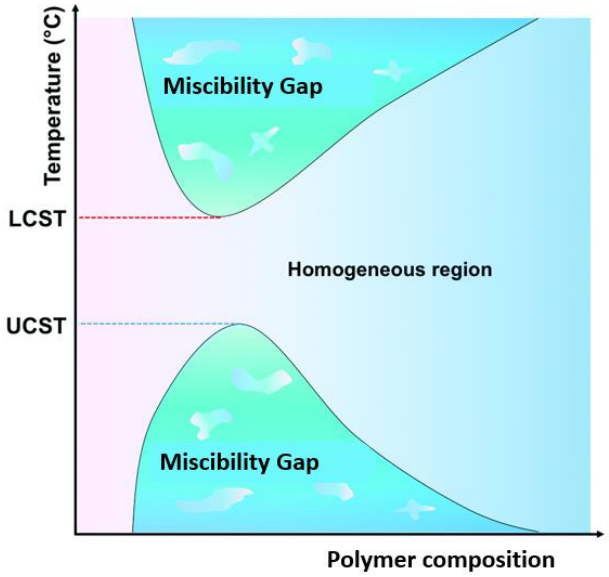

Figure 2. The temperature-composition diagram of thermoresponsive polymers aqueous solution. Reprinted from ref [21], copyright (2017) Royal Society of Chemistry, license number: 4342511322624.

P(NIPAM) is one of the typical LCST polymers widely used for bilayer actuator. For actuator application, P(NIPAM) needs to be stable in water and should keep the structure for a long time, such as films & fibers. There are several strategies of keeping P(NIPAM) stable in water without losing its thermoresponsive property, such as block copolymers with hydrophobic monomers or cross-linkable monomers. In the first case, there are two aspects should be paid attention to: 1) Although as the introduction of hydrophobic segments, the LCST of P(NIPAM) can be shifted to lower temperatures, thus keeping P(NIPAM) stable in water for a broader temperature range,[32-34] there is still a limitation that when the temperature is lower than the LCST, it becomes water soluble again; 2) By

applying P(NIPAM) block copolymer with hydrophobic monomer, physical cross-links can be created by hydrophobic interactions. Through this method, although the fromed P(NIPAM) gel is stable in water without losing its thermoresponsive ability, the physical cross-links are not permanent in nature and it is reversible.[35-38] Therefore, it introduces risks associated with actuation application. In contrast, it is more convenient and useful to take the strategy of using cross-linkable monomer. For instance, photo cross-linker of 4-acryloyl benzophenone(ABP) is usually used to make insoluble P(NIPAM). A small amount of ABP can crosslink P(NIPAM) without changing LCST too much. [39, 40] As it is shown in the **Figure 3**, free radicals produced from benzophenone fragment by UV irradiation result in crosslinking. It is chemical crosslinking. Be different from the physical crosslinking, when the temperature is below LCST, the chemic cross-linked P(NIPAM) performs swelling in water rather than dissolving. Therefore, this type of cross-linked P(NIPAM) by covalent bonds can keep the structures stable in water without losing its thermoresponsive property.

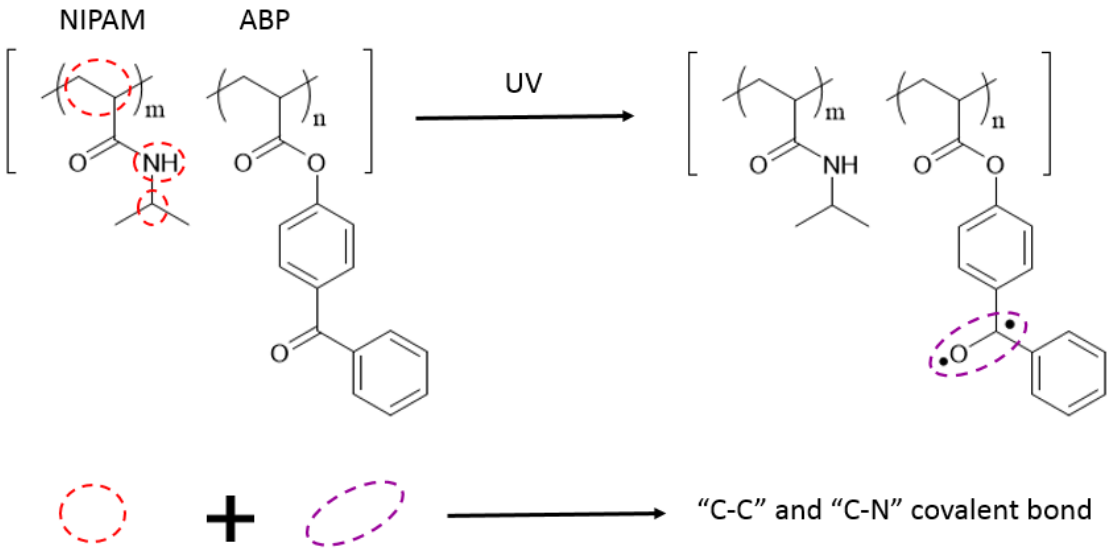

Figure 3. Mechanism of UV crosslinking. When the free radicals are produced from benzophenone fragment by UV irradiation, the "C-C" or "C-N" are built between the activated benzophenone and the NIPAM part from another polymer chain, thus resulting in crosslinking.

A polymeric actuator composed of the active layer of crosslinked P(NIPAM) is capable of reversible bending upon responding to temperature. When the temperature is higher/lower than the LCST, the active layer shrinks/swells, but the size of the passive layer is stable, thus leading to the bending actuation.[39] (**Figure 4**) Depending on the different stimuli, various kinds of materials could be employed as active layer, such as ones triggered by temperature,[39, 41-50], light,[48, 51-58] and pH[2, 49, 52, 59].

Furthermore, not only single stimuli polymers but also the multi-stimuli responsive polymers could be used to produce the active layer. From the

point of view of applications, multi-responsive polymers would be more interesting to scientists, owing to their ability to respond to several stimuli simultaneously.[60-66] Poly(N-isopropylacrylamide-co-Acrylic Acid) P(NIPAM-AA) is a dual-responsive polymer which can be synthesized by combining two components of NIPAM and AA.[67-70] In addition, because of the thermoresponsive part of NIPAM and the pH-responsive aspect of AA, P(NIPAM-AA) appears to have characteristics of both thermoresponsive and pH- responsive.[67-71]. Moreover, it is able to exhibit volume/(dissolving /precipitation) change triggered by the temperature and pH value of the surrounding medium.[72, 73] The polymeric actuators made of these type of dual-responsive polymers are capable of performing actuation triggered by temperature and pH. Li et al. reported an temperature and pH dual responsive polymeric actuator that undergoes reversible bidirectional bending behavior upon responding to temperature and pH stimuli based on this concept.[49] (**Figure 5)**

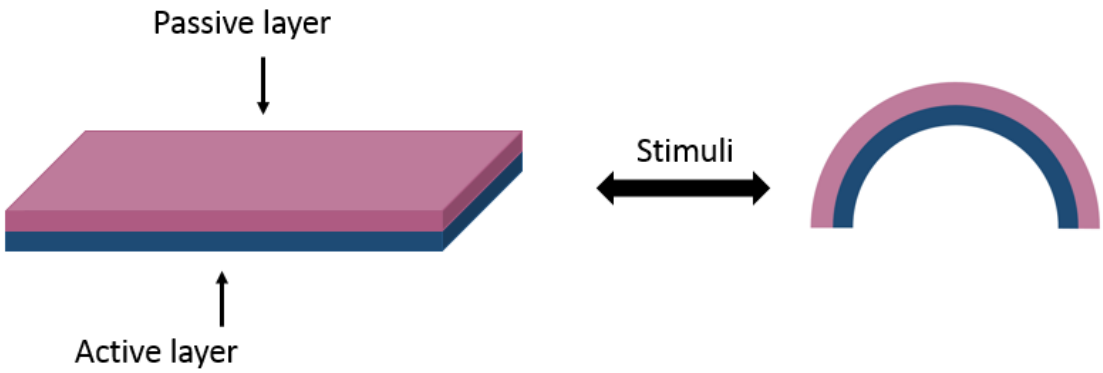

Figure 4. Schematic of bilayer polymeric actuator.

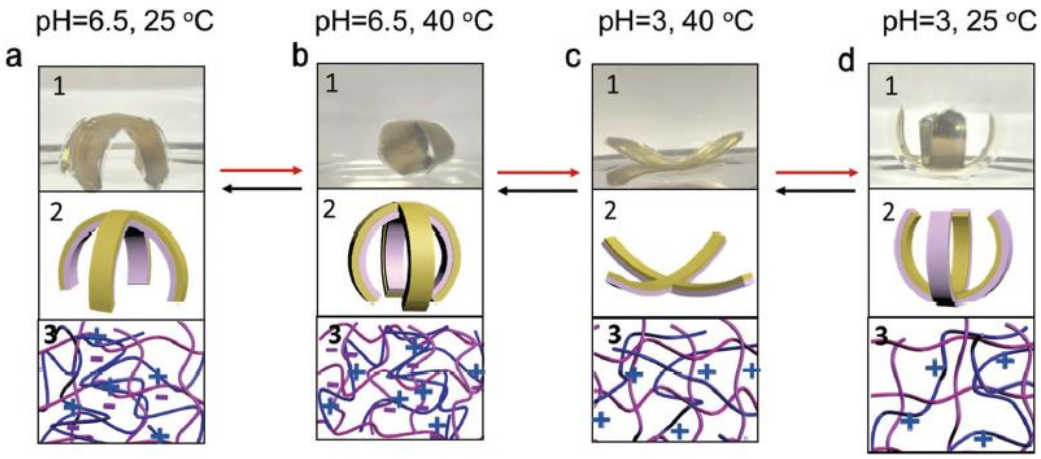

Figure 5. Images of reversible bending behavior of 1) photos, 2) schematics and 3) the corresponding polymer chains. The golden one is the passible layer and the active layer is made of poly(NIPAm-AA) in the presence of poly(diallyldimethylammonium chloride) PDADMAC. Reprinted from ref [49], copyright (2017) Royal Society of Chemistry, license number: 4342521000764.

In addition, the materials of passive layer are not restricted to general polymers, stimuli-responsive polymers can be applied as the passive layer as well. Chen et al. presented a LCST-UCST bilayer structure as actuator, in which, the active layer was made from the LCST polymer of P(NIPAM), but the passive layer is the gel of poly(acrylic acid-co-acrylamide) (P(AAc-co-AAm)), a kind of UCST polymer. (**Figure 6**) When the temperature is below the LCST and UCST, the LCST layer swells and the UCST layer shrinks, and vice versa.[74] Due to their opposite thermoresponsive property, this bilayer actuator was able to exhibit

reversible bidirectional bending behavior upon responding to temperature as well. In conclusion, regarding to the design of bilayer polymeric actuators, it is unnecessary to use the common materials, stimuli-responsive polymers can also be a candidate as long as there is anisotropy along the cross-section between the two layers.

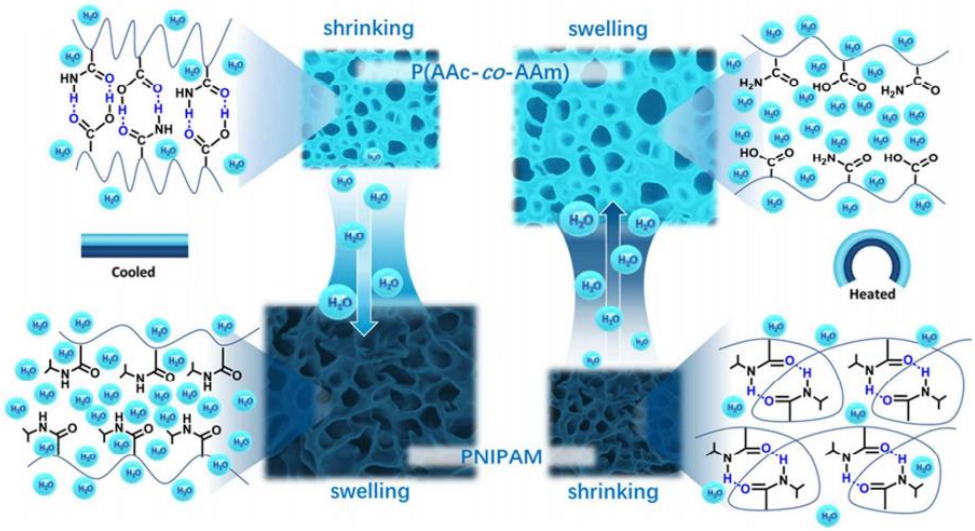

Figure 6. The mechanism of bending behavior of UCST-LCST bilayer structure actuator. At low temperature (15°C), the PNIPAM layer is swollen by water. Increasing temperature to 40°C leads to a shrinking of the PNIPAM layer, a directional water transfer to the P(AAc-co-AAm) layer that consequently swells and in result lets the bilayer hydrogel bends. Reprinted from,[74] copyright (2017), Royal Society of Chemistry, license number: 4342521434124.

1.4 Porous polymeric/soft actuators

The actuators mentioned above are capable of demonstrating controlled

shape deformation or motion, but the ones with higher sensitivity and fast response ability are rare. In general, polymeric/soft actuators respond slowly to external stimuli, because the corresponding swelling/shrinkage process is closely associated with the diffusion of water or ions or with the energy transfer. Generally, high diffusion rate generates high responding behavior.[75, 76] The diffusion rate is determined by the collective diffusion coefficient and the structure of the matrix.[76] For example, the porous structure is always used to increase the thermoresponsive ability of P(NIPAM). When a P(NIPAM) gel is immersed into the cold water with the temperature lower than the LCST, the swelling behavior is determined by the water molecules diffusion from the surrounding into the gel network.[77] Porous structure can provide more channels for the diffusion of water molecules, which indicates high water diffusion rate. When the P(NIPAM) gel is immersed into the higher temperature water (above the LCST), the shrinkage may mostly occur in the surface region at the beginning. The resultant dense skin layer as a barrier prevent the water molecules from further diffusion out from the gel matrix.[76, 78] However, P(NIPAM) gel with high porous structure which increases the contact area between the gel and the water can have more mass transfers of water resulting in high water diffusion rate.[76, 79] Moreover, Bell and Grosberg found that the diffusion coefficient is in direct proportion to the porosity. As the porosity increasing, more gas can go through the materials.[80]

Therefore, in comparison to the common film polymeric actuators whose smooth surface and compact structure slows down the diffusion in/out of water or ions or the energy transfer, the porous polymeric actuators could demonstrate distinguished actuation with the help of this "porous-diffusion" concept.

Zhao et al., designed a polymeric/soft actuator with a porous architecture, whose actuation happens within one second.[81] (**Figure 7)** However, this polymeric actuator has to be triggered by acetone, tetrahydrofuran (THF) or some other organic solvents which would limit the application in biomedical field. A lot of success have been achieved in fast actuation by the introduction of porous structure into the films.[82-86] By comparison, electrospinning could be a new optimal approach to design polymeric/soft actuators with outstanding properties.

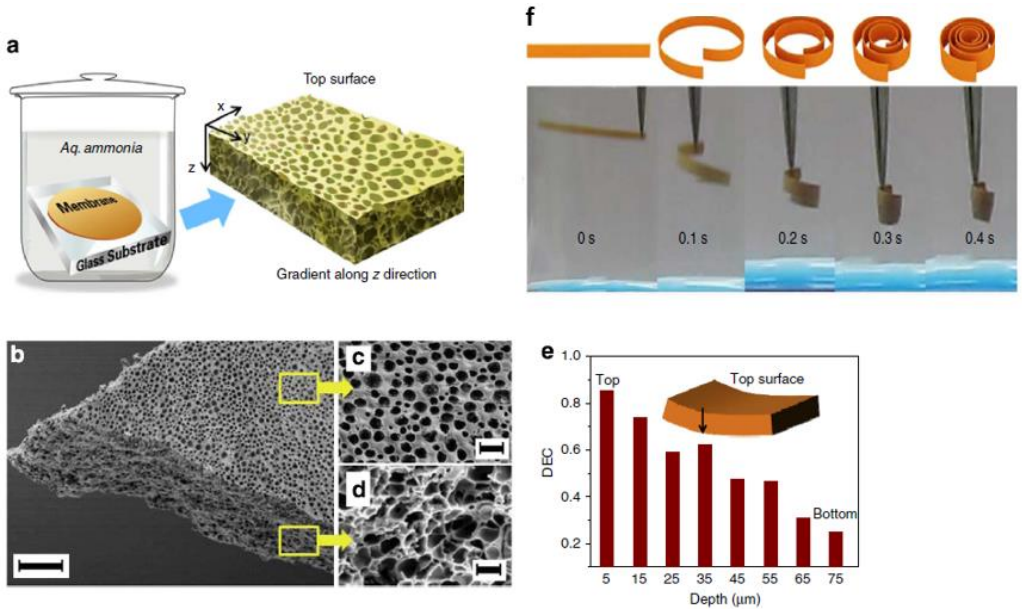

Figure 7. The concept, gradient structure characterization, and actuation of the polymeric actuator . (a) A scheme fabricating the actuator (b, scale

bar (black), 30 mm); top surface (c, scale bar, 3 mm); and cross-section (d, scale bar: 1 mm); (e) the DEC gradient along the thickness direction (from top to down). (f) fast actuation response to acetone vapor. Reproduced from [81], copyright (2014) Springer Nature, license number: 4342530538058.

1.5 Electrospinning

Electrospinning is the most common procedure to produce nanofibers. The **Figure 8** reveals that electrospinning is a current topic of interest for scientists, and the number of papers related to electrospinning increases year by year. Moreover, electrospinning technology has been introduced as an nanofibers fabrication method in nearly half of the scientific papers that refer to nanofibers fabrication.[87-90].

Electrospinning can be divided into solution electrospinning and melt electrospinning.[91-95] Generally, the electrospinning process contains three parts: the power supplier, which provides high voltage; the needle, which is used to form the Taylor cone;[96-98] and the two electrodes that form the potential difference.[87, 99-101] When the formed repulsive force overcomes the surface tension at the Taylor cone, the charged polymer solution is ejected. During the ejecting process, most of solvent is evaporated and finally, the nanofibers are collected by the counter electrode.[96, 102-106] (**Figure 9**) Different from other nanofiber

fabrication methods,[87, 96, 100, 101, 107-132] one of the most important features of electrospinning is that there is no special requirement put on the materials to be used that could limit the application; instead, various types of polymers and inorganic materials can be transformed into nanofibers.[96, 101, 106, 133, 134] Besides, electrospinning nanofiber production can be enhanced by applying either multi-syringe or needleless electrospinning.[135-137] More importantly, this method is able to manage the diameter of the nanofibers by varying the processing parameters such as concentration, voltage, and the distance between the needle and the collector.[98]. Well-known already, when the dimensions of the fiber materials are reduced to nanoscale, some outstanding properties appear, such as an ultrahigh aspect ratio, a large specific surface area, high porosity, and flexibility in surface functionalities.[138-143]

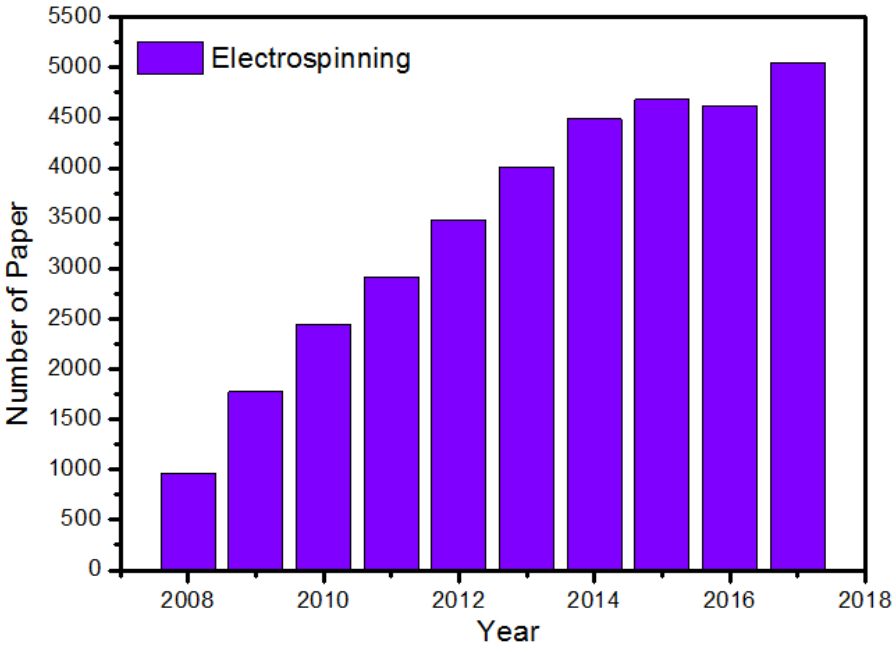

Figure 8. Growth of research of electrospinning. The increasing number of scientific papers containing the keyword "electrospinning" from SciFinder indicates the upward trend of electrospinning.

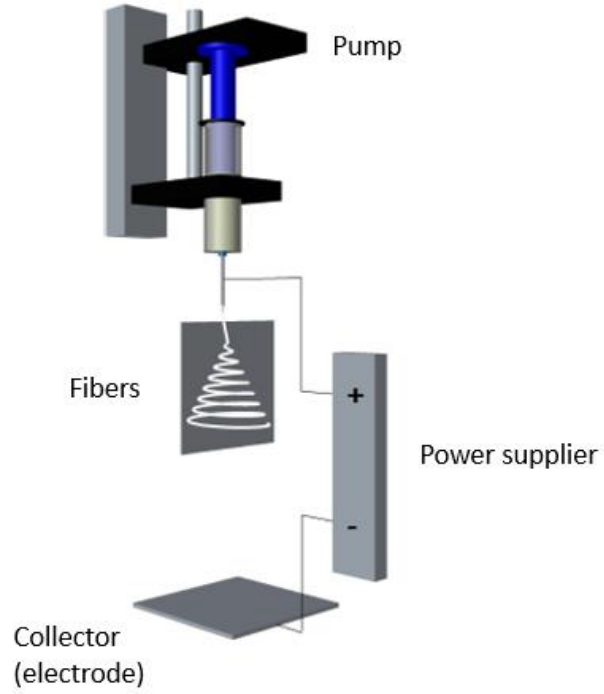

Figure 9. The set-up of electrospinning

1.5.1 Large aspect ratio

Nano-fibers are fibers with diameters in the nanometer range. They must be a type of linear one dimension object of longitudinal extension. The nanofibers' aspect ratio refers to the proportions of the length and diameter of the fibers. The aspect ratio of nano-fibers can be as high as 1000:1 or 10,000:1, and even higher.[144] Owing to their outstanding aspect ratio,

nano-fibers have a special anisotropy between longitudinal and lateral directions, which could be used to design polymeric actuators.

1.5.2 Large specific area and high porosity

It is already well-known that as the dimension of fibers is decreased to nanoscale, the specific area will be increased dramatically.[145] The **Figure 10** demonstrates a survey result that the decreasing diameter results in a large specific surface area. Polymeric actuators consist of smart materials that could exhibit property changes upon responding toexternal stimuli such as light, temperature, and pH, among others. A large specific area can provide fibrous polymeric actuators with more contact area to respond to the stimuli more efficiently.[146] In addition, the large surface area can offer many more positions for cell growth and the opportunities for biomedical application.[147] On the other hand, compared with polymer film, the fibrous mat has the unique characteristic of high porosity. The porosity of nano-fibrous materials can amount to more than 90%,[148-150] which can promote the diffusion in/out of water or ions or the energy transfer, thus resulting in high sensitivity. Electrospinning as a cost-effective, versatile, and fascinating technology has been recognized as the most efficient method for the fabrication of continuous polymer nanofibers.[151] In addition to be the easier way to construct porous

architecture, electrospinning is a convenient way to provide nanofibers with various kinds of morphologies and structures, which expands its application.[106, 152-158]. For example, the porous structure also plays a significant role in the scaffold.[148, 149, 159, 160] Therefore, electrospinning promises great potential in designing polymeric actuator, which should receive more attention.

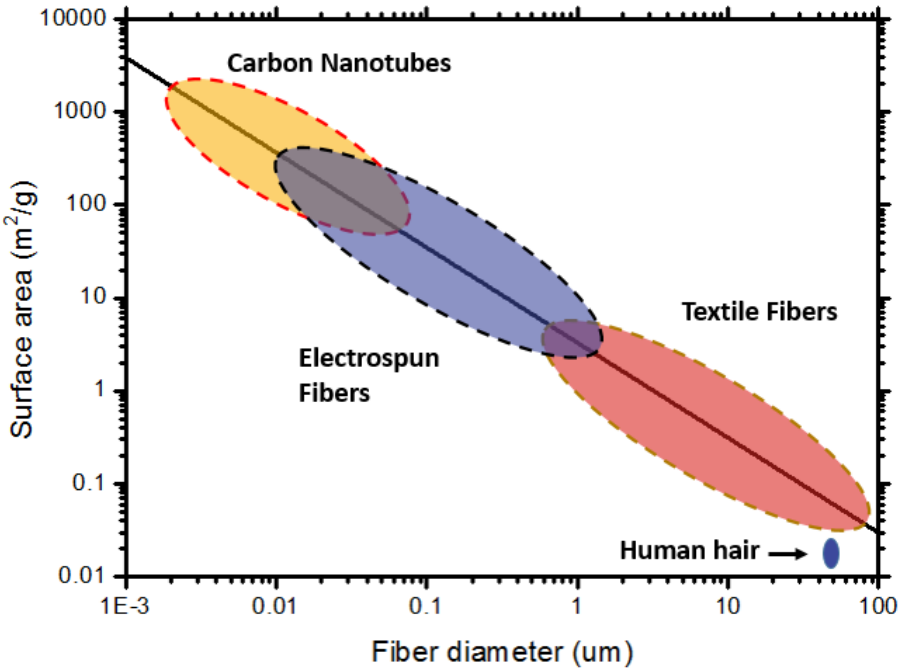

Figure 10. Schematic illustrating the relationship of the diameter of fibers and its specific area. Reproduced from [145], copyright (2001) Elsevier Science B.V., license number: 4342531220951.

1.5.3 Electrospun polymeric/soft actuators

To the best of my knowledge, including but not limited to, the earliest fibrous mat actuator made by electrospinning was designed in 2010.[161] Nakagawa *et al*. used electrospinning to fabricate a pH-responsive actuator. By controlling the feeding rate of the pump, he obtained a fibrous mat with diameter anisotropy in thickness direction, which exhibits a simple bending behavior response to an external pH change. Later, an electrospun polymeric actuator was developed by our group.[40] An unusual bilayer thermoresponsive actuator was fabricated by electrospinning. It exhibited ultrafast temperature-triggered actuation. Later, in 2018, 3D printing technology was combined with electrospinning for rapid response and enhanced designability of hydrogel actuators. Through this innovational approach, a range of controlled hydrogel actuators are constructed with various unique responsive motions. In addition, this framework can be extended to other responsive polymers.[162] Similarly, much success has been achieved by another electrospun polymeric/soft actuators.[163-167]

1.6 Directionally controlled polymeric/soft actuators

In the past decades, the bending forward and backward of polymeric/soft actuators have been achieved by inducing anisotropy along the cross-section.[42, 44, 46, 49, 53, 55, 58, 59, 83, 86, 167-173] Recently, being

inspired by the plants in nature, directionally controlled actuation was introduced as a new property to be given to polymeric/soft actuators. For sclerenchymal tissues whose fibrous cell walls consist of lots of stiff cellulose fibrils with a directional orientation. Arising from the preferred fibrils alignment, such as during the the penetration of wheat seeds into soil and the opening of chiral seed pods, the tissues exhibit preferred directionally motion when expelling/absorbing water.[174, 175] The natural analogues of such systems rely on the anisotropic restricted shrinkage along prescribed directions. Although it is intrinsic to the system of nature, this strategy paved the way for the design of polymeric/soft actuators with directionally controlled ability. Wu et al., reported a polymeric/soft actuator with directionally controlled actuation by combing fiber-like regions with different swelling behaviors in one single-layer hydrogel sheet.[176] Zhang et al., incorporated prescribed parallel glass fibers into agarose. The forming composite actuator realized directionally controlled actuation upon responding to humidity.[177] (**Figure 11)** Thus, the prescribed aligned architecture plays an important role in directionally controlled actuation.[13, 54, 178-181] However, none of those approaches enable directionally controlled actuation with high sensitivity to occur in one polymeric/soft actuator.

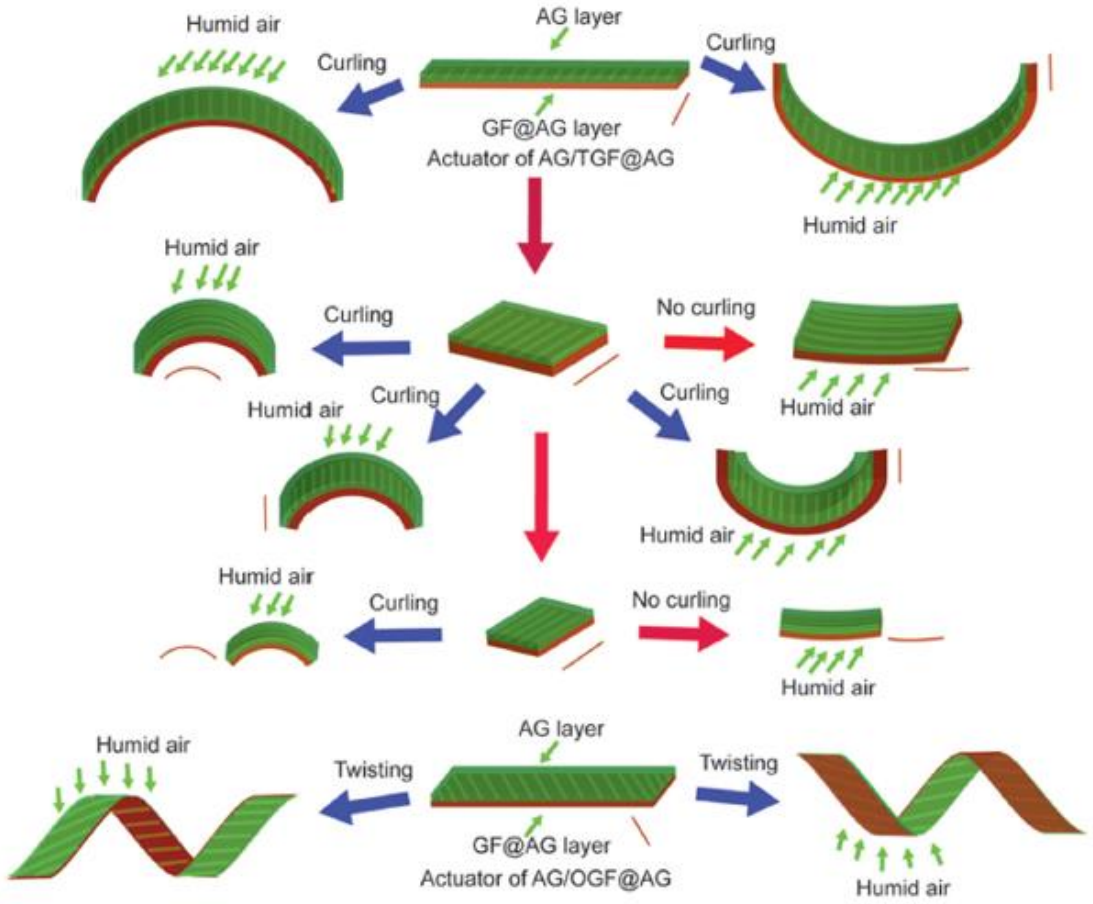

Figure 11. The schematic of actuation of the composite, in which, parallel glass fibers embedded within the agarose, in response to humidity. Reprinted from [177] copyright (2015) John Wiley and Sons, license number: 4342540024870.

1.7 Fabrication of polymeric/soft actuators by electrospinning

In this study, to obtain a thermoresponsive polymeric actuator with fast response, directional controlled actuation, electrospinning is used as a tool to get porous membrane for fast actuation. A vertically rotating disc with fast rotation was employed as a collector and provided parallel aligned

fibers whose porosity and alignment are extremely high, presenting the potential of high sensitivity and directionally controlled actuation. The aligned fibrous mats made of stimuli responsive polymers can demonstrate different size changes between longitudinal and lateral directions upon responding to external stimuli. When they are combined with another passive layer, the obtained bilayer actuator could reveal a directionally controlled actuation with high sensitivity due to its porous architecture and anisotropy longitudinal and lateral directions.

The stimuli responsive polymers used in this study are P(NIPAM) and another thermo- and pH- dual responsive polymer P(NIPAM-AA). Be different from the fabrication of polymeric actuators triggered by only temperature, this dual responsive polymeric actuator is a composite, in which, the aligned P(NIPAM-AA) fibrous mat embedded within a passive thermoplastic polyurethane (TPU) matrix by dropping dilute TPU/THF solution on the fibrous mat.

1.8 References

[1] H. Ko, A. Javey, Smart Actuators and Adhesives for Reconfigurable Matter, Acc Chem Res 50(4) (2017) 691-702.

[2] J. Duan, X. Liang, K. Zhu, J. Guo, L. Zhang, Bilayer hydrogel actuators with tight interfacial adhesion fully constructed from natural polysaccharides, Soft Matter 13(2) (2017) 345-354.

[3] S. Kim, C. Laschi, B. Trimmer, Soft robotics: a bioinspired evolution in robotics, Trends in biotechnology 31(5) (2013) 287-294.

[4] S. Singamaneni, M.C. LeMieux, H.P. Lang, C. Gerber, Y. Lam, S. Zauscher, P.G. Datskos, N.V. Lavrik, H. Jiang, R.R. Naik, T.J. Bunning, V.V. Tsukruk, Bimaterial Microcantilevers as a Hybrid Sensing Platform, Advanced Materials 20(4) (2008) 653-680.

[5] R. Bashir, J. Hilt, O. Elibol, A. Gupta, N. Peppas, Micromechanical cantilever as an ultrasensitive pH microsensor, Applied Physics Letters 81(16) (2002) 3091-3093.

[6] C. Dawson, J.F.V. Vincent, A.-M. Rocca, How pine cones open, Nature 390 (1997) 668.

[7] J.W.C. Dunlop, R. Weinkamer, P. Fratzl, Artful interfaces within biological materials, Materials Today 14(3) (2011) 70-78.

[8] I. Burgert, P. Fratzl, Actuation systems in plants as prototypes for bioinspired devices, Philos Trans A Math Phys Eng Sci 367(1893) (2009) 1541-57.

[9] S. Armon, E. Efrati, R. Kupferman, E. Sharon, Geometry and mechanics in the opening of chiral seed pods, Science 333(6050) (2011) 1726-30.

[10] S.-J. Jeon, A.W. Hauser, R.C. Hayward, Shape-Morphing Materials from Stimuli-Responsive Hydrogel Hybrids, Accounts of Chemical Research 50(2) (2017) 161-169.

[11] L. Ionov, Hydrogel-based actuators: possibilities and limitations, Materials Today 17(10) (2014) 494-503.

[12] K.D. Harris, R. Cuypers, P. Scheibe, C.L. van Oosten, C.W. Bastiaansen, J. Lub, D.J. Broer, Large amplitude light-induced motion in high elastic modulus polymer actuators, Journal of Materials Chemistry 15(47) (2005) 5043-5048.

[13] J. Kim, S.E. Chung, S.E. Choi, H. Lee, J. Kim, S. Kwon, Programming magnetic anisotropy in polymeric microactuators, Nat Mater 10(10) (2011) 747-52.

[14] K.D. Harris, C.W.M. Bastiaansen, D.J. Broer, A Glassy Bending-Mode Polymeric Actuator Which Deforms in Response to Solvent Polarity, Macromolecular Rapid Communications 27(16) (2006) 1323-1329.

[15] L.T. de Haan, J.M. Verjans, D.J. Broer, C.W. Bastiaansen, A.P. Schenning, Humidity-responsive liquid crystalline polymer actuators with an asymmetry in the molecular trigger that bend, fold, and curl, J Am Chem Soc 136(30) (2014) 10585-8.

[16] K.D. Harris, C.W. Bastiaansen, J. Lub, D.J. Broer, Self-assembled polymer films for controlled agent-driven motion, Nano letters 5(9) (2005) 1857-1860.

[17] W. Wu, L. Yao, T. Yang, R. Yin, F. Li, Y. Yu, NIR-light-induced deformation of cross-linked liquid-crystal polymers using upconversion nanophosphors, J Am Chem Soc 133(40) (2011) 15810-3.

[18] Y.H.P. Zhang, J. Cui, L.R. Lynd, L.R. Kuang, A Transition from Cellulose Swelling to Cellulose Dissolution by o-Phosphoric Acid: Evidence from Enzymatic Hydrolysis and Supramolecular Structure, Biomacromolecules 7(2) (2006) 644-648.

[19] D. Klemm, B. Philipp, T. Heinze, U. Heinze, W. Wagenknecht, Endpapers, Comprehensive Cellulose Chemistry: Functionalization of Cellulose, Volume 2 (1998).

[20] E. Reyssat, L. Mahadevan, How wet paper curls, EPL (Europhysics Letters) 93(5) (2011) 54001.

[21] Y.-J. Kim, Y.T. Matsunaga, Thermo-responsive polymers and their application as smart biomaterials, Journal of Materials Chemistry B 5(23) (2017) 4307-4321.

[22] A.S. Hoffman, "Intelligent" Polymers in Medicine and Biotechnology, Artificial Organs 19(5) (1995) 458-467.

[23] A.S. Hoffman, Stimuli-responsive polymers: Biomedical applications and challenges for clinical translation, Advanced Drug Delivery Reviews

65(1) (2013) 10-16.

[24] X. Yin, A.S. Hoffman, P.S. Stayton, Poly(N-isopropylacrylamide-co-propylacrylic acid) Copolymers That Respond Sharply to Temperature and pH, Biomacromolecules 7(5) (2006) 1381-1385.

[25] D. Roy, W.L. Brooks, B.S. Sumerlin, New directions in thermoresponsive polymers, Chem Soc Rev 42(17) (2013) 7214-43.

[26] Y. Lu, M. Ballauff, Thermosensitive core–shell microgels: From colloidal model systems to nanoreactors, Progress in Polymer Science 36(6) (2011) 767-792.

[27] J. Seuring, S. Agarwal, Polymers with Upper Critical Solution Temperature in Aqueous Solution: Unexpected Properties from Known Building Blocks, ACS Macro Letters 2(7) (2013) 597-600.

[28] J. Seuring, F.M. Bayer, K. Huber, S. Agarwal, Upper Critical Solution Temperature of Poly(N-acryloyl glycinamide) in Water: A Concealed Property, Macromolecules 45(1) (2011) 374-384.

[29] A. Gandhi, A. Paul, S.O. Sen, K.K. Sen, Studies on thermoresponsive polymers: Phase behaviour, drug delivery and biomedical applications, Asian Journal of Pharmaceutical Sciences 10(2) (2015) 99-107.

[30] X. Wang, X. Qiu, C. Wu, Comparison of the Coil-to-Globule and the Globule-to-Coil Transitions of a Single Poly(N-isopropylacrylamide) Homopolymer Chain in Water, Macromolecules 31(9) (1998) 2972-2976.

[31] C. Wu, X. Wang, Globule-to-Coil Transition of a Single

Homopolymer Chain in Solution, Physical Review Letters 80(18) (1998) 4092-4094.

[32] A.A. Alexander-Bryant, W.S. Vanden Berg-Foels, X. Wen, Bioengineering strategies for designing targeted cancer therapies, Adv Cancer Res 118 (2013) 1-59.

[33] Y.G. Takei, T. Aoki, K. Sanui, N. Ogata, T. Okano, Y. Sakurai, Temperature-responsive bioconjugates. 2. Molecular design for temperature-modulated bioseparations, Bioconjugate chemistry 4(5) (1993) 341-346.

[34] Y.-J. Liu, A. Pallier, J. Sun, S. Rudiuk, D. Baigl, M. Piel, E. Marie, C. Tribet, Non-monotonous variation of the LCST of light-responsive, amphiphilic poly(NIPAM) derivatives, Soft Matter 8(32) (2012) 8446.

[35] K. Troll, A. Kulkarni, W. Wang, C. Darko, A.M. Bivigou Koumba, A. Laschewsky, P. Müller-Buschbaum, C.M. Papadakis, The collapse transition of poly(styrene-b-(N-isopropyl acrylamide)) diblock copolymers in aqueous solution and in thin films, Colloid and Polymer Science 286(8-9) (2008) 1079-1092.

[36] T. Tang, V. Castelletto, P. Parras, I.W. Hamley, S.M. King, D. Roy, S. Perrier, R. Hoogenboom, U.S. Schubert, Thermo-responsive Poly(methyl methacrylate)-block-poly(N-isopropylacrylamide) Block Copolymers Synthesized by RAFT Polymerization: Micellization and Gelation, Macromolecular Chemistry and Physics 207(19) (2006) 1718-1726.

[37] J. Maitra, V.K. Shukla, Cross-linking in hydrogels-a review, American Journal of Polymer Science 4(2) (2014) 25-31.

[38] S. Harms, K. Ratzke, F. Faupel, W. Egger, L. Ravello, A. Laschewsky, W. Wang, P. Muller-Buschbaum, Free Volume and Swelling in Thin Films of Poly(N-isopropylacrylamide) End-Capped with n-Butyltrithiocarbonate, Macromol Rapid Commun 31(15) (2010) 1364-7.

[39] G. Stoychev, N. Puretskiy, L. Ionov, Self-folding all-polymer thermoresponsive microcapsules, Soft Matter 7(7) (2011) 3277.

[40] S. Jiang, F. Liu, A. Lerch, L. Ionov, S. Agarwal, Unusual and Superfast Temperature-Triggered Actuators, Adv Mater 27(33) (2015) 4865-70.

[41] G. Stoychev, S. Turcaud, J.W.C. Dunlop, L. Ionov, Hierarchical Multi-Step Folding of Polymer Bilayers, Advanced Functional Materials 23(18) (2013) 2295-2300.

[42] V. Stroganov, S. Zakharchenko, E. Sperling, A.K. Meyer, O.G. Schmidt, L. Ionov, Biodegradable Self-Folding Polymer Films with Controlled Thermo-Triggered Folding, Advanced Functional Materials 24(27) (2014) 4357-4363.

[43] X. Zhang, C.L. Pint, M.H. Lee, B.E. Schubert, A. Jamshidi, K. Takei, H. Ko, A. Gillies, R. Bardhan, J.J. Urban, M. Wu, R. Fearing, A. Javey, Optically- and thermally-responsive programmable materials based on carbon nanotube-hydrogel polymer composites, Nano Lett 11(8) (2011) 3239-44.

[44] V. Stroganov, M. Al-Hussein, J.U. Sommer, A. Janke, S. Zakharchenko, L. Ionov, Reversible thermosensitive biodegradable polymeric actuators based on confined crystallization, Nano Lett 15(3) (2015) 1786-90.

[45] G. Stoychev, S. Zakharchenko, S.b. Turcaud, J.W. Dunlop, L. Ionov, Shape-programmed folding of stimuli-responsive polymer bilayers, ACS nano 6(5) (2012) 3925-3934.

[46] L. Zhang, I. Desta, P. Naumov, Synergistic action of thermoresponsive and hygroresponsive elements elicits rapid and directional response of a bilayer actuator, Chem Commun (Camb) 52(35) (2016) 5920-3.

[47] Z. Hu, X. Zhang, Y. Li, Synthesis and application of modulated polymer gels, Science 269(5223) (1995) 525-527.

[48] E. Zhang, T. Wang, W. Hong, W. Sun, X. Liu, Z. Tong, Infrared-driving actuation based on bilayer graphene oxide-poly(N-isopropylacrylamide) nanocomposite hydrogels, Journal of Materials Chemistry A 2(37) (2014) 15633.

[49] X. Li, X. Cai, Y. Gao, M.J. Serpe, Reversible bidirectional bending of hydrogel-based bilayer actuators, Journal of Materials Chemistry B 5(15) (2017) 2804-2812.

[50] C. Yao, Z. Liu, C. Yang, W. Wang, X.-J. Ju, R. Xie, L.-Y. Chu, Poly(N-isopropylacrylamide)-Clay Nanocomposite Hydrogels with Responsive Bending Property as Temperature-Controlled Manipulators, Advanced

Functional Materials 25(20) (2015) 2980-2991.

[51] X. Zhang, Z. Yu, C. Wang, D. Zarrouk, J.W. Seo, J.C. Cheng, A.D. Buchan, K. Takei, Y. Zhao, J.W. Ager, J. Zhang, M. Hettick, M.C. Hersam, A.P. Pisano, R.S. Fearing, A. Javey, Photoactuators and motors based on carbon nanotubes with selective chirality distributions, Nat Commun 5 (2014) 2983.

[52] P. Techawanitchai, M. Ebara, N. Idota, T.-A. Asoh, A. Kikuchi, T. Aoyagi, Photo-switchable control of pH-responsive actuators via pH jump reaction, Soft Matter 8(10) (2012) 2844.

[53] D. Niu, W. Jiang, H. Liu, T. Zhao, B. Lei, Y. Li, L. Yin, Y. Shi, B. Chen, B. Lu, Reversible Bending Behaviors of Photomechanical Soft Actuators Based on Graphene Nanocomposites, Sci Rep 6 (2016) 27366.

[54] J. Deng, J. Li, P. Chen, X. Fang, X. Sun, Y. Jiang, W. Weng, B. Wang, H. Peng, Tunable Photothermal Actuators Based on a Pre-programmed Aligned Nanostructure, J Am Chem Soc 138(1) (2016) 225-30.

[55] Z. Lei, W. Zhu, S. Sun, P. Wu, MoS2-based dual-responsive flexible anisotropic actuators, Nanoscale 8(44) (2016) 18800-18807.

[56] H. Lim, T. Park, J. Na, C. Park, B. Kim, E. Kim, Construction of a photothermal Venus flytrap from conductive polymer bimorphs, NPG Asia Materials 9(6) (2017) e399.

[57] J. Mu, C. Hou, H. Wang, Y. Li, Q. Zhang, M. Zhu, Origami-inspired active graphene-based paper for programmable instant self-folding

walking devices, Science advances 1(10) (2015) e1500533.

[58] M. Ji, N. Jiang, J. Chang, J. Sun, Near-Infrared Light-Driven, Highly Efficient Bilayer Actuators Based on Polydopamine-Modified Reduced Graphene Oxide, Advanced Functional Materials 24(34) (2014) 5412-5419.

[59] Y. Cheng, K. Ren, D. Yang, J. Wei, Bilayer-type fluorescence hydrogels with intelligent response serve as temperature/pH driven soft actuators, Sensors and Actuators B: Chemical 255 (2018) 3117-3126.

[60] Y. Zhao, H. Su, L. Fang, T. Tan, Superabsorbent hydrogels from poly (aspartic acid) with salt-, temperature-and pH-responsiveness properties, Polymer 46(14) (2005) 5368-5376.

[61] M.K. Krušić, J. Filipović, Copolymer hydrogels based on N-isopropylacrylamide and itaconic acid, Polymer 47(1) (2006) 148-155.

[62] M.D. Determan, J.P. Cox, S. Seifert, P. Thiyagarajan, S.K. Mallapragada, Synthesis and characterization of temperature and pH-responsive pentablock copolymers, Polymer 46(18) (2005) 6933-6946.

[63] S.Y. Kim, S.M. Cho, Y.M. Lee, S.J. Kim, Thermo-and pH-responsive behaviors of graft copolymer and blend based on chitosan and N-isopropylacrylamide, Journal of Applied Polymer Science 78(7) (2000) 1381-1391.

[64] T.G. Park, A.S. Hoffman, Synthesis and characterization of pH-and/or temperature-sensitive hydrogels, Journal of Applied Polymer Science 46(4)

(1992) 659-671.

[65] T. Serizawa, K. Wakita, T. Kaneko, M. Akashi, Thermoresponsive properties of porous poly (N-isopropylacrylamide) hydrogels prepared in the presence of nanosized silica particles and subsequent acid treatment, Journal of Polymer Science Part A: Polymer Chemistry 40(23) (2002) 4228-4235.

[66] H.K. Ju, S.Y. Kim, S.J. Kim, Y.M. Lee, pH/temperature-responsive semi-IPN hydrogels composed of alginate and poly (N-isopropylacrylamide), Journal of applied polymer science 83(5) (2002) 1128-1139.

[67] K. Kratz, T. Hellweg, W. Eimer, Influence of charge density on the swelling of colloidal poly (N-isopropylacrylamide-co-acrylic acid) microgels, Colloids and Surfaces A: Physicochemical and Engineering Aspects 170(2-3) (2000) 137-149.

[68] M.J. Snowden, B.Z. Chowdhry, B. Vincent, G.E. Morris, Colloidal copolymer microgels of N-isopropylacrylamide and acrylic acid: pH, ionic strength and temperature effects, Journal of the Chemical Society, Faraday Transactions 92(24) (1996) 5013-5016.

[69] C. Johansson, J. Gernandt, M. Bradley, B. Vincent, P. Hansson, Interaction between lysozyme and colloidal poly (NIPAM-co-acrylic acid) microgels, Journal of colloid and interface science 347(2) (2010) 241-251.

[70] H. Chen, Y.L. Hsieh, Ultrafine hydrogel fibers with dual temperature-

and pH-responsive swelling behaviors, Journal of Polymer Science Part A: Polymer Chemistry 42(24) (2004) 6331-6339.

[71] W.F. Lee, C.H. Shieh, pH–thermoreversible hydrogels. II. Synthesis and swelling behaviors of N-isopropylacrylamide-co-acrylic acid-co-sodium acrylate hydrogels, Journal of applied polymer science 73(10) (1999) 1955-1967.

[72] J. Zhang, L.-Y. Chu, Y.-K. Li, Y.M. Lee, Dual thermo- and pH-sensitive poly(N-isopropylacrylamide-co-acrylic acid) hydrogels with rapid response behaviors, Polymer 48(6) (2007) 1718-1728.

[73] C.M. Schilli, M. Zhang, E. Rizzardo, S.H. Thang, Y.K. Chong, K. Edwards, G. Karlsson, A.H.E. Müller, A New Double-Responsive Block Copolymer Synthesized via RAFT Polymerization: Poly(N-isopropylacrylamide)-block-poly(acrylic acid), Macromolecules 37(21) (2004) 7861-7866.

[74] J. Zheng, P. Xiao, X. Le, W. Lu, P. Théato, C. Ma, B. Du, J. Zhang, Y. Huang, T. Chen, Mimosa inspired bilayer hydrogel actuator functioning in multi-environments, Journal of Materials Chemistry C 6(6) (2018) 1320-1327.

[75] Y. Kaneko, K. Sakai, A. Kikuchi, R. Yoshida, Y. Sakurai, T. Okano, Influence of freely mobile grafted chain length on dynamic properties of comb-type grafted poly (N-isopropylacrylamide) hydrogels, Macromolecules 28(23) (1995) 7717-7723.

[76] X.-Z. Zhang, Y.-Y. Yang, T.-S. Chung, K.-X. Ma, Preparation and characterization of fast response macroporous poly (N-isopropylacrylamide) hydrogels, Langmuir 17(20) (2001) 6094-6099.

[77] S. Jin, F. Bian, M. Liu, S. Chen, H. Liu, Swelling mechanism of porous P(VP-co-MAA)/PNIPAM semi-IPN hydrogels with various pore sizes prepared by a freeze treatment, Polymer International 58(2) (2009) 142-148.

[78] X. Zhang, R. Zhuo, Synthesis of Temperature-Sensitive Poly(N-isopropylacrylamide) Hydrogel with Improved Surface Property, J Colloid Interface Sci 223(2) (2000) 311-313.

[79] O. Hirasa, S. Ito, A. Yamauchi, S. Fujishige, H. Ichijo, Thermoresponsive polymer hydrogel, Polymer Gels, Springer1991, pp. 247-256.

[80] J.R. Bell, P. Grosberg, Diffusion Through Porous Materials, Nature 189 (1961) 980.

[81] Q. Zhao, J.W. Dunlop, X. Qiu, F. Huang, Z. Zhang, J. Heyda, J. Dzubiella, M. Antonietti, J. Yuan, An instant multi-responsive porous polymer actuator driven by solvent molecule sorption, Nat Commun 5 (2014) 4293.

[82] H. Lin, J. Gong, H. Miao, R. Guterman, H. Song, Q. Zhao, J.W. Dunlop, J. Yuan, Flexible and Actuating Nanoporous Poly (Ionic Liquid)–Paper-Based Hybrid Membranes, ACS applied materials & interfaces 9(17)

(2017) 15148-15155.

[83] M.K. Khan, W.Y. Hamad, M.J. Maclachlan, Tunable mesoporous bilayer photonic resins with chiral nematic structures and actuator properties, Adv Mater 26(15) (2014) 2323-8.

[84] Q. Zhao, J. Heyda, J. Dzubiella, K. Tauber, J.W. Dunlop, J. Yuan, Sensing Solvents with Ultrasensitive Porous Poly(ionic liquid) Actuators, Adv Mater 27(18) (2015) 2913-7.

[85] W.E. Lee, Y.J. Jin, L.S. Park, G. Kwak, Fluorescent Actuator Based on Microporous Conjugated Polymer with Intramolecular Stack Structure, Advanced Materials 24(41) (2012) 5604-5609.

[86] Y. Zhang, L. Ionov, Actuating porous polyimide films, ACS Appl Mater Interfaces 6(13) (2014) 10072-7.

[87] D. Li, Y. Xia, Electrospinning of Nanofibers: Reinventing the Wheel?, Advanced Materials 16(14) (2004) 1151-1170.

[88] R. Sarbatly, D. Krishnaiah, Z. Kamin, A review of polymer nanofibres by electrospinning and their application in oil-water separation for cleaning up marine oil spills, Mar Pollut Bull 106(1-2) (2016) 8-16.

[89] AZoNano, Polymer Nanofibers - an Overview of Applications and Current Research into Processing Techniques, AZONANO (2005).

[90] P. Katta, M. Alessandro, R. Ramsier, G. Chase, Continuous electrospinning of aligned polymer nanofibers onto a wire drum collector, Nano letters 4(11) (2004) 2215-2218.

[91] P.D. Dalton, D. Grafahrend, K. Klinkhammer, D. Klee, M. Möller, Electrospinning of polymer melts: Phenomenological observations, Polymer 48(23) (2007) 6823-6833.

[92] Z.K. Nagy, A. Balogh, G. Drávavölgyi, J. Ferguson, H. Pataki, B. Vajna, G. Marosi, Solvent-free melt electrospinning for preparation of fast dissolving drug delivery system and comparison with solvent-based electrospun and melt extruded systems, Journal of pharmaceutical sciences 102(2) (2013) 508-517.

[93] D.W. Hutmacher, P.D. Dalton, Melt electrospinning, Chemistry–An Asian Journal 6(1) (2011) 44-56.

[94] J. Lyons, C. Li, F. Ko, Melt-electrospinning part I: processing parameters and geometric properties, Polymer 45(22) (2004) 7597-7603.

[95] S. Agarwal, A. Greiner, On the way to clean and safe electrospinning-green electrospinning: emulsion and suspension electrospinning, Polymers for Advanced Technologies 22(3) (2011) 372-378.

[96] J. Doshi, D.H. Reneker, Electrospinning process and applications of electrospun fibers, Journal of electrostatics 35(2-3) (1995) 151-160.

[97] A.L. Yarin, S. Koombhongse, D.H. Reneker, Taylor cone and jetting from liquid droplets in electrospinning of nanofibers, Journal of Applied Physics 90(9) (2001) 4836-4846.

[98] S.A. Theron, E. Zussman, A.L. Yarin, Experimental investigation of the governing parameters in the electrospinning of polymer solutions,

Polymer 45(6) (2004) 2017-2030.

[99] S.R. Merritt, A.A. Exner, Z. Lee, H.A. von Recum, Electrospinning and Imaging, Advanced Engineering Materials 14(5) (2012) B266-B278.

[100] W.E. Teo, S. Ramakrishna, A review on electrospinning design and nanofibre assemblies, Nanotechnology 17(14) (2006) R89-R106.

[101] Z.-M. Huang, Y.Z. Zhang, M. Kotaki, S. Ramakrishna, A review on polymer nanofibers by electrospinning and their applications in nanocomposites, Composites Science and Technology 63(15) (2003) 2223-2253.

[102] D.H. Reneker, A.L. Yarin, H. Fong, S. Koombhongse, Bending instability of electrically charged liquid jets of polymer solutions in electrospinning, Journal of Applied Physics 87(9) (2000) 4531-4547.

[103] H. Fong, I. Chun, D. Reneker, Beaded nanofibers formed during electrospinning, Polymer 40(16) (1999) 4585-4592.

[104] K. Lee, H. Kim, H. Bang, Y. Jung, S. Lee, The change of bead morphology formed on electrospun polystyrene fibers, Polymer 44(14) (2003) 4029-4034.

[105] A. Frenot, I.S. Chronakis, Polymer nanofibers assembled by electrospinning, Current Opinion in Colloid & Interface Science 8(1) (2003) 64-75.

[106] A. Greiner, J.H. Wendorff, Electrospinning: a fascinating method for the preparation of ultrathin fibers, Angew Chem Int Ed Engl 46(30) (2007)

5670-703.

[107] R. Vasita, D.S. Katti, Nanofibers and their applications in tissue engineering, International Journal of nanomedicine 1(1) (2006) 15.

[108] P.X. Ma, R. Zhang, Synthetic nano-scale fibrous extracellular matrix, (1999).

[109] C.A. Martínez-Pérez, I. Olivas-Armendariz, J.S. Castro-Carmona, P.E. García-Casillas, Scaffolds for tissue engineering via thermally induced phase separation, Advances in Regenerative Medicine, InTech2011.

[110] P.X. Ma, Scaffolds for tissue fabrication, Materials today 7(5) (2004) 30-40.

[111] U.G. Micropipettes, Drawing Suspended Polymer Micro/Nanofibers.

[112] T. Ondarcuhu, C. Joachim, Drawing a single nanofibre over hundreds of microns, EPL (Europhysics Letters) 42(2) (1998) 215.

[113] C.R. Martin, Template synthesis of electronically conductive polymer nanostructures, Accounts of chemical research 28(2) (1995) 61-68.

[114] C.R. Martin, Nanomaterials: a membrane-based synthetic approach, Science 266(5193) (1994) 1961-1966.

[115] N.B. Malkar, J.L. Lauer-Fields, D. Juska, G.B. Fields, Characterization of Peptide− Amphiphiles Possessing Cellular Activation Sequences, Biomacromolecules 4(3) (2003) 518-528.

[116] C. Zhang, X. Xue, Q. Luo, Y. Li, K. Yang, X. Zhuang, Y. Jiang, J.

Zhang, J. Liu, G. Zou, Self-assembled peptide nanofibers designed as biological enzymes for catalyzing ester hydrolysis, Acs Nano 8(11) (2014) 11715-11723.

[117] E.S. Medeiros, G.M. Glenn, A.P. Klamczynski, W.J. Orts, L.H.C. Mattoso, Solution blow spinning: A new method to produce micro- and nanofibers from polymer solutions, Journal of Applied Polymer Science 113(4) (2009) 2322-2330.

[118] R. Barhate, S. Ramakrishna, Nanofibrous filtering media: Filtration problems and solutions from tiny materials, Journal of Membrane Science 296(1-2) (2007) 1-8.

[119] C.J. Ellison, A. Phatak, D.W. Giles, C.W. Macosko, F.S. Bates, Melt blown nanofibers: Fiber diameter distributions and onset of fiber breakup, Polymer 48(11) (2007) 3306-3316.

[120] K. Nakata, K. Fujii, Y. Ohkoshi, Y. Gotoh, M. Nagura, M. Numata, M. Kamiyama, Poly(ethylene terephthalate) Nanofibers Made by Sea–Island-Type Conjugated Melt Spinning and Laser-Heated Flow Drawing, Macromolecular Rapid Communications 28(6) (2007) 792-795.

[121] W.C. Hinds, Aerosol technology: properties, behavior, and measurement of airborne particles, John Wiley & Sons2012.

[122] B.Y. Yeom, B. Pourdeyhimi, Aerosol filtration properties of PA6/PE islands-in-the-sea bicomponent spunbond web fibrillated by high-pressure water jets, Journal of Materials Science 46(17) (2011) 5761-5767.

[123] M.A. Hammami, M. Krifa, O. Harzallah, Centrifugal force spinning of PA6 nanofibers – processability and morphology of solution-spun fibers, The Journal of The Textile Institute 105(6) (2014) 637-647.

[124] K. Lozano, K. Sarkar, Methods and apparatuses for making superfine fibers, Patent Application, US, 2009.

[125] S. Padron, R. Patlan, J. Gutierrez, N. Santos, T. Eubanks, K. Lozano, Production and characterization of hybrid BEH-PPV/PEO conjugated polymer nanofibers by forcespinning™, Journal of Applied Polymer Science 125(5) (2012) 3610-3616.

[126] K. Sarkar, C. Gomez, S. Zambrano, M. Ramirez, E. de Hoyos, H. Vasquez, K. Lozano, Electrospinning to forcespinning™, Materials Today 13(11) (2010) 12-14.

[127] K. Shanmuganathan, Y. Fang, D.Y. Chou, S. Sparks, J. Hibbert, C.J. Ellison, Solventless High Throughput Manufacturing of Poly(butylene terephthalate) Nanofibers, ACS Macro Letters 1(8) (2012) 960-964.

[128] W.J. Morton, Method of dispersing fluids, Patent US, 1902.

[129] J.F. Cooley, Apparatus for electrically dispersing fluids, Patent US, 1902.

[130] F. Anton, Method and apparatus for the production of artificial fibers, Patent, US 1939.

[131] D.H. Reneker, A.L. Yarin, Electrospinning jets and polymer nanofibers, Polymer 49(10) (2008) 2387-2425.

[132] L. Persano, A. Camposeo, C. Tekmen, D. Pisignano, Industrial Upscaling of Electrospinning and Applications of Polymer Nanofibers: A Review, Macromolecular Materials and Engineering 298(5) (2013) 504-520.

[133] S. Agarwal, A. Greiner, J.H. Wendorff, Functional materials by electrospinning of polymers, Progress in Polymer Science 38(6) (2013) 963-991.

[134] S. Agarwal, A. Greiner, J.H. Wendorff, Electrospinning of Manmade and Biopolymer Nanofibers-Progress in Techniques, Materials, and Applications, Advanced Functional Materials 19(18) (2009) 2863-2879.

[135] D. Petras, L. Mares, D. Stranska, Method and device for production of nanofibres from the polymeric solution through electrostatic spinning, Patent Application US, 2008.

[136] J.A. Robertson, A.S. Scott, Electrospraying/electrospinning array utilizing a replacement array of individual tip flow restriction, Patent, US, 2009.

[137] H. Niu, T. Lin, X. Wang, Needleless electrospinning. I. A comparison of cylinder and disk nozzles, Journal of Applied Polymer Science 114(6) (2009) 3524-3530.

[138] Kenry, C.T. Lim, Nanofiber technology: current status and emerging developments, Progress in Polymer Science 70 (2017) 1-17.

[139] J.N. Tiwari, R.N. Tiwari, K.S. Kim, Zero-dimensional, one-

dimensional, two-dimensional and three-dimensional nanostructured materials for advanced electrochemical energy devices, Progress in Materials Science 57(4) (2012) 724-803.

[140] R. Nirmala, K.T. Nam, S.-J. Park, Y.-S. Shin, R. Navamathavan, H.Y. Kim, Formation of high aspect ratio polyamide-6 nanofibers via electrically induced double layer during electrospinning, Applied Surface Science 256(21) (2010) 6318-6323.

[141] R. Nirmala, H.R. Panth, C. Yi, K.T. Nam, S.-J. Park, H.Y. Kim, R. Navamathavan, Effect of solvents on high aspect ratio polyamide-6 nanofibers via electrospinning, Macromolecular Research 18(8) (2010) 759-765.

[142] K. Müller, J.F. Quinn, A.P.R. Johnston, M. Becker, A. Greiner, F. Caruso, Polyelectrolyte Functionalization of Electrospun Fibers, Chemistry of Materials 18(9) (2006) 2397-2403.

[143] U. Boudriot, R. Dersch, A. Greiner, J.H. Wendorff, Electrospinning approaches toward scaffold engineering—a brief overview, Artificial organs 30(10) (2006) 785-792.

[144] S. Agarwal, M. Burgard, A. Greiner, J.H. Wendorff, Electrospinning: A Practical Guide to Nanofibers, DE GRUYTER2016.

[145] P. Gibson, H. Schreuder-Gibson, D. Rivin, Transport properties of porous membranes based on electrospun nanofibers, Colloids and Surfaces A: Physicochemical and Engineering Aspects 187 (2001) 469-481.

[146] R.V. Samatham, Sub-micron diameter electrospun polyacrylonitrile fibers as potential linear actuator, (2005).

[147] M.M. Stevens, J.H. George, Exploring and engineering the cell surface interface, Science 310(5751) (2005) 1135-8.

[148] V.J. Chen, P.X. Ma, Nano-fibrous poly(l-lactic acid) scaffolds with interconnected spherical macropores, Biomaterials 25(11) (2004) 2065-2073.

[149] W.J. Li, C.T. Laurencin, E.J. Caterson, R.S. Tuan, F.K. Ko, Electrospun nanofibrous structure: a novel scaffold for tissue engineering, Journal of Biomedical Materials Research Part A 60(4) (2002) 613-621.

[150] C.P. Barnes, S.A. Sell, E.D. Boland, D.G. Simpson, G.L. Bowlin, Nanofiber technology: designing the next generation of tissue engineering scaffolds, Adv Drug Deliv Rev 59(14) (2007) 1413-33.

[151] S. Agarwal, J.H. Wendorff, A. Greiner, Progress in the field of electrospinning for tissue engineering applications, Adv Mater 21(32-33) (2009) 3343-51.

[152] D. Li, Y. Xia, Direct fabrication of composite and ceramic hollow nanofibers by electrospinning, Nano letters 4(5) (2004) 933-938.

[153] S. Jiang, G. Duan, E. Zussman, A. Greiner, S. Agarwal, Highly flexible and tough concentric triaxial polystyrene fibers, ACS Appl Mater Interfaces 6(8) (2014) 5918-23.

[154] X. Lu, C. Wang, Y. Wei, One-dimensional composite nanomaterials:

synthesis by electrospinning and their applications, Small 5(21) (2009) 2349-70.

[155] V. Kalra, P.A. Kakad, S. Mendez, T. Ivannikov, M. Kamperman, Y.L. Joo, Self-Assembled Structures in Electrospun Poly(styrene-block-isoprene) Fibers, Macromolecules 39(16) (2006) 5453-5457.

[156] H. Hou, D.H. Reneker, Carbon nanotubes on carbon nanofibers: a novel structure based on electrospun polymer nanofibers, Advanced Materials 16(1) (2004) 69-73.

[157] M. Bognitzki, M. Becker, M. Graeser, W. Massa, J.H. Wendorff, A. Schaper, D. Weber, A. Beyer, A. Gölzhäuser, A. Greiner, Preparation of Sub-micrometer Copper Fibers via Electrospinning, Advanced Materials 18(18) (2006) 2384-2386.

[158] H. Hou, Z. Jun, A. Reuning, A. Schaper, J.H. Wendorff, A. Greiner, Poly (p-xylylene) nanotubes by coating and removal of ultrathin polymer template fibers, Macromolecules 35(7) (2002) 2429-2431.

[159] J. Mitra, G. Tripathi, A. Sharma, B. Basu, Scaffolds for bone tissue engineering: role of surface patterning on osteoblast response, RSC Advances 3(28) (2013) 11073.

[160] V. Karageorgiou, D. Kaplan, Porosity of 3D biomaterial scaffolds and osteogenesis, Biomaterials 26(27) (2005) 5474-91.

[161] H. Nakagawa, Y. Hara, S. Maeda, S. Hashimoto, A novel design of nanofibrous gel actuator by electrospinning, Nanotechnology (IEEE-

NANO), 2010 10th IEEE Conference on, IEEE, 2010, pp. 1135-1138.

[162] T. Chen, H. Bakhshi, L. Liu, J. Ji, S. Agarwal, Combining 3D Printing with Electrospinning for Rapid Response and Enhanced Designability of Hydrogel Actuators, Advanced Functional Materials (2018) 1800514.

[163] H. Nakagawa, Y. Hara, S. Maeda, S. Hasimoto, A pendulum-like motion of nanofiber gel actuator synchronized with external periodic pH oscillation, Polymers 3(1) (2011) 405-412.

[164] J. Li, S. Vadahanambi, C.D. Kee, I.K. Oh, Electrospun fullerenol-cellulose biocompatible actuators, Biomacromolecules 12(6) (2011) 2048-54.

[165] M. Beregoi, A. Evanghelidis, V.C. Diculescu, H. Iovu, I. Enculescu, Polypyrrole Actuator Based on Electrospun Microribbons, ACS applied materials & interfaces 9(43) (2017) 38068-38075.

[166] F. Zhang, Z. Zhang, T. Zhou, Y. Liu, J. Leng, Shape Memory Polymer Nanofibers and Their Composites: Electrospinning, Structure, Performance, and Applications, Frontiers in Materials 2 (2015).

[167] H. Kato, A. Shimizu, T. Sato, M. Kushida, Fabrication of Carbon Nanotube Polymer Actuator Using Nanofiber Sheet, Journal of Physics: Conference Series 924 (2017) 012005.

[168] C. Ma, W. Lu, X. Yang, J. He, X. Le, L. Wang, J. Zhang, M.J. Serpe, Y. Huang, T. Chen, Bioinspired Anisotropic Hydrogel Actuators with On-

Off Switchable and Color-Tunable Fluorescence Behaviors, Advanced Functional Materials 28(7) (2018) 1704568.

[169] C.O. Baker, B. Shedd, P.C. Innis, P.G. Whitten, G.M. Spinks, G.G. Wallace, R.B. Kaner, Monolithic Actuators from Flash-Welded Polyaniline Nanofibers, Advanced Materials 20(1) (2008) 155-158.

[170] N. Terasawa, High-performance ionic and non-ionic fluoropolymer/ionic liquid gel hybrid actuators based on single-walled carbon nanotubes, RSC Advances 7(5) (2017) 2443-2449.

[171] J. Li, W. Ma, L. Song, Z. Niu, L. Cai, Q. Zeng, X. Zhang, H. Dong, D. Zhao, W. Zhou, S. Xie, Superfast-response and ultrahigh-power-density electromechanical actuators based on hierarchal carbon nanotube electrodes and chitosan, Nano Lett 11(11) (2011) 4636-41.

[172] T.-a. Asoh, M. Matsusaki, T. Kaneko, M. Akashi, Fabrication of Temperature-Responsive Bending Hydrogels with a Nanostructured Gradient, Advanced Materials 20(11) (2008) 2080-2083.

[173] K. Mukai, K. Asaka, T. Sugino, K. Kiyohara, I. Takeuchi, N. Terasawa, D.N. Futaba, K. Hata, T. Fukushima, T. Aida, Highly Conductive Sheets from Millimeter-Long Single-Walled Carbon Nanotubes and Ionic Liquids: Application to Fast-Moving, Low-Voltage Electromechanical Actuators Operable in Air, Advanced Materials 21(16) (2009) 1582-1585.

[174] R. Elbaum, L. Zaltzman, I. Burgert, P. Fratzl, The Role of Wheat

Awns in the Seed Dispersal Unit, Science 316(5826) (2007) 884-886.

[175] E. Reyssat, L. Mahadevan, Hygromorphs: from pine cones to biomimetic bilayers, Journal of the Royal Society Interface 6(39) (2009) 951-957.

[176] Z.L. Wu, M. Moshe, J. Greener, H. Therien-Aubin, Z. Nie, E. Sharon, E. Kumacheva, Three-dimensional shape transformations of hydrogel sheets induced by small-scale modulation of internal stresses, Nat Commun 4 (2013) 1586.

[177] L. Zhang, S. Chizhik, Y. Wen, P. Naumov, Directed Motility of Hygroresponsive Biomimetic Actuators, Advanced Functional Materials 26(7) (2016) 1040-1053.

[178] A.S. Gladman, E.A. Matsumoto, R.G. Nuzzo, L. Mahadevan, J.A. Lewis, Biomimetic 4D printing, Nat Mater 15(4) (2016) 413-8.

[179] H. Therien-Aubin, Z.L. Wu, Z. Nie, E. Kumacheva, Multiple shape transformations of composite hydrogel sheets, J Am Chem Soc 135(12) (2013) 4834-9.

[180] S. Iamsaard, S.J. Asshoff, B. Matt, T. Kudernac, J.J. Cornelissen, S.P. Fletcher, N. Katsonis, Conversion of light into macroscopic helical motion, Nat Chem 6(3) (2014) 229-35.

[181] R.M. Erb, J.S. Sander, R. Grisch, A.R. Studart, Self-shaping composites with programmable bioinspired microstructures, Nat Commun 4 (2013) 1712.

2. Thesis Overview

Polymeric actuators inspired from bio-architecture are very well-known in the literature. They are mostly based on a bilayer structure with asymmetrical swelling/shrinkage. The existing problems in the field of soft actuators are: slow speed of the actuation, control over direction missing of movements and multi-responsive ability. The aim of my work is to have detailed studies with respect to the responsive polymeric actuators with high sensitivity (fast actuation), directionally controlled actuation and multi-responsive ability. For enhancing the speed of actuation, porous fibrous mats were used in this work with a hypothesis of increasing the water mass transport and thus resulting in high speed of actuation. Electrospinning was used as a tool for making porous fibrous mats.

Direction control in the actuation is achieved by aligning fibers at different angles in the active layer. This result in asymmetric swelling/shrinkage & hence controls the direction of motion.

Firstly, through combining the passive layer of aligned thermoplastic polyurethane (TPU) fibrous mat and the active layer of poly(n-isopropylarylamide) P(NIPAM), a bilayer thermoresponsive polymeric actuator is obtained. It demonstrates the following highlights: 1) ultra-fast actuation between 0.6 – 5 s; 2) reversible directionally controlled

movement (rolls, tubes, helices); 3) there was not only shape changes but also surface changes triggered by temperature.

Secondly, a stable one-component polymeric actuator was created by electrospinning a random P(NIPAM) fibrous mat and an aligned P(NIPAM) fibrous mat. The combined bilayer thermoresponsive actuator consists of only one component of P(NIPAM) and the actuation of this actuator is irreversible. In addition, the temperature-triggered formed size could be controlled by temperature. Moreover, the actuation is directionally controlled depending on the angles between fiber alignment and long axis and it is demonstrated that by numerical simulations the observed behaviour is the unique combination of anisotropic thermal expansion with an equally anisotropic elastic modulus of the employed material as well.

Thirdly, a dual-responsive composite actuator composed of thermo- and pH-responsive poly(N-isopropylacrylamide-co-acrylic acid) (poly(NIPAm-AA)) fibers (average diameter ~ 905 nm) embedded within a passive thermoplastic polyurethane (TPU) matrix at different angles with degree of alignment as high as 98% was presented. The actuation direction were depended on the angles between fiber alignment and long axis. The actuation and the actuated tube was independent of temperature at pH 7 and above. However, temperature can be used to control the size of the actuated tubes at lower pH. Although the polymeric actuator is only 5.8 mg, it was able to reversibly lift and release ~426 times weight of their own

mass (2.47 g metal ring).

In summary, it is worth noting that our strategy, through which it is very convenient to obtain porous structure and directionally controlled actuation, is not only applicable to P(NIPAM) and P(NIPAM-AA), but also to other "smart" polymers, which therefore enriches the designs of versatile polymeric actuators with high sensitivity.

2.1 Giving direction to motion and surface with ultra-fast speed using oriented hydrogel fibers

Li Liu, Shaohua Jiang, Yue Sun, and Seema Agarwal*, "Giving direction to motion and surface with ultra‐fast speed using oriented hydrogel fibers", *Advanced Functional Materials*, 2016, 26(7), 1021-1027.

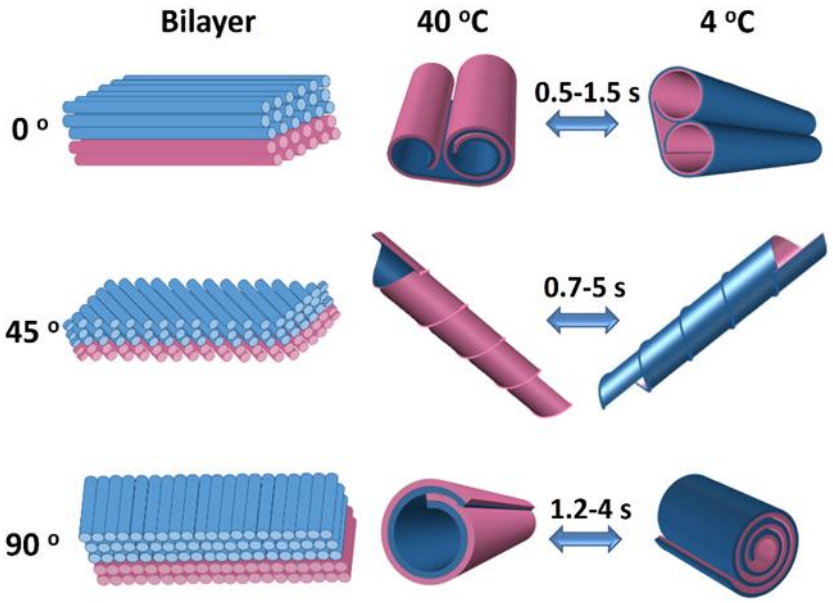

Abstract

This work presented the first time to present thermoresponsive hydrogel fibrous membranes demonstrating directionally controlled actuation and surface change with ultra-fast speed. Reversible bending, coiling, twisting and rolling deformations are exhibited in different controllable directions for many cycles (＞50 cycles) with inside-out change in surfaces and shapes. In order to make synthetic actuators inspired from natural materials

or otherwise, speed, reversibility, large-scale deformations and, most importantly, control over the direction of deformation is required. A polymeric actuator possessing all these properties still remains a challenge. This issue was addressed in this work and provide a very simple strategy fulfilling all these requirements by combining porosity and asymmetric planar size change (swelling/shrinking) via orientation of hydrogel fibers at different angles in a fibrous membrane. Electrospinning was as used as a tool for making membranes with fibers oriented at different angles.

In order to get aligned fibrous mat, a vertical rotating wheel with fast speed was used to collect fibers. After the TPU and P(NIPAM-ABP) solution were sequentially electrospun, obtained bilayer porous mats were pressed and transferred under UV- lamp for cross-linking. Then it is easy to get samples with various angles between fiber alignment and long axis by cutting. **(Figure 12)**

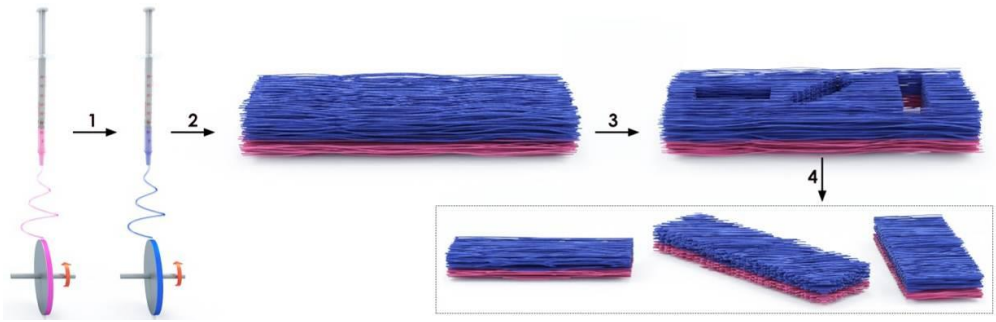

Figure 12. Schematic showing the formation of bilayer actuators by sequential electrospinning of TPU and P(NIPAM-ABP) followed by UV

cross-linking (steps 1 and 2). The samples were cut at different angles to get varied orientations of thermoresponsive P(NIPAM-ABP) fibers (steps 3 and 4). The TPU and P(NIPAM-ABP) solutions were mixed with rhodamine B (RB) and methylene blue, respectively to observe the actuation phenomenon optically better. Copyright (2015), John Wiley and Sons, license number: 4342540732801.

The alignment degree of P(NIPAM-ABP) and TPU are ~ 95 % and ~ 82 %, respectively. The porosity of P(NIPAM-ABP) fibrous mat was about 56 %. The SEM image shows a strong interface in the actuator between P(NIPAM) and TPU layer. (**Figure 13**)

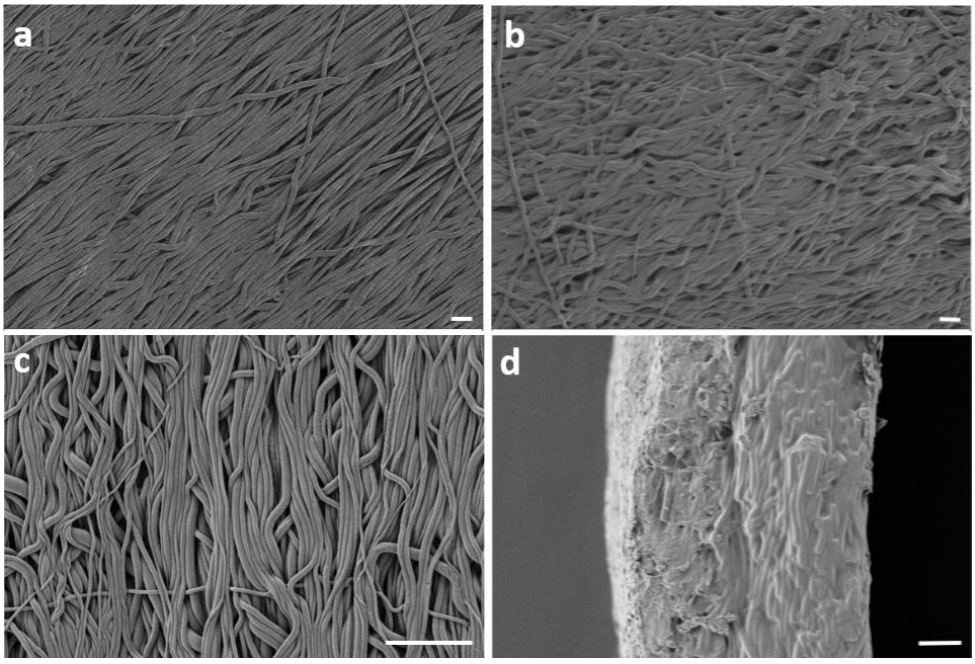

Figure 13. SEM images of a) P(NIPAM-ABP) side – as spun bilayer membrane, b) P(NIPAM-ABP) side - after treatment with hot water, c) TPU side- as spun bilayer membrane and d) the cross-section of the bilayer sample in water at 40 ^{o}C after drying shows a strong interface between TPU

(left side) and P(NIPAM-ABP) (right side). Scale bar = 10 μm. Copyright (2015), John Wiley and Sons, license number: 4342540732801.

This polymeric actuator made by electrospinning exhibits temperature-triggered ultrafast and directionally controlled actuation owing to the high porosity and fiber alignment degree. (**Figure 14**) No matter what the temperature is, it is always following the rule that in cold water (4 °C), it rolls in the perpendicular direction to the fiber alignment with the TPU layer inward and in hot water (40 °C) it rolls along fiber alignment with TPU layer outward. This process is reversible and highly repeated for more than 100 cycles.

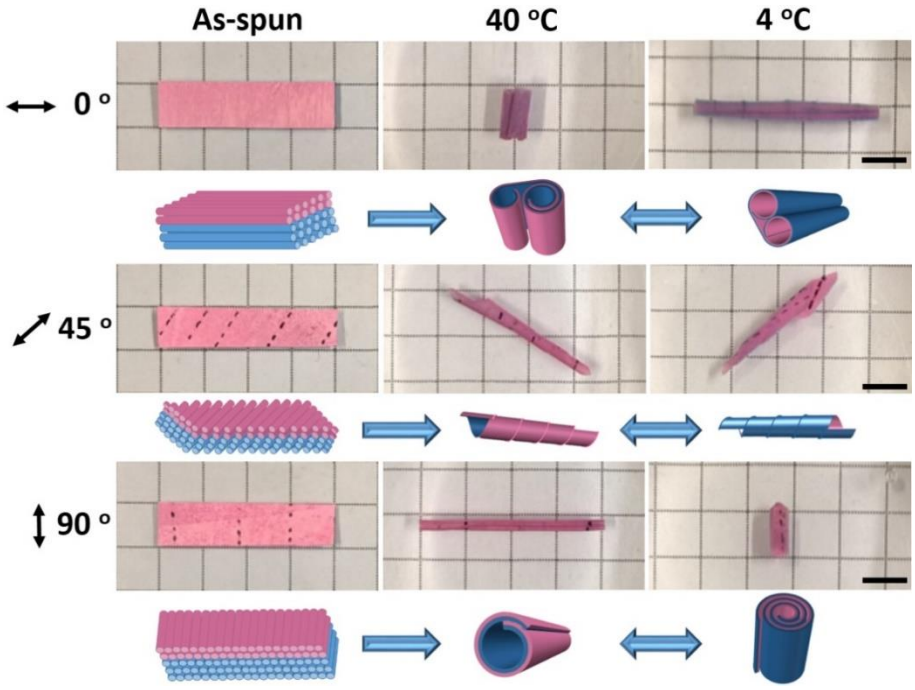

Figure 14. Fiber orientation-dependent actuation behaviour of bilayer TPU (pink)/P(NIPAM-ABP) (blue) fibrous membranes (length: 2.0 cm, width:

0.5 cm) in water at different temperatures. Black arrows show the fibre orientation direction, 0, 45 and 90^{o} are angles between the fibre direction and the long axis of the sample, as indicated by a black dotted line on the sample. Scale bar = 0.5 cm. The TPU and P(NIPAM-ABP) were dyed to get a better contrast but in real photos and movies the contrast might not be visible as P(NIPAM-ABP) becomes transparent in contact with water.

Although reversibility is considered as one of the advantages giving repeatable actuation for many cycles, in many applications, reversibility advantage is not seen as an expected process. Therefore, further efforts were put to generate novel concepts for making irreversible actuators as described in the next section.

2.2 One-component dual actuation: Only Poly(NIPAM) can actuate to stable 3D forms with reversible size change

Li Liu, Ali Ghaemi, Stephan Gekle, and Seema Agarwal*, "One-component dual actuation: Only Poly(NIPAM) can actuate to stable 3D forms with reversible size change ", Advanced Materials, 2016, 28(44), 9792-9796.

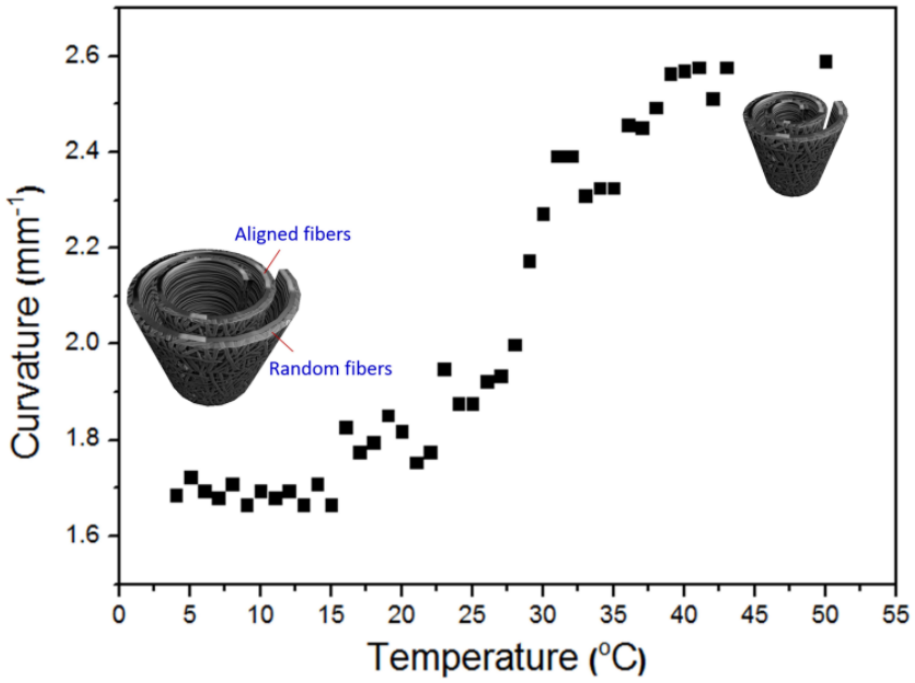

Abstract

In this work, a rare example of a one‐component dual actuator is provided, which displays irreversible change in shape by rolling on contact with water and reversible size change on changing the temperature. The actuator has a bilayer structure with aligned and randomly oriented fibers of poly(N-

isopropyl acrylamide) P(NIPAM). A combination of anisotropic E-modulus and temperature dependent swelling/shrinkage provides the dual actuation.

The anisotropy in swelling/shrinkage along cross-section required for irreversible actuation is created by electrospinning random P(NIPAM) fibrous mat and aligned P(NIPAM) fibrous mat. (**Figure 15 a**) The combined bilayer thermoresponsive actuator exhibits fast, directionally controlled and stable/irreversible actuation triggered by temperature. It is easy to get the actuator with different angles by cutting, thus achieving the directionally controlled actuation.(**Figure 15 b**) The result of numerical simulation done by group of Prof. Dr. Stephan Gekle correspond to the experiment findings.(**Figure 15 c**) No matter what angle it is, it always follows the rule that it always rolls along fiber alignment with the random layer outside. The shape of this formed tube is very stable, the size of the rolled tube can be controlled by altering temperature. (**Figure 16**)

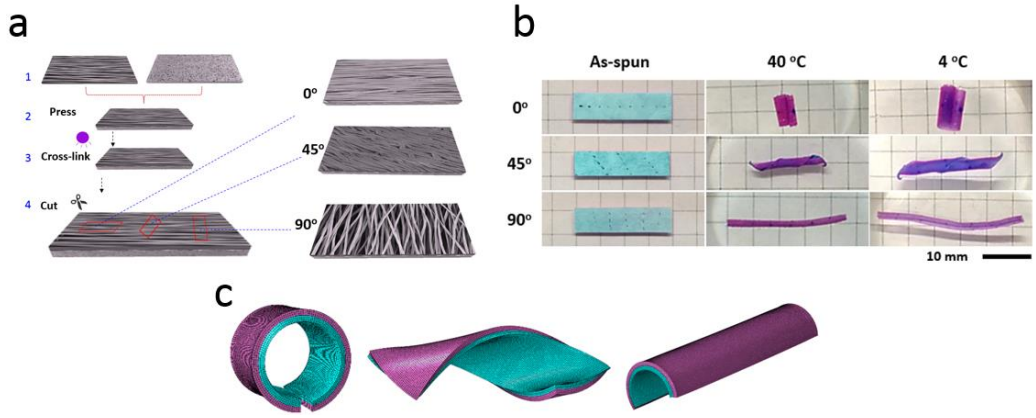

Figure 15. a) Schematic of formation of Bi-PNIPAM-0^{o}, 45^{o}, 90^{o} actuator by electrospinning of aligned layer and random layer, respectively (step 1), followed by pressing and cross-linking (steps 2 and 3). At last, the samples were cut into pieces at different angles (step 4); b) One component PNIPAM directionally controlled actuation: movement of Bi-PNIPAM-0o, 45o, 90o mat (aligned (blue)/random (pink) (length: 2.0 cm, width: 0.5 cm) with the thickness ratio (aligned / bilayer) of 0.65) in water at different temperatures. Fiber alignment direction was indicated by a black dotted line on the sample. The good color contrast by dying the aligned and random mats might be invisible due to the transparency of P(NIPAM-ABP) in water; c) Equilibrium shapes of bilayer mats obtained from finite-element simulations in 40° water. From left to right are 0°, 45°, and 90° fiber orientations. By using anisotropic expansion coefficients in combination with an anisotropic elastic modulus, good agreement with the experimental shapes in Fig. 1b is obtained. Copyright (2016), John Wiley and Sons, license number: 4342541040242.

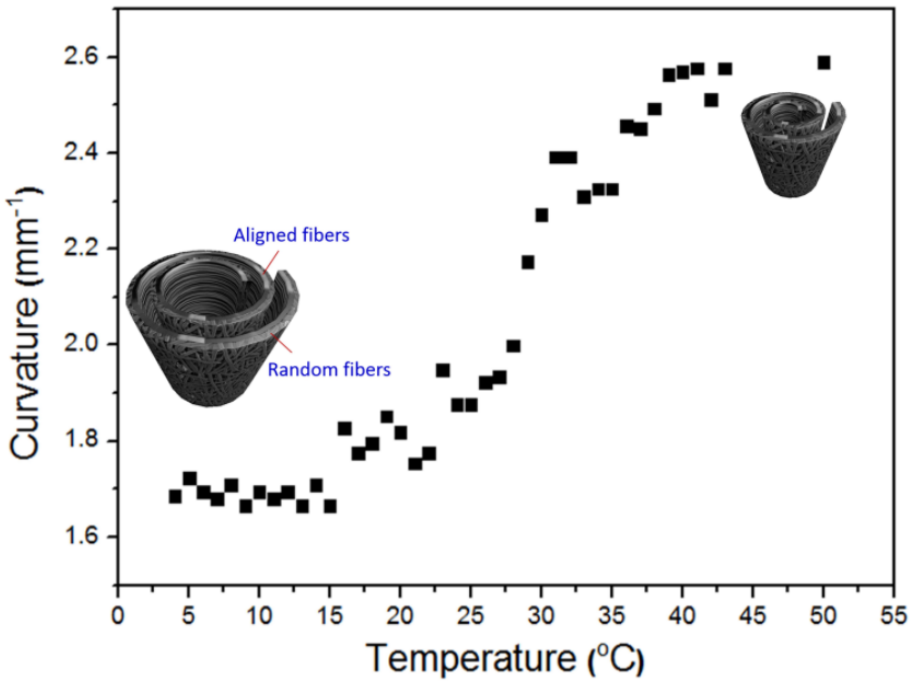

Figure 16. The effect of temperature of water on the curvature of Bi-PNIPAM-0° mat with the thickness ratio (aligned / bilayer) of 0.65. Curvature=1/r. Copyright (2016), John Wiley and Sons, license number: 4342541040242.

Furthermore, it is of interest to control actuation by multiple stimuli. Complexity of actuation be increased by use of more than one stimuli was for central question. Therefore, dual responsive polymers (pH- & thermo-responsive) was used as active system in polymeric actuator and results are described in the next section.

2.3 Composite Polymeric Membranes with Directionally Embedded Fibers for Controlled Dual Actuation

Li Liu, Hadi Bakhshi, Shaohua Jiang, Holger Schmalz and Seema Agarwal*, "Composite Polymeric Membranes with Directionally Embedded Fibers for Controlled Dual Actuation", *Macromolecular rapid communications*, 2018, 1800082.

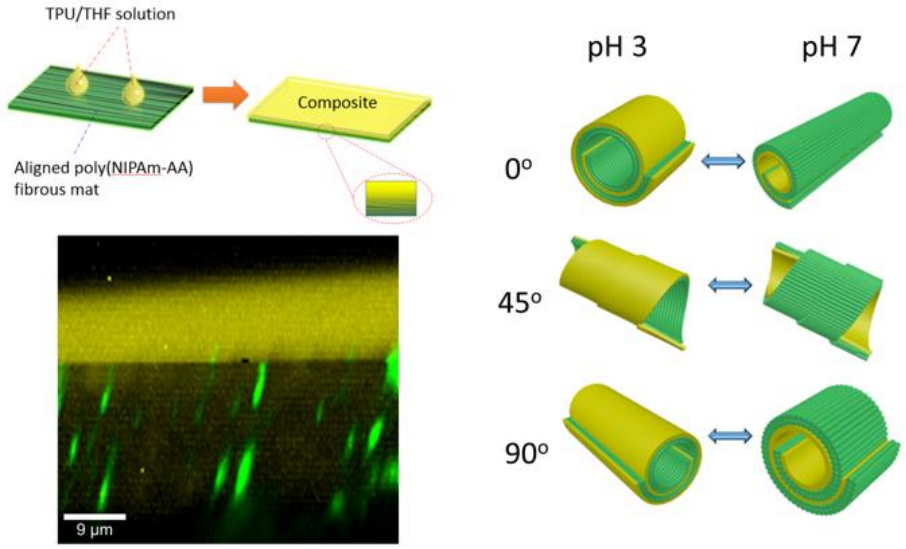

Abstract

Dual-responsive composite actuator composed of thermo- and pH-responsive poly(N-isopropylacrylamide-co-acrylic acid) (poly(NIPAm-AA)) fibers (average diameter ~ 905 nm) embedded within a passive thermoplastic polyurethane (TPU) matrix at different angles with degree of alignment as high as 98% was presented. The actuation direction were

depended on the angles between fiber alignment and long axis. The actuation and the actuated tube are independent of temperature at pH 7 and above. However, temperature can be used to control the size of the actuated tubes at lower pH. Although the polymeric actuator is only 5.8 mg, it was able to reversibly lift and release ~426 times weight of their own mass (2.47 g metal ring).

Be different from the last two works, this work is referring to dual responsive actuator. A cross-linkable dual aligned fibrous mat made of P(NIPAM-AA) was fabricated by electrospinning. After it was pressed and UV cross-linked, a composite was obtained by dropping TPU/THF dilute solution on it, as it is shown in **Figure 17 a**. Due to the penetration of TPU solution, a TPU-gradient structure of the composite membrane was formed and studied via Raman-AFM imaging (**Figure 17 b, c, d**). The image of Raman cross-section perfectly demonstrated the gradient structure and the distribution of TPU (yellow) on the underlying P(NIPAM-AA) fibrous mat (green), where the amount of TPU component obviously declined near the fibrous mat (**Figure 17 c**). By applying this simple dropping method, a composite with strong interface and repeatable thickness ratio can be obtained. The morphology of the composite membrane was examined by SEM as well. (**Figure 17 e-h**) The SEM image (**Figure 17 g**) presented a dense TPU layer with the thickness of 16 μm on a porous P(NIPAM-AA)

layer reinforced with aligned fibers with the hickness of 35 µm. A strong interface between the TPU layer and the fibrous mat could be observed from **Figure 17 h**.

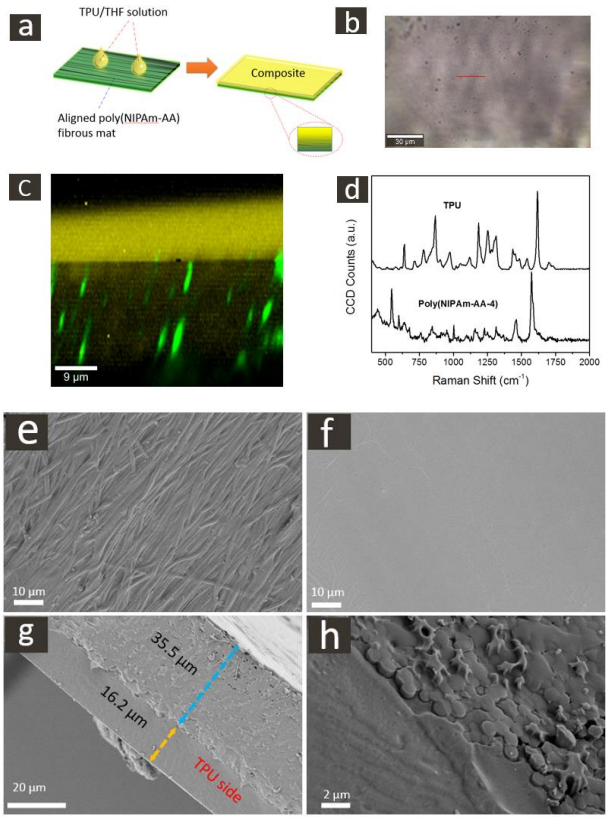

Figure 17. (a) Schematic fabrication of the composite membrane. (b-d) Raman-AFM imaging of the composite membrane; (b) optical microscope image with position of Raman cross-section (red line), (c) Raman cross-section with domains rich in TPU colored in yellow and those rich in poly(NIPAm-AA) in green and (d) Raman spectra of neat components, i.e., TPU and poly(NIPAm-AA). (e-h) SEM images of the composite membrane; (e) poly(NIPAm-AA) aligned fibrous mat side, (f) TPU side, (g) cross-section and (h) interface between aligned poly(NIPAm-AA)

fibers and TPU.

And this composite shows a dual responsive directionally actuation triggered by temperature and pH. Here it is the rule that in pH 3, it always is folding along the fiber alignment with TPU layer outside, but in pH 7 and 10, it is folding in perpendicular direction to the fiber alignment.(**Figure 18**)

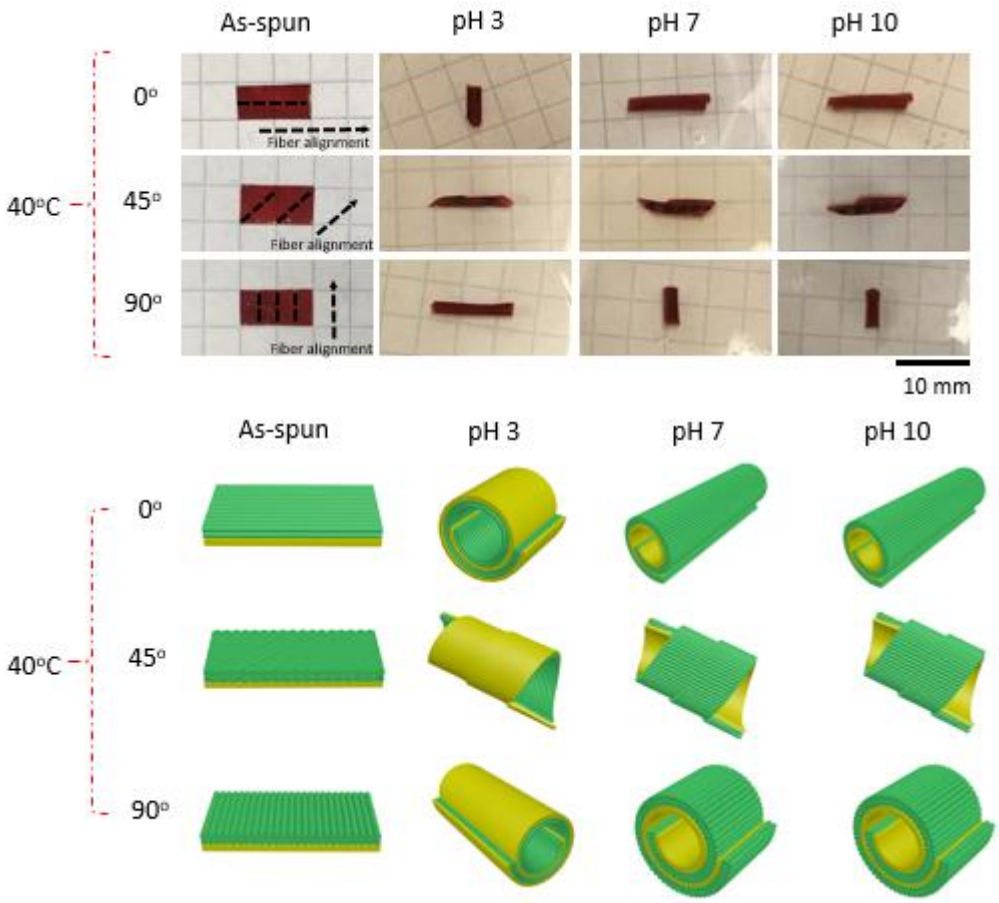

Figure 18. (a) Actuation of the composite membrane in buffer solution with different pH at 40 °C. (b) The corresponding schematics for the actuation of composite membrane at 40 °C. Poly(NIPAm-AA) is colored in

green and TPU in yellow.

2.4 Individual Contribution to Joint Publications

Publication 1: Giving direction to motion and surface with ultra-fast speed using oriented hydrogel fibers

This work has been published in *Advanced Functional Materials*, **2016**, 26(7): 1021-1027.

By **Li Liu**, Shaohua Jiang, Yue Sun, and Seema Agarwal*

I and Shaohua Jiang contributed equally to this work. Prof. Dr. Seema Agarwal, I and Shaohua Jiang designed the experiments. I performed the experiments. Yue Sun draw the actuation schematic, TOC and took part in discussion. Prof. Dr. Seema Agarwal proposed the idea, help write the paper and in charge of guidance and supervision of this work.

Publication 2: One-component dual actuation: Only Poly(NIPAM) can actuate to stable 3D forms with reversible size change

This work has been published in *Advanced Materials*, **2016**, 28(44): 9792-9796..

By **Li Liu**, Ali Ghaemi, Stephan Gekle, Seema Agarwal*

I performed the experiments which were designed by me and Prof. Dr. Seema Agarwal. Prof. Dr. Stephan Gekle and Ali Ghaemi performed the numerical simulation part. Prof. Dr. Seema Agarwal proposed the idea, and in charge of guidance and supervision of this work. All authors contributed to paper writing.

Publication 3: Composite Polymeric Membranes with Directionally Embedded Fibers for Controlled Dual Actuation

This work has been published in *Macromolecular rapid communications*, **2018**, 1800082.

By **Li Liu**, Hadi Bakhshi, Shaohua Jiang, Holger Schmalz and Seema Agarwal*

I and Hadi Bakhshi contributed equally to this work. Experiments were designed by Prof. Dr. Seema Agarwal, me and shaohua Jiang. I performed the experiments except the synthesis of dual responsive polymers which was done by Hadi Bakhshi. The Raman measurements were performed by Holger Schmalz. Prof. Dr. Seema Agarwal proposed the idea, and in charge of guidance and supervision of this work. All authors contributed to the paper writing.

3. Outlook

Currently, regarding polymeric actuators, most scientists are focusing only on the 3D transforms, such as bending, rolling and folding. However, the investigation of polymeric actuators' mechanical properties is rare. First, compared with the general mechanical robot, the advantages of polymeric actuators are few. Nonetheless, polymeric actuator with strong mechanicals could be more interesting.

Second, how strong are they ? or how much force could they generate ? According to recently published papers, this type of generated force is very small, which could limit the polymeric actuators' application.

Third, although polymeric actuators can perform 3D transforms, it could be helpful to discover how they could exhibit smarter and complex actuation behavior, thus realizing real time control as the electric mechanic robot does.

Furthermore, another important factor is that the degree of freedom a polymeric actuator can generate is too low. For example, the most common bilayer-type polymeric actuator generally realizes a transform in two directions. Could we create an actuator that can perform a controllable transform in any direction ?

In addition, more effort could be forced on the application of polymeric actuators, such as real blood vessel fabrication. This objective could propel

the polymeric actuator one significant step forward.

4. Acknowledgement

Firstly, I am deeply grateful to my supervisor Prof. Dr. Seema Agarwal for the opportunity to work in her group on this hot and interesting topic and her kindly supervision. With her great guidance and help, she brings me not only the science knowledge in this filed but also a lot of personal useful suggestions which could be great helpful in my life and work of future. I deeply appreciate her contributions during this 4 years from the depth from my heart.

Secondly, I would like to thank Prof. Dr. Andreas Greiner for his encourage and the enlightening suggestions and numerous useful comments.

Also, I want to thank Chinese Scholarship Council (CSC) for its financial supporting in this 4 years.

Thanks to Mrs. Gaby Rösner-Oliver, Mr. Niko Plocher and Ms. Annette Krökel for making administrative issue much easier.

Especial thanks to Dr. Shaohua Jiang for his so much help for discussion and suggestions about my work and my life.

To my best German friend Florian Käfer who always endures my mistakes in the lab but still kindly help me solve problems.

I received the technical support and discussion from Dr. Fangyao Liu, Matthias Burgard, Dr. Holger Schmalz, Rika Schneider, Dr. Roland Dersch, Bianca Uch, Martina Heider, Judith Schöbel, Mahsa Mafi, Dr. Mellisa Köhn-Serrano, Michael Mader, Pin Hu, Steffen Reich, Xiaojian Liao, Jian Zhu, Julia Kronawitt, Ling Peng, Martin Pretscher, Tingting Chen.

I am also grateful to my colleges for the help and good research atmosphere during these 4 years, Dr. Gaigai Duan, Yinfeng Shi, Amir Reza Bagheri, Dr. Oliver Hauenstein, Dr. Hui Wang, Amanda Pineda, Lothar Benker, Dr. Holger Pletch, Mina Heidari, Chen Liang, Tobias Moss, Simon Neumann and all the other actual and former MCII members, respectively.

Further, special thanks were given to Welcome Center and International Office of University Bayreuth, they gave me clear guideline to get familiar with environment as I came here in 2014.

Last but not least, I want to express my appreciations to my family for their support and also to my girlfriend Yue Sun who is always standing by me.

5. Appendix

5.1 Publication 1: Giving direction to motion and surface with ultra-fast speed using oriented hydrogel fibers

Li Liu, Shaohua Jiang, Yue Sun, and Seema Agarwal*, "Giving direction to motion and surface with ultra‐fast speed using oriented hydrogel fibers", *Advanced Functional Materials*, 2016, 26(7), 1021-1027.

Materials Views
www.MaterialsViews.com

ADVANCED FUNCTIONAL MATERIALS
www.afm-journal.de

FULL PAPER

Giving Direction to Motion and Surface with Ultra-Fast Speed Using Oriented Hydrogel Fibers

*Li Liu, Shaohua Jiang, Yue Sun, and Seema Agarwal**

Thermoresponsive hydrogel fibrous membranes showing directionally controlled movements and surface change with ultra-fast speed are presented for the first time. They show reversible coiling, rolling, bending, and twisting deformations in different controllable directions for many cycles (at least 50 cycles tried) with inside-out change in surfaces and shapes. Speed, reversibility, large-scale deformations and, most importantly, control over the direction of deformation is required in order to make synthetic actuators inspired from natural materials or otherwise. A polymeric synthetic material combining all these properties is still awaited. This issue is addressed and provide a very simple system fulfilling all these requirements by combining porosity and asymmetric swelling/shrinking via orientation of hydrogel fibers at different angles in a fibrous membrane. Electrospinning is used as a tool for making membranes with fibers oriented at different angles.

1. Introduction

The utility of external stimuli triggered movements of polymeric materials is undisputable in many fields of application. Speed, reversibility, large-scale deformations and, most importantly, the control over the direction of movement is desired in order to make synthetic replicas inspired from natural materials or otherwise. Although innovative concepts for polymeric actuation triggered by, for example, electrical stimulation,[1–3] light,[4–6] magnetic field,[7] pH,[8] humidity and water,[9–13] and many others[14,15] are shown covering the last few years, a polymeric synthetic actuator with control in direction of movement and reversible change in shapes at high speed is still awaited. The pioneering work of Hu et al.[16] regarding actuation based on differential swelling/shrinking of two layers triggered by water and temperature in a bilayer polymeric system remains the basis of thermoresponsive polymeric actuators, highly interesting for applications in tissue engineering, cell encapsulation, microfabrication, robotics, smart drug carrier, etc. In such actuators, poly(*N*-isopropyl acrylamide) (PNIPAM) is often used as the thermoresponsive active hydrogel layer undergoing swelling and shrinking below and above the lower critical solution temperature (LCST). The outcome is mostly reversible bending and rolling motions in the time range from many seconds to hours, depending upon the size and shape.[17,18] The instant actuation is not possible due to the use of bulk hydrogel films with slow fluid transport. Further, the bilayers change shape reversibly, mostly from flat objects to either curved (with varied degree of curvatures), circular, or bent structures, depending upon the dimensions and thickness of the two layers with hydrogel as outside layer. Control over the direction of deformation and surface side is not possible due to isotropic swelling and shrinking.

The problem of control over the direction of deformation was tackled in a work by Studart and co-workers[12] by using constrained swelling/shrinking of hydrogels in water with or without a temperature trigger. For this purpose, aluminium oxide platelets (7.5 mm diameter, 200 nm thickness) coated with superparamagnetic iron oxide nanoparticles were fixed in different orientations in hydrogel forming materials such as alginate, gelatin, and PNIPAM using a magnetic field. The presence of oriented particles restricted swelling/shrinking in the direction of reinforcement providing different deformation patterns, such as bending and twisting, but lacked fast deformations. The reversible bending and twisting took several minutes to hours. Similar movements in multistrip hydrogels with compositional gradient also took several hours.[19]

In another work, irrespective of the hydrogels, the self-assembled superparamagnetic nanoparticles were also fixed in other polymer matrix and actuation was achieved using a magnetic field. The actuator showed small-scale bending and recoiling in different directions.[7] Alignment of mesogenic units in a polymer matrix via rubbing or photoalignment also provides directional control to actuation.[20,21] Inspired by chiral seed pods, flat to helical transitions were achieved in a synthetic system by using the shrinkage of two layers in perpendicular directions. The uniaxial stretched layers along perpendicular directions cut at different angles will either bend or make helices, depending upon the orientation on the relief of strain.[22]

Porous materials with an increased rate of solvent diffusion show faster swelling in comparison to the bulk materials.[23,24]

L. Liu, Dr. S. Jiang, Y. Sun, Prof. S. Agarwal
Macromolecular Chemistry II and Bayreuth Center for Colloids and Interfaces
Universität Bayreuth
Universitätsstraße 30, 95440 Bayreuth, Germany
E-mail: agarwal@uni-bayreuth.de

DOI: 10.1002/adfm.201503612

ADVANCED FUNCTIONAL MATERIALS
www.afm-journal.de

Materials Views
www.MaterialsViews.com

High porosity was utilized in providing fast actuation to polymeric actuators with acetone, camphor sulphonic acid, ethanol, and sodium hydroxide as solvents.[2,21,25] We recently showed the fastest temperature-triggered bilayer polymeric actuators, with a thickness of more than 100 µm and planar size of 25 × 5 mm, reversibly bending and rolling to tubes in less than 1 s.[26] But a still unresolved challenge is to control the direction of movement without sacrificing instant/fast reversible large-scale actuation. We addressed the issue and in this work, present a large size temperature-triggered polymeric actuator with control in the direction of movement at ultra-fast speed, i.e., ≈0.6–5 s depending upon the type of movement. There is a complete reversal in direction of movement providing not only switch between two shapes (rolls, tubes, helices) but also between two different surfaces with temperature.

2. Results and Discussion

A fibrous bilayer system with thermoplastic polyurethane (TPU) and cross-linked PNIPAM fibers, oriented at different angles as passive and active layers, respectively, is used for directional controlled movement. The angle of fiber orientation controls the direction of movement. The bilayers are made by sequential electrospinning of TPU with a small amount of photo cross-linker (4-acryloylbenzophenone, ABP) and thermoresponsive copolymer of *N*-isopropyl acrylamide with 2 mol% of photo cross-linker acryloylbenzophenone (P(NIPAM-ABP)), followed by pressing at 300 bar for 20 min and photo cross-linking. The fibers were collected on a rotating disc (diameter 20 cm, disc rim 4 cm) at 850 rpm to obtain a parallel alignment of fibers. The alignment degree was ≈95% for P(NIPAM-ABP) and ≈82% for TPU (**Figure 1**), and porosity was about 56%. The aligned fibers did not show any molecular orientation as seen by polarized FT-IR (Figure S1, Supporting Information). The average fiber diameters of TPU and P(NIPAM-ABP) were 501 ± 149 and 1368 ± 185 nm, respectively. The bilayers were cut at different angles (0°-fibers oriented parallel to the long axis; 90°-fibers oriented perpendicular to the long axis; 45°-fibers oriented 45° to the long axis) to get a varied orientation of P(NIPAM-ABP) fibers with respect to the long axis of the sample (**Scheme 1**) for controlling the direction of actuation.

Pure TPU fibrous membrane with oriented fibers did not show any change in dimensions in water at different temperatures (Figure S2, Supporting Information) and acted as a passive layer in the present bilayer membrane system. By contrast, the P(NIPAM-ABP) fiber mat with oriented fibers shows reversible anisotropic swelling/shrinking in water with respect to the dry as-spun fibrous membrane with changes in temperature (**Figure 2**). The degree of anisotropic swelling/shrinking is dependent upon the angle of orientation of the P(NIPAM-ABP) fibers with respect to the long axis of the sample and made basis of directionally controlled movement. The as-spun fiber mat (length (L) × width (W) × thickness (t): 2.0 cm × 0.5 cm × 46 µm) with P(NIPAM-ABP) fibers aligned parallel to each other in the direction of the long axis (0° orientation) in water at 40 °C (above LCST; the LCST of P(NIPAM-ABP) fiber mat is 27 °C as measured by micro-DSC (differential scanning calorimetry) (Figure S3, Supporting Information); it is taken as the peak temperature in micro-DSC heat flow curve) showed a shrinkage in length by about 35%, but an increase in the width and thickness by 15% and 41%, respectively, in comparison to the dry state (**Table 1**). No change in dimensions is expected for hydrogel bulk films at 40 °C in comparison to the dry film. The

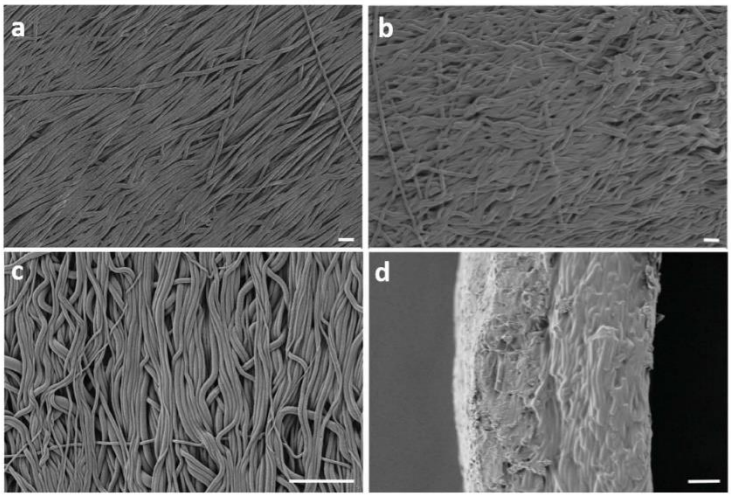

Figure 1. SEM images of a) P(NIPAM-ABP) side—as spun bilayer membrane, b) P(NIPAM-ABP) side—after treatment with hot water, c) TPU side—as spun bilayer membrane, and d) the cross section of the bilayer sample in water at 40 °C after drying shows a strong interface between TPU (left side) and P(NIPAM-ABP) (right side). Scale bar = 10 µm.

Materials Views
www.MaterialsViews.com

ADVANCED FUNCTIONAL MATERIALS
www.afm-journal.de

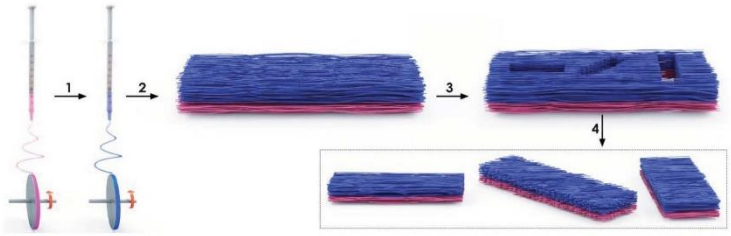

Scheme 1. Schematic showing the formation of bilayer actuators by sequential electrospinning of TPU and P(NIPAM-ABP) followed by UV cross-linking (steps 1 and 2). The samples were cut at different angles to get varied orientations of thermoresponsive P(NIPAM-ABP) fibers (steps 3 and 4). The TPU and P(NIPAM-ABP) solutions were mixed with rhodamine B (RB) and methylene blue, respectively, to observe the actuation phenomenon optically better.

significant shrinkage in the direction of fiber orientation on putting the fiber mat in water at 40 °C is due to the relaxation of the electrospun fibers to the lower energy coiled conformation (Figure 1). During fiber formation, the electrospun fibers are deposited in the stretched state due to very fast evaporation of solvent. This is a very well-known fact and this behavior is similar to the solvent-triggered shape-memory polymers and temperature-driven contraction of electrospun fibers.[2,27,28] Also, the oriented fibers are present in a layer-by-layer structure with many contact points between the fibers. The shrinkage in the direction of fiber orientation together with expulsion of water between the fibers lead to the slight expansion in the direction perpendicular to the fiber orientation.

In dropping from 40 to 4 °C, the same mat in water below LCST is expected to be hydrophilically swollen in all directions. In fact, symmetric swelling in planar dimensions (length and width) was observed at 4 °C. The fiber mat showed about 38% expansion in length and width in comparison to the fiber mat at 40 °C. If we compare the expanded dimensions at 4 °C to the as-spun fiber mat, the swelling is anisotropic. The increase in width was 58%, whereas the length reduced by about 9% in comparison to as-spun fibers. In brief, in going from the as-spun bilayer mat to the wet states, the shrinkage in length (direction of fiber orientation) dominates the increase in width above LCST, whereas expansion in width (perpendicular to the direction of fiber orientation) dominates the shrinkage in the length below LCST. The increase in thickness above and below LCST was 41% and 326%, respectively.

The trend is just the opposite for P(NIPAM-ABP) membrane with fibers oriented perpendicular to the long axis of the sample (fiber orientation 90°). The membrane shrinks more in the width (direction of fibers) at 40 °C, whereas it swells more in the perpendicular direction at 4 °C (Table 1, Figure 2).

The change in dimensions of a P(NIPAM-ABP) fibrous mat with fibers aligned at different angles in water at different temperatures was reflected in directionally controlled movement of a

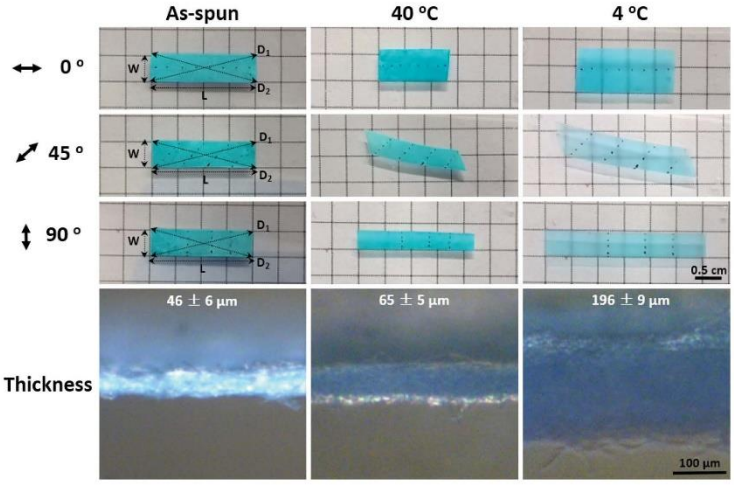

Figure 2. Size change of cross-linked P(NIPAM-ABP) fibrous membrane (original size: 2.0 cm × 0.5 cm × 46 µm) in water at different temperatures.

ADVANCED FUNCTIONAL MATERIALS
www.afm-journal.de
www.MaterialsViews.com

Table 1. Size change of pure P(NIPAM-ABP) fibrous membranes with fibers oriented at different angles (0°, 45°, and 90°) to the direction of the long axis of the sample in water at different temperatures (40 and 4 °C). *L*: length; *W*: width; D_1 and D_2: diagonal lengths.

	0°			45°			90°		
	As-spun	40 °C	4 °C	As-spun	40 °C	4 °C	As-spun	40 °C	4 °C
L [cm]	2.041	1.332	1.845	2.028	1.858	2.535	1.979	2.308	3.015
W [cm]	0.534	0.612	0.845	0.521	0.446	0.624	0.521	0.340	0.485
D_1 [cm]	2.090	1.461	2.049	2.084	1.656	2.321	2.067	2.341	3.221
D_2 [cm]	2.083	1.402	2.010	2.103	2.078	2.971	2.066	2.356	3.248

bilayer membrane with TPU. The thickness of the P(NIPAM-ABP) and TPU layers were 53 ± 9 µm and 18 ± 3 µm (Figure S4, Supporting Information), respectively, in bilayer membrane. TPU is used as a representative example for passive layer. It would also work with other hydrophobic polymers. At 40 °C (temperature above LCST), the P(NIPAM-ABP) layer with parallel orientation (0°) of fibers in the bilayer membrane shrinks in the direction of fiber orientation and, therefore, rolls sideways along the direction of fiber orientation with P(NIPAM-ABP) making inside surface of the rolls (**Figure 3**). On transferring the sample to water at 4 °C (below LCST), a directional change with opening of the rolls followed by re-rolling in the direction perpendicular to the fiber orientation with the P(NIPAM-ABP) layer now making the outside surface was observed. The rolling-re-rolling was reversible for many cycles without showing any sign of delamination. The bilayer interface as observed from the cross section of the sample is shown in Figure 1D. The actuation was ultra-fast, took ≈0.6 s from 4 to 40 °C, whereas the reversal of the process took ≈1.4 s (**Figure 4**, Movie S1, Supporting Information). Further experiments were carried out to study the actuation behavior at temperatures other than 40 and 4 °C. The bilayers showed sideways rolling along the direction of fiber orientation with P(NIPAM-ABP) making inside surface of the rolls at temperatures 25 °C and above. At 25 °C, the time required for rolling was about 15 s, whereas at temperatures 27 °C and above the process was very fast with complete rolling in less than 2 s (Figure S5, Supporting Information). The heat flow versus temperature transition in micro-DSC for P(NIPAM-ABP) was broad starting from 19 °C and the peak temperature (27 °C) was considered as LCST (Figure S3, Supporting Information). The opening of rolls followed by re-rolling in the direction perpendicular to the fiber orientation was possible at all temperatures below 19 °C. At temperature between 19 and 25 °C, the rolls simply open up but do not re-roll in another direction. The bilayer fibrous mat in hot water (above 27 °C) could lift ≈13.4 times mass of its own weight (55 mg was lifted by a bilayer membrane of 4.11 mg) (Figure S6, Supporting Information).

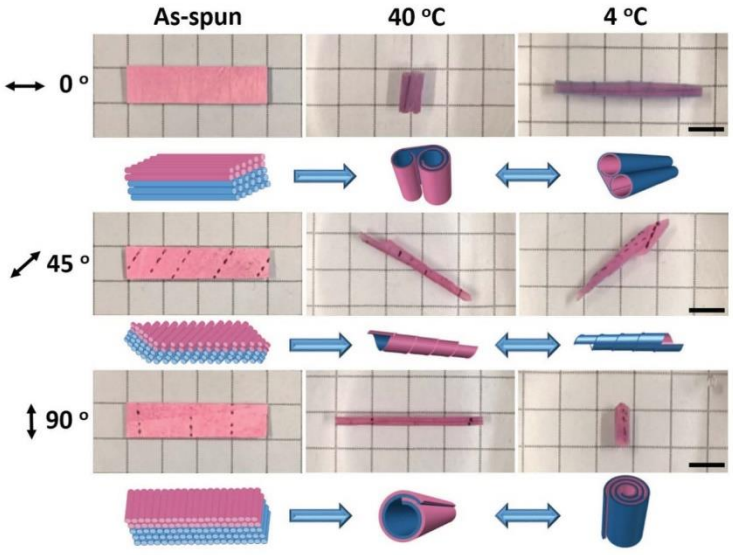

Figure 3. Fiber orientation-dependent actuation behavior of bilayer TPU (pink)/P(NIPAM-ABP) blue) fibrous membranes (length: 2.0 cm, width: 0.5 cm) in water at different temperatures. Black arrows show the fiber orientation direction, 0°, 45°, and 90° are angles between the fiber direction and the long axis of the sample, as indicated by a black dotted line on the sample. Scale bar = 0.5 cm. The TPU and P(NIPAM-ABP) were dyed to get a better contrast but in real photos and movies the contrast might not be visible as P(NIPAM-ABP) becomes transparent in contact with water.

Materials Views
www.MaterialsViews.com

ADVANCED FUNCTIONAL MATERIALS
www.afm-journal.de

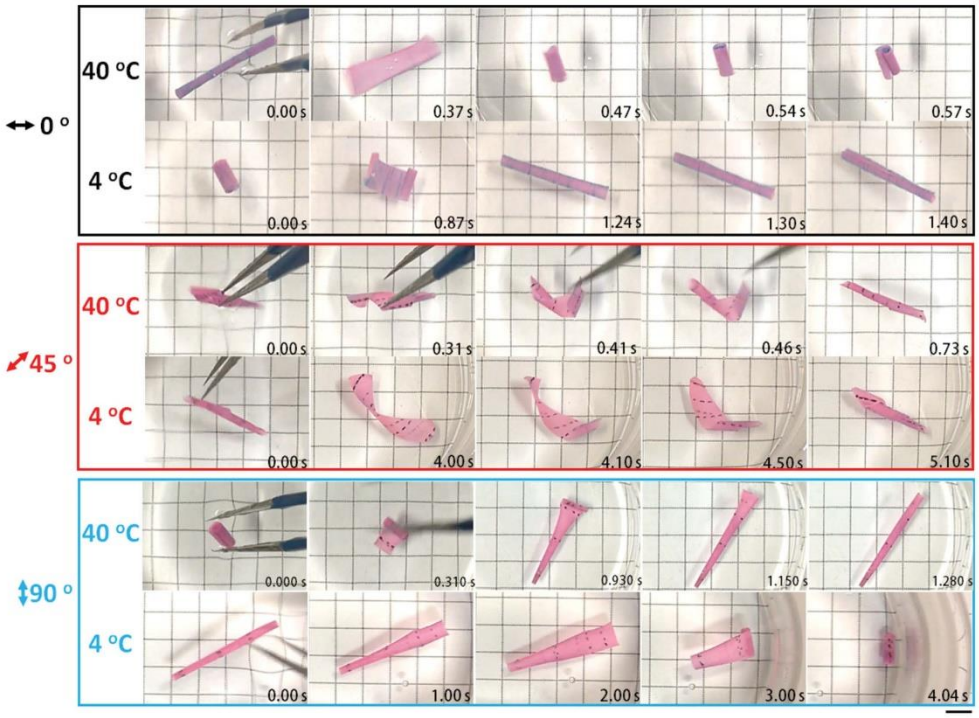

Figure 4. Actuation time of the bilayer TPU/P(NIPAM-ABP) fibrous membrane with different orientations of fibers at 0°, 45°, and 90° with respect to the long axis of the sample (original length: 2.0 cm, width: 0.5 cm) in water at 40 and 4 °C, respectively. Scale bar = 0.5 cm.

When fibers were oriented at 90° (perpendicular to the long axis), similar control over direction, shape, and surface was observed. The difference was the sideways rolling (perpendicular to the direction of fiber orientation) at 4 °C with the P(NIPAM-ABP) layer on the outside (actuation time ≈4.0 s) and rolling along the direction of fibers at 40 °C with P(NIPAM-ABP) layer inside (actuation time ≈1.3 s) (Figures 3 and 4, Movie S2, Supporting Information).

The P(NIPAM-ABP) mat with fibers oriented at 45° with respect to the long axis showed shrinkage along the fiber directions at 40 °C reflecting a very significant reduction in diagonal length D_1 in comparison to D_2 (Figure 2, Table 1). At 4 °C, the swelling took place in all directions almost symmetrically if we consider dimensions, in comparison to that of the sample at 40 °C. In comparison to the as-spun dry fiber, the swelling was asymmetrical, with more swelling in diagonal direction D_2. Asymmetrical swelling and shrinkage was reflected in the twisting of the bilayer membrane with direction control. At 40 °C, the twisting followed shrinking parallel to the fiber orientation with right-handed twists leading to a tubular structure with P(NIPAM-ABP) as the inside layer. Whereas at 4 °C, swelling in a perpendicular direction led to the opening of the right-handed helix followed by rolling diagonally in the direction perpendicular to the fiber orientation giving a helically rolled tubular structure, with P(NIPAM-ABP) as the outside layer. The complete inversion of the tube (inside out) took place in ≈0.7 s at 40 °C and ≈5 s at 4 °C (Figure 4, Movie S3, Supporting Information).

Furthermore, fast actuation with similar directional control is possible for samples of different sizes as shown in **Figure 5**. The bigger sample requires more time for mass transport and therefore an increase in the time of actuation. Also, the curvature and the number of turns in a tubular coil can be controlled by changing the thickness ratio of the two layers. A thickness ratio (P(NIPAM-ABP):TPU) of 0.4 (sample size: 20 mm × 5 mm) for a sample with parallel arrangement of fibers (0° alignment) is not sufficient for making rolls/coils (**Figure 6**). The sample simply bended. The complete rolling took place at P(NIPAM-ABP):TPU thickness ratio ≈1.0. On increasing the thickness ratio, the coiling took place with increase in number of turns and curvature. Moreover, complex shapes can also be made by simply cutting the bilayer membranes into different patterns. As an example, one of the shapes provided a synthetic analogue of a Venus fly trap, mimicking only its movement pattern and actuation time in our case even with water vapors (Movie S4, Supporting Information).

ADVANCED FUNCTIONAL MATERIALS
www.afm-journal.de
Materials Views
www.MaterialsViews.com

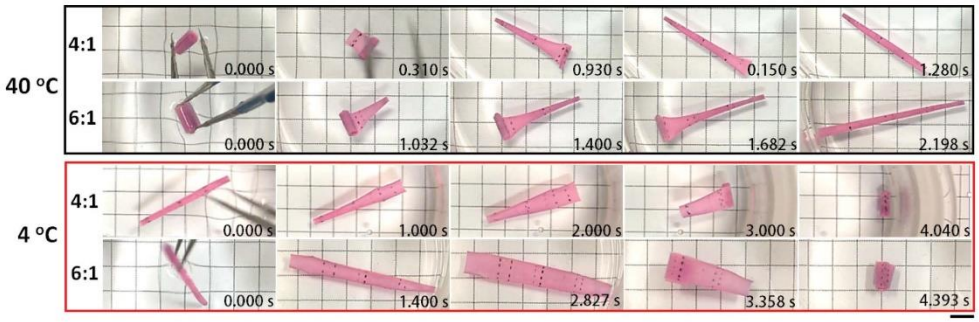

Figure 5. Size-dependent actuation of the bilayered TPU/P(NIPAM-ABP) fibrous membrane (fibers are oriented at 90° with respect to the direction of long axis of the sample) (original size: length: 2.0 cm, width: 0.5 cm and length: 3.0 cm, width: 0.5 cm) in water at 40 and 4 °C, respectively. Scale bar = 0.5 cm.

3. Conclusion

In conclusion, we show the first ever large size thermoresponsive polymeric actuator with directionally controlled reversible movements with very high speed. The movements led to the formation of tubes, coils, and helices, reversibly changing their shapes and surface sides with temperature. The inherent porosity, deposition of electrospun fibers in stretched state, and alignment in a simple way by collecting fibers on a rotating wheel provided the desired all-in-one actuators. Based on this concept, the appropriate combination of materials in bilayers can also provide polymeric actuators triggered by other stimuli in the future. The method is simple, versatile, and suitable for making large samples.

4. Experimental Section

Materials: Cross-linkable PNIPAM (M_n = 12 × 10^4 g mol^{-1}, M_w = 41 × 10^4 g mol^{-1}) was made by free-radical copolymerization of NIPAM and photo cross-linker ABP, designated as (P(NIPAM-ABP) according to the previous report.[26] TPU (Desmopann DP 2590, Bayer Materials Science, M_n = 8.89 × 10^4 g mol^{-1}, M_w = 14.5 × 10^4 g mol^{-1}) and *N,N'*-dimethylformamide (DMF, 99.8%, Aldrich) were used as received.

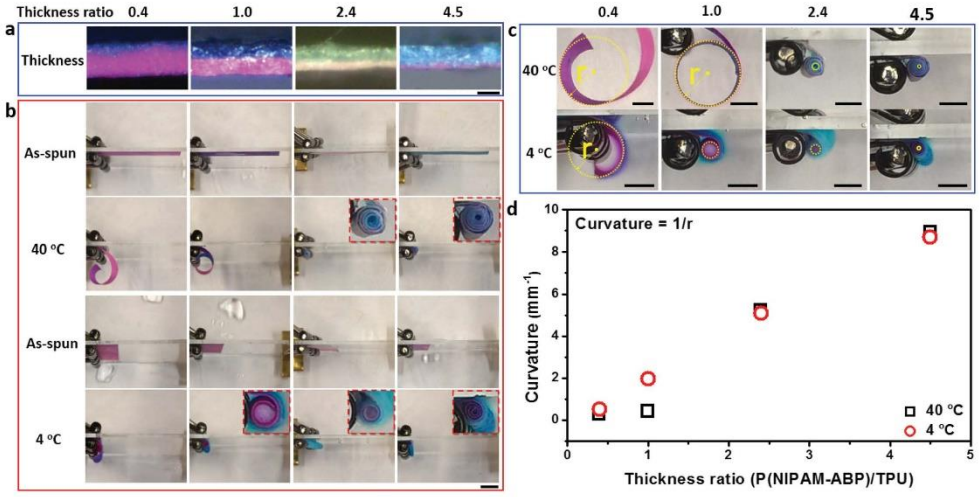

Figure 6. Thickness ratio (PNIPAM-ABP/TPU) dependent bending of 0°-bilayered TPU/P(NIPAM-ABP) fiber mats (20 mm × 5 mm). a) Cross section of samples with different thickness ratio (pink side is TPU; scale bar = 50 μm); b) in water at different temperatures (scale bar = 5 mm); c) determination of radius (*r*) (scale bar = 2 mm); and d) plot of curvature against thickness ratio of P(NIPAM-ABP)/TPU. The curvature is taken as 1/*r*. The bended arch is assumed as an imaginary circle for the determination of *r* and for coils the radius of the inner most circle is taken for comparison purpose.

www.MaterialsViews.com

ADVANCED FUNCTIONAL MATERIALS
www.afm-journal.de

Preparation of Fibrous Membranes: The pure TPU, P(NIPAM-ABP), and bilayer fibrous membranes were prepared by electrospinning of the corresponding polymers from DMF. The spinning conditions are given in Table S1 (Supporting Information). The TPU spinning solution had 4 wt% of UV cross-linker ABP, with respect to the weight of TPU, to cross-link the two layers at the interface in bilayer membranes. An amount of 0.4 wt% of Rhodamine B (RB) and methylene blue (MB), with respect to the weight of the corresponding polymer, were added to the TPU and P(NIPAM-ABP) solutions, respectively, to obtain color contrast in the bilayer. A rotating disc (diameter 20 cm, disc rim 4 cm) with a rotation speed of 850 rpm was used as a collector and provided parallel-aligned fibers. The bilayer TPU/P(NIPAM-ABP) aligned-fiber mat was made by sequential spinning of the two polymer solutions, i.e., first, pure TPU was spun, followed by the spinning of P(NIPAM-ABP). Subsequently, the bilayer nanofiber mats were pressed at 300 bar for 20 min at room temperature and cross-linked by UV light (Honle UVAHAND 250 GS) for 4 h for each side.

Characterization: A scanning electron microscope (SEM) (Zeiss Leo 1530) was used to observe the morphology and diameter of fibers (Image J software). Before scanning, 3.0 nm of platinum (Pt) coating was applied to increase the conductivity of the samples. All the photos of the actuation process were captured by Video Remaker software from the corresponding videos. Micro-DSC was measured on a Setaram Micro-DSC III at a heating/cooling rate of 0.25 °C min^{-1}. The molecular weight of P(NIPAM-ABP) was determined by gel permeation chromatography using DMF as the eluent at a flow rate of 0.5 mL min^{-1} at 25 °C.

The degree of fiber alignment (d_{Fa}) was calculated according to the previous literature using the following equation[29]

$$d_{Fa} = \frac{3\cos^2\theta - 1}{2} \quad (1)$$

where θ is the angle the individual fiber forms with the preferred direction controlled by the rotating collector. The values given are an average of a minimum of 100 fibers.

The porosity (P) of the electrospun nanofiber mat was calculated using Equations (2)–(4)

$$\rho_{mat} = \frac{\text{mass}_{mat}}{\text{area}_{mat} \times \text{thickness}_{mat}} \quad (2)$$

$$\rho_{film} = \frac{\text{mass}_{film}}{\text{area}_{film} \times \text{thickness}_{film}} \quad (3)$$

$$P = \left(1 - \frac{\rho_{mat}}{\rho_{film}}\right) \times 100\% \quad (4)$$

where ρ_{mat} and ρ_{film} are the density of the pressed UV cross-linked P(NIAPM-ABP) electrospun fibrous membrane (mat) and film, respectively.

Supporting Information

Supporting Information is available from the Wiley Online Library or from the author.

Acknowledgements

L.L. and S.J. contributed equally to this work. The authors would like to acknowledge financial support from Deutsche Forschungsgemeinschaft (DFG). The work was carried out in the frame of SFB 840. L.L. thanks China Scholarship Council for awarding fellowship for carrying out Ph.D. in Germany in the lab of Prof. Seema Agarwal.

Received: August 26, 2015
Revised: November 8, 2015
Published online: December 28, 2015

[1] Y. Osada, H. Okuzaki, H. Hori, *Nature* **1992**, *355*, 242.
[2] Q. Zhao, J. W. C. Dunlop, X. Qiu, F. Huang, Z. Zhang, J. Heyda, J. Dzubiella, M. Antonietti, J. Yuan, *Nat. Commun.* **2014**, *5*, 4293.
[3] S. Taccola, F. Greco, E. Sinibaldi, A. Mondini, B. Mazzolai, V. Mattoli, *Adv. Mater.* **2015**, *27*, 1668.
[4] S. Iamsaard, S. J. Aßhoff, B. Matt, T. Kudernac, J. J. L. M. Cornelissen, S. P. Fletcher, N. Katsonis, *Nat. Chem.* **2014**, *6*, 229.
[5] X. Zhang, Z. Yu, C. Wang, D. Zarrouk, J.-W. T. Seo, J. C. Cheng, A. D. Buchan, K. Takei, Y. Zhao, J. W. Ager, J. Zhang, M. Hettick, M. C. Hersam, A. P. Pisano, R. S. Fearing, A. Javey, *Nat. Commun.* **2014**, *5*, 2983.
[6] H. Yu, T Ikeda, *Adv. Mater.* **2011**, *23*, 2149.
[7] J. Kim, S. E. Chung, S.-E. Choi, H. Lee, J. Kim, S. Kwon, *Nat. Mater.* **2011**, *10*, 747.
[8] S. J. Kim, M. S. Kim, S. I. Kim, G. M. Spinks, B. C. Kim, G. G. Wallace, *Chem. Mater.* **2006**, *18*, 5805.
[9] K. Zhang, A. Geissler, M. Standhardt, S. Mehlhase, M. Gallei, L. Chen, C. M. Thiele, *Sci. Rep.* **2015**, *5*, 11011.
[10] M. Ma, L. Guo, D. G. Anderson, R. Langer, *Science* **2013**, *339*, 186.
[11] A. Sidorenko, T. Krupenkin, A. Taylor, P. Fratzl, J. Aizenberg, *Science* **2007**, *315*, 487.
[12] R. M. Erb, J. S. Sander, R. Grisch, A. R. Studart, *Nat. Commun.* **2013**, *4*, 1712.
[13] F. Liu, S. Jiang, L. Ionov, S. Agarwal, *Polym. Chem.* **2015**, *6*, 2769.
[14] E. T. Roche, R. Wohlfarth, J. T. B. Overvelde, N. V. Vasilyev, F. A. Pigula, D. J. Mooney, K. Bertoldi, C. J. A Walsh, *Adv. Mater.* **2014**, *26*, 1200.
[15] C. Ohm, M. Brehmer, R. Zentel, *Adv. Mater.* **2010**, *22*, 3366.
[16] Z. Hu, X. Zhang, Y. Li, *Science* **1995**, *269*, 525.
[17] L. Ionov, *e-Polymers* **2014**, *14*, 109.
[18] G. Stoychev, S. Turcaud, J. W. C. Dunlop, L. Ionov, *Adv. Funct. Mater.* **2013**, *23*, 2295.
[19] Z. L. Wu, M. Moshe, J. Greener, H. Therien-Aubin, Z. Nie, E. Sharon, E. Kumacheva, *Nat. Commun.* **2013**, *4*, 1586.
[20] L. T. de Haan, C. Sánchez-Somolinos, C. M. W. Bastiaansen, A. P. H. J. Schenning, D. J. Broer, *Angew. Chem., Int. Ed.* **2012**, *51*, 12469.
[21] W. E. Lee, Y. J. Jin, L. S. Park, G. Kwak, *Adv. Mater.* **2012**, *24*, 5604.
[22] S. Armon, E. Efrati, R. Kupferman, E. Sharon, *Science* **2011**, *333*, 1726.
[23] D. Kuckling, J. Hoffmann, M. Plötner, D. Ferse, K. Kretschmer, H.-J. P. Adler, K.-F. Arndt, R. Reichelt, *Polymer* **2003**, *44*, 4455.
[24] L.-W. Xia, R. Xie, X.-J. Ju, W. Wang, Q. Chen, L.-Y. Chu, *Nat. Commun.* **2013**, *4*, 2226.
[25] C. O. Baker, B. Shedd, P. C. Innis, P. G. Whitten, G. M. Spinks, G. G. Wallace, R. B. Kaner, *Adv. Mater.* **2008**, *20*, 155.
[26] S. Jiang, F. Liu, A. Lerch, L. Ionov, S. Agarwal, *Adv. Mater.* **2015**, *27*, 4865.
[27] C. Azra, D. Alhazov, E. Zussman, *Polymer* **2015**, *58*, 162.
[28] R. Xiao, J. Guo, D. L. Safranski, T. D. Nguyen, *Soft Matter* **2015**, *11*, 3977.
[29] R. Dersch, T. Liu, A. K. Schaper, A. Greiner, J. H. Wendorff, *J. Polym. Sci., Part A: Polym. Chem.* **2003**, *41*, 545.

ADVANCED FUNCTIONAL MATERIALS

Supporting Information

for *Adv. Funct. Mater.*, DOI: 10.1002/adfm.201503612

Giving Direction to Motion and Surface with Ultra-Fast Speed Using Oriented Hydrogel Fibers

*Li Liu, Shaohua Jiang, Yue Sun, and Seema Agarwal**

WILEY-VCH

Supporting Information

Giving direction to motion and surface with ultra-fast speed using oriented hydrogel fibers

Li Liu[1], Shaohua Jiang[1], Yue Sun, and Seema Agarwal[*]

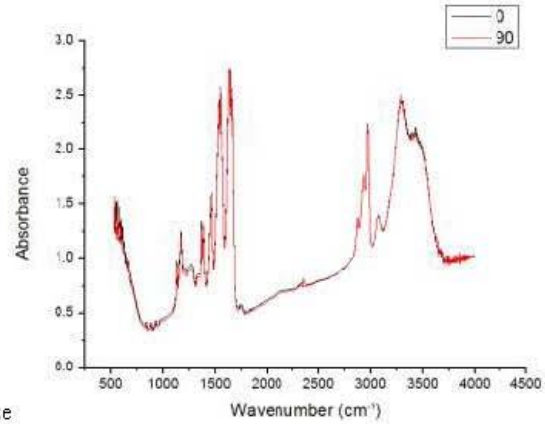

Figure S1. Polarized mat. Note: 0 and 90 are the angles between fiber alignment and light.

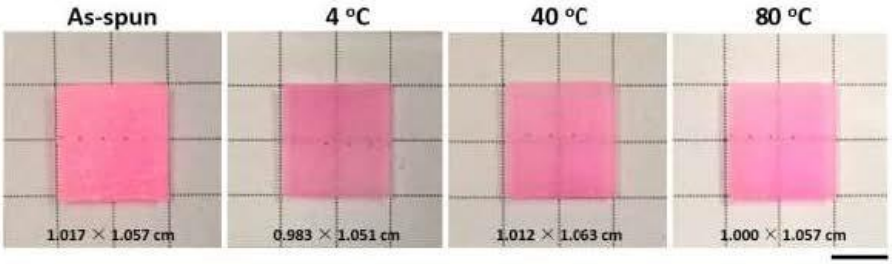

Figure S2. TPU fibrous membrane does not show appreciable size change in water at different temperatures (original size: ~ 1.0 cm × 1.0 cm). Scale bar = 0.5 cm.

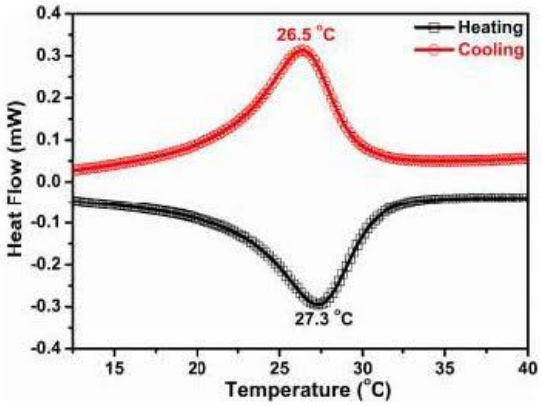

Figure S3. Micro-DSC measurement of cross-linked P(NIPAM-ABP) fibrous membrane showing LCST around 27 °C.

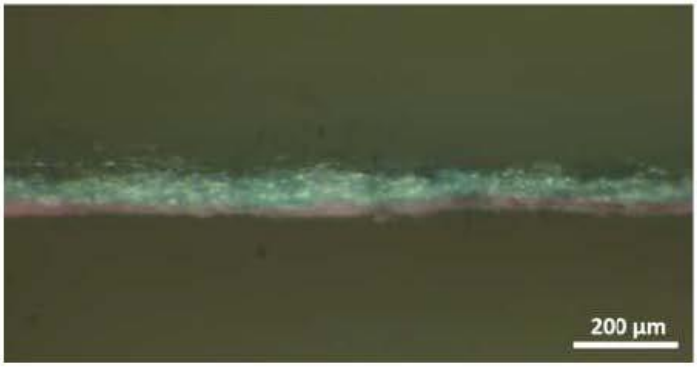

Figure S4. Digital microscope picture of the bilayered TPU/P(NIPAM-ABP) fibrous membrane. The thickness of PNIPAM layer is 53 ± 9 µm and of TPU is 18 ± 3 µm.

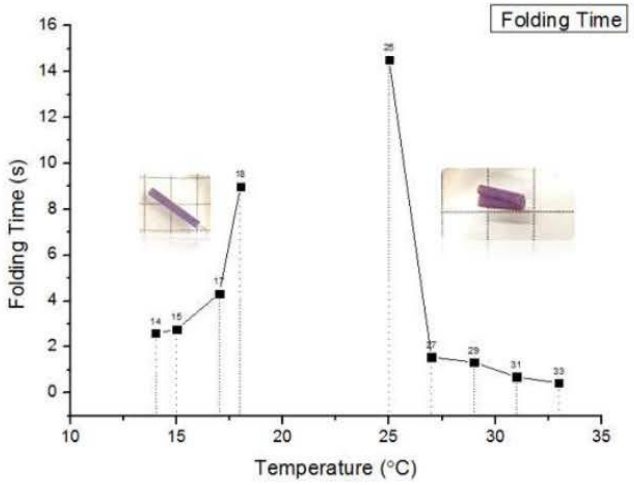

Figure S5. Effect of water temperature on folding time (0° sample; original size: length: 2.0 cm, width: 0.5 cm).

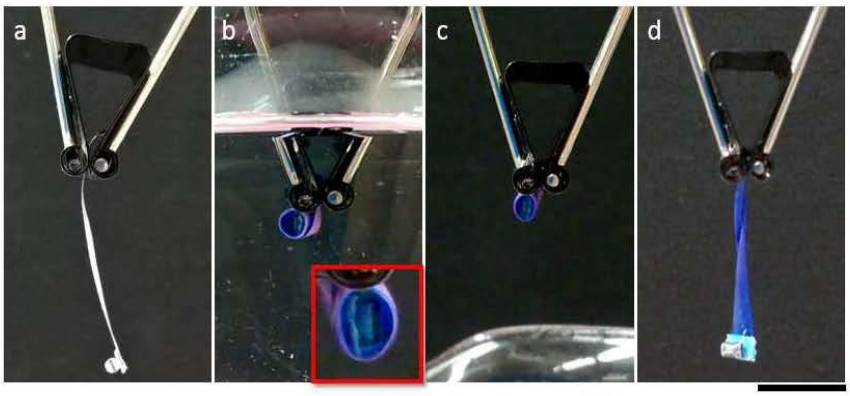

Figure S6. Lifting of weight by fibrous bilayer membrane (sample 0°) a) bilayer sample (4.11 mg) in air with a weight of 55 mg glued at its one end, b) the sample rolled with attached weight in water at 40°C, c) rolled sample in air at room temperature (22°C), d) rolled sample de-rolls in 136s. Scale bar = 8 mm.

Table S1. The electrospinning parameters used for making fibrous membranes. DMF was used as solvent.

	Solution concentration (wt%)	Voltage (kV)	Flowrate (ml/h)	Spinning volume (ml)	Needle diameter (mm)	Collecting distance (cm)
P(NIPAM-ABP)	40	18	1.3	2	0.6	20
TPU	25	18	1.3	4	0.6	20

Movies 1-4 showing membrane movements.

5.2 Publication 2: One-component dual actuation: Only Poly(NIPAM) can actuate to stable 3D forms with reversible size change

Li Liu, Ali Ghaemi, Stephan Gekle, and Seema Agarwal*, " One-component dual actuation: Only Poly(NIPAM) can actuate to stable 3D forms with reversible size change ", *Advanced Materials*, 2016, 28(44), 9792-9796.

Materials Views
www.MaterialsViews.com

ADVANCED MATERIALS
www.advmat.de

COMMUNICATION

One-Component Dual Actuation: Poly(NIPAM) Can Actuate to Stable 3D Forms with Reversible Size Change

*Li Liu, Ali Ghaemi, Stephan Gekle, and Seema Agarwal**

In the last several years, artificial polymeric bilayer architectures inspired from nature have been used for light, temperature, moisture, or electric- and magnetic-field-triggered reversible twisting, bending, and curling motions.[1–15] One of these most studied bilayer systems makes use of thermoresponsive hydrogels as an active layer, undergoing temperature dependent swelling/shrinking in water/humid air in combination with a hydrophobic (passive) polymer inert layer, leading to shape change.[16–22] Fast actuation, large deformations, reversibility, direction control maintaining low cost, and simple procedures of production of thermoresponsive bilayer actuators have already been achieved in one way or the other as evidenced from the literature.[21–23] A piece of paper, though only one component, also curls or bends on a water surface due to the differential swelling across the paper thickness. The curvature increases with time to a maximum and then flattens as the sheet becomes completely wet.[24] Artificial one component thermo-/hydro-responsive actuation is a rare phenomenon as special procedures are required for creating structural anisotropy. In one of the studies, which in real sense is not one component, the anisotropy was generated by orientation of stiff inorganic particles within the swellable/shrinkable polymer hydrogel or thermoresponsive gel along the layer thickness using a weak external magnetic field. The hydrogels reversibly changed shape in accordance to the orientation of the particles.[25] A graphene paper with a gradient of reduced graphene oxide (hydrophobic)/graphene oxide (hydrophilic) showed reversible deformations with moisture and heat due to water driven differential expansion/contraction.[26] The gradient along the thickness can also be achieved by differential molar mass of the base polymer or cross-link density.[27,28] A gradient along the thickness in a poly (*N*-isopropyl acrylamide) (poly(NIPAM)) film was created by concentrating silica particles on one side of the film by electrophoresis followed by photo-polymerization. The cross-linked poly(NIPAM) gel in water bent at 40 °C with the silica side outside. The removal of silica particles can provide gradient porous poly(NIPAM) gel bending in opposite direction.[29]

Reversibility in actuation is seen as one of the advantages providing performance for many cycles. The majority of thermoresponsive actuators are reversible showing opening and closing of tubes, curls, inversion of surfaces (inside-out) with change in temperature. For many applications, such as externally triggered formation of 2D and 3D scaffolds, reversibility of actuation is not desired as a slight change in temperature would reverse the process destroying the scaffold structure. Therefore, very fast irreversible actuation/shape/form change making 2D and 3D stable structures via temperature as external trigger in a simple way on a large scale is also a challenge. Here we report our new findings regarding dual one-component thermoresponsive actuator with the following highlights: (1) actuation of only-poly(NIPAM) membranes without any additional components; (2) formation of very fast 3D hollow tubes by temperature triggered self-rolling and curling in an irreversible way in different directions and being stable at all temperatures in water once they are formed; (3) actuation in size depending upon the temperature; (4) the observed behaviour is traced back to the unique combination of anisotropic thermal expansion with a similarly anisotropic elastic modulus of the employed material as demonstrated by numerical simulations.

Cross-linked poly(NIPAM) fibrous membranes made by electrospinning show temperature and fiber alignment dependent swelling and shrinkage in water.[21,22] Two such differently swellable/shrinkable poly(NIPAM) fibrous mats were combined together to generate a swelling/shrinkage gradient along the membrane thickness (perpendicular to the interface) to create temperature triggered irreversible very fast actuation. The gradient thickness can be easily adjusted by the time of spinning. For making such membranes, randomly aligned fibers were first spun on a horizontally rotating disc of diameter 13 cm at 30 rpm followed by deposition of aligned fibers on a vertically rotating disc of diameter 20 cm and disc rim of 4 cm with a rotating speed of 800 rpm. The degree of alignment of fibers, as calculated by Formula 1 (Supporting Information) was 97%. The fibrous mat was pressed at room temperature at 300 bars for 20 min and photo cross-linked to get a strong interface between the fiber layers (**Figure 1**a, Figure S1, Supporting Information). This method of making a stable fibrous layered membrane (no delamination on repeated use in water) was established in our previous work on bicomponent membranes.[21] The porosity, as determined by Equations (2–4) (Supporting Information), was 40% and 33%, respectively, for random and aligned fibrous layers. The average diameters of as-spun random and aligned fibers were 1.5 and 1.3 μm, respectively (Figure S1, Supporting Information). The resulting sample with asymmetric alignment of fibers was cut at varied angles to provide samples with

L. Liu, Prof. S. Agarwal
Macromolecular Chemistry II, and Bayreuth Center for Colloids and Interfaces
Universität Bayreuth
Universitätsstraße 30, 95440 Bayreuth, Germany
E-mail: agarwal@uni-bayreuth.de
A. Ghaemi, Prof. S. Gekle
Biofluid Simulation and Modeling
Fachbereich Physik, and Bayreuth Center for Colloids and Interfaces
Universität Bayreuth
Universitätsstraße 30, 95440 Bayreuth, Germany

DOI: 10.1002/adma.201603677

ADVANCED MATERIALS
www.advmat.de
www.MaterialsViews.com

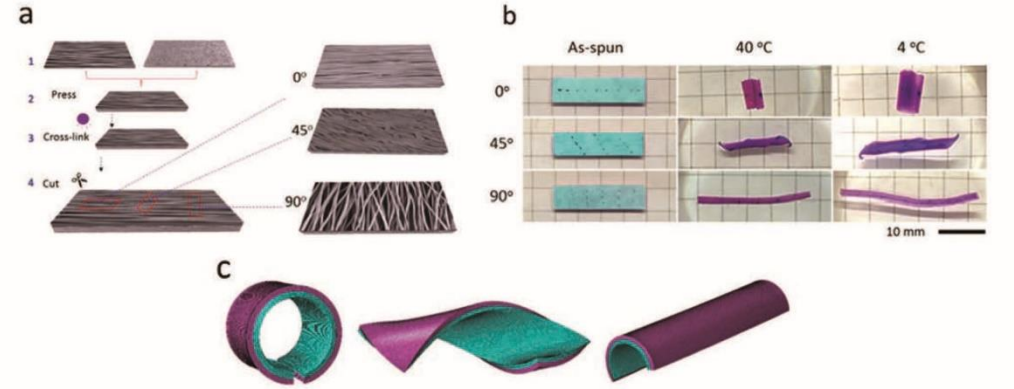

Figure 1. a) Schematic of formation of Bi-PNIPAM-0°, Bi-PNIPAM-45°, Bi-PNIPAM-90° actuator by electrospinning of aligned layer and random layer, respectively (Step 1), followed by pressing and cross-linking (Steps 2 and 3). At last, the samples were cut into pieces at different angles (Step 4); b) one component poly(NIPAM) directionally controlled actuation: movement of Bi-PNIPAM-0°, Bi-PNIPAM-45°, Bi-PNIPAM-90° mat (aligned (blue)/random (pink) (length: 2.0 cm, width: 0.5 cm) with the thickness ratio (aligned/bilayer) of 0.65) in water at different temperatures. Fiber alignment direction was indicated by a black dotted line on the sample. The good color contrast by dying the aligned and random mats might be invisible due to the transparency of poly(NIPAM-ABP) in water; c) equilibrium shapes of bilayer mats obtained from finite-element simulations in 40 °C water. From left to right are 0°, 45°, and 90° fiber alignments in one of the two layers. By using anisotropic expansion coefficients in combination with an anisotropic elastic modulus, good agreement with the experimental shapes in (b) is obtained.

randomly arranged fibers in one layer and parallel arranged (Bi-PNIPAM-0°), perpendicularly arranged (Bi-PNIPAM-90°), and fibers arranged at 45° (Bi-PNIPAM-45°) with respect to the long axis in the second layer as shown in Figure 1a.

For comparison purposes, poly(NIPAM) individual random (mono-ran-PNIPAM), and aligned fibrous mats (PNIPAM-0°; PNIPAM-90°; PNIPAM-45°) were also prepared. Temperature and fiber alignment dependent swelling and shrinking of individual poly(NIPAM) fibrous mats with different fiber alignments is shown in Figure S2 in the Supporting Information and Table 1. The mat with fibers aligned parallel to the long axis of the fibers (PNIPAM-0°) showed around 33% shrinkage and 18% swelling in the direction parallel and perpendicular to the fiber alignment, respectively, whereas fiber mats with random alignment of fibers (mono-ran-PNIPAM) shrank ≈11% in both directions on putting in water at 40 °C in a similar way as described previously.[21,22] When two such fibrous mats (PNIPAM-0° and mono-ran-PNIPAM) were combined together in the form of a layered structure (thickness of PNIPAM-0° and mono-ran-PNIPAM fibrous mats were 33.9 and 17.9 µm, respectively; size: 2.0 cm × 0.5 cm length (L) × width (W)) and immersed in water at 40 °C, the structure showed rolling along the fiber alignment direction with the randomly oriented mono-ran-PNIPAM fibrous layer forming the outside of the rolls (Figure 1b, Movie 1, Supporting Information) due to the gradient in differential shrinkage along the thickness. The high shrinkage of PNIPAM-0° compresses the mono-ran-PNIPAM layer all along the interface leading to rolling. Based on the naive assumption of an isotropic E modulus, the differential swelling and shrinkage pattern in Table 1 would suggest that rolling perpendicular to the direction of fiber alignment should also happen for a bilayer of PNIPAM-0° and mono-ran-PNIPAM. The preference of rolling along the length of the fiber mat can be explained by a significant difference in E modulus of the aligned PNIPAM-0° fibrous mat in parallel and perpendicular directions. Indeed, we measured the E modulus of the aligned fibrous mats in the dry state (Figure S3, Supporting Information) and find that in the perpendicular direction it is much smaller than in parallel direction. Thus, even though the material does attempt to increase its size in the perpendicular direction, the resulting stress is too small to create buckling in this direction. Although a similar mechanical test on wet samples could not give any accurate quantitative values due to handling and gripping problems together with the difficulty of

Table 1. Size change of poly(NIPAM) fiber mats with different alignment of fibers in water at different temperatures (40 and 4 °C). The similar mats were used in the previous work for getting reversible thermoresponsive actuation in shape by making bicomponent mats.[21,22]

	0°			45°			90°			Random		
	As-spun	40 °C	4 °C	As-spun	40 °C	4 °C	As-spun	40 °C	4 °C	As-spun	40 °C	4 °C
L [cm]	1.976	1.319	1.85	2.005	1.831	2.617	2.1015	2.355	3.508	2.117	1.887	2.71
W [cm]	0.524	0.62	0.932	0.524	0.464	0.677	0.5165	0.3355	0.4985	0.539	0.479	0.669
D_1 [cm]	2.041	1.447	2.049	2.071	2.086	3.041	2.163	2.371	3.548	2.193	1.956	2.777
D_2 [cm]	2.048	1.454	2.071	2.073	1.656	2.364	2.17	2.376	3.534	2.181	1.948	2.783

Adv. Mater. 2016,
DOI: 10.1002/adma.201603677

Materials Views
www.MaterialsViews.com

ADVANCED MATERIALS
www.advmat.de

keeping uniform shape which is a general problem of all soft gels, a qualitatively similar trend is expected. We note that a similar mechanical anisotropy with a higher modulus in parallel direction in comparison to that in perpendicular direction is known for other soft gels.[30]

The rolled tubes, when taken out from water, and dried, either at room temperature or at 60 °C, in a vacuum oven for 24 h did not return back to the original flat shape. However, they showed reversible change in size on changing the water temperature from 40 to 4 to 40 °C keeping its tubular shape for at least 30 cycles. On transferring the rolled 3D structures in water from 40 to 4 °C and vice versa led to no significant change in shape. Indeed, for a shape change when going from 40 to 4 °C (the temperature below lower critical solution temperature (LCST) of poly(NIPAM), which in the first instant should be opening of the tube, two possible scenarios are (1) the inside layer swells in parallel direction and the outside layer does not change its length, (2) both layers swell in parallel direction with the inside layer swelling appreciably more than the outside layer. Under both these conditions, the compressive force generated along the interface would open the tube. But from Table 1, it is evident that both mono-ran-PNIPAM (the outside layer) and PNIPAM-0° (inside layer) swell to almost the same extent in parallel direction. The mono-ran-PNIPAM increases in length by ≈43%, whereas PNIPAM-0° showed ≈40% increase. Therefore, in our case there is no net compressive force on the interface to open the tube. This explains irreversible shape change.

Once the tubes are formed, the change in water temperature to 4 °C and vice versa led to an almost instant reversible change in size. The tubes swell (both length and width) at 4 °C and shrink at 40 °C. This is simply due to swelling of poly(NIPAM) in cold water (4 °C) and shrinkage in hot water (40 °C), an inherent property of poly(NIPAM) irrespective of fiber alignment direction. 4 and 40 °C were arbitrarily chosen as two temperatures below and above the LCST (26 °C) of poly(NIPAM) fibrous mat as observed by micro-DSC.[22] In short, there are two different processes: (1) from as spun (dry) state to wet and (2) from wet (hot) to wet (cold) and vice versa. The first process decides the shape and is irreversible. The second process decides the tube size and is reversible.

The same behavior, i.e., movement along fiber alignment, was observed in other samples with one layer made up of randomly arranged fibers and another layer with fiber alignments perpendicular and 45° (Bi-PNIPAM-90° and Bi-PNIPAM-45°) (Figure 1b). In case of PNIPAM-45, compared to the random layer (mono-ran-PNIPAM), on going from dry as spun fibers to wet state at 40 °C, the dimensional change (shrinkage) of aligned layer along the fiber orientation (diagonal D_2) dominated that along the direction perpendicular to the fiber orientation (diagonal D_1) (Figure S2, Supporting Information) leading to a helix with the randomly aligned fibrous layer outside. Also, Bi-PNIPAM-90° showed bilayer movement along the direction of fiber alignment due to the combined effect of the anisotropic E modulus and asymmetrical differential change in length and width as explained above for Bi-PNIPAM-0° sample. The width of PNIPAM-90° decreased by ≈35% whereas mono-ran-PNIPAM showed only 11% shrinkage. The differential shrinkage in width led to the formation of a tube by rolling along the fiber alignment, i.e., perpendicular to the long axis. Shape changes in all these cases were very fast in less than 3 s depending upon the direction of fiber alignment due to highly porous membranes. Fast shape change is also possible even for larger size samples. 2.28, 2.97, and 3.37 s, respectively were required for Bi-PNIPAM-0° (thickness ratio (aligned:bilayer) 0.65) samples with ratio of L:W 2:1, 4:1, and 6:1 at 40 °C, respectively (**Figure 2**a,b).

Furthermore, the effect of temperature on rolling behavior was studied for Bi-PNIPAM-0° by following the curvature. The rolling took place on placing the as spun dry sample in water at all temperatures between 4 and 40 °C. There was a significant increase in curvature on going from 23 to 37 °C and the change was maximum at 26 °C, the cloud point of poly(NIPAM) fibrous mat (Figure 2c).

In **Figure 3**, we show that the curvature normalized by the total thickness reaches its maximum point when the thickness ratio is around 0.48 and decreases again afterward. A reminiscent behavior with zero curvature for the extreme thickness ratios of 0 (random layer only) and 1 (aligned layer only) together with a maximum in between occurs in metallic bilayers under thermal expansion.[31] A similar trend was seen

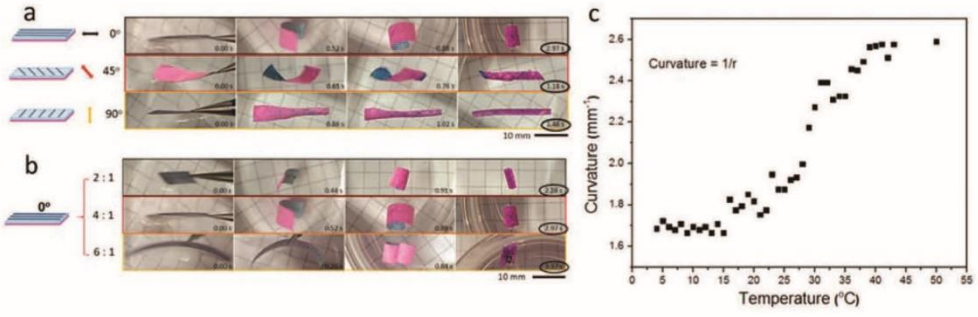

Figure 2. Actuation process and effect of temperature. a) Actuation process of Bi-PNIPAM-0°, Bi-PNIPAM-45°, Bi-PNIPAM-90° mats (thickness ratio : 0.65 (aligned/random); L:W = 4:1) with time in water at 40 °C; b) Size-dependent actuation process of Bi-PNIPAM-0° mats (thickness ratio: 0.65 (Aligned/random)) with time in water at 40 °C. L:W ratios were 2:1, 4:1, and 6:1; c) The effect of temperature of water on the curvature of Bi-PNIPAM-0° mat with the thickness ratio (aligned/random) of 0.65.

ADVANCED MATERIALS
www.advmat.de
www.MaterialsViews.com

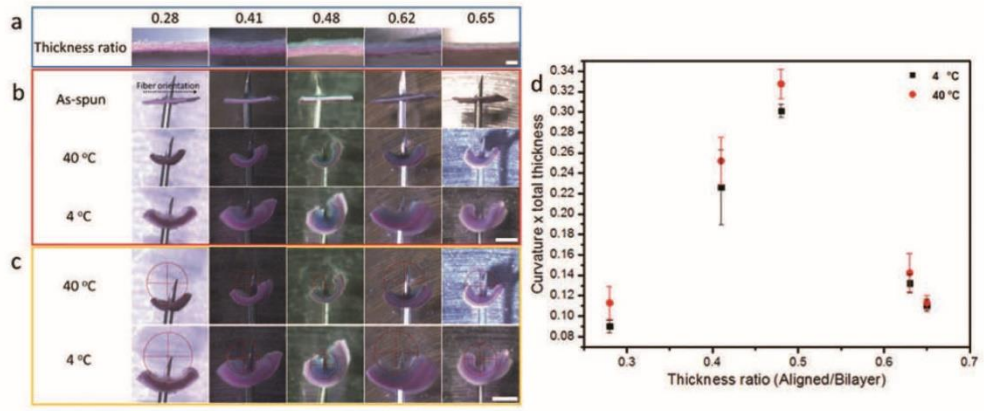

Figure 3. Effect of thickness ratio (aligned/random) on "curvature × total thickness" of Bi-PNIPAM-0° mats (size: $L{:}W = 2$ mm:3.5 mm) in water at different temperatures. a) Cross-section of Bi-PNIPAM-0° samples with different thickness ratio (blue side is aligned layer; scale bar = 100 µm); b) in water at different temperatures (scale bar = 1 mm); c) radius (r) determination (scale bar = 1 mm); d) "curvature × total thickness" against thickness ratio of aligned/random. The curvature is taken as $1/r$.

in samples with high aspect ratio ($L/W = 4{:}1$) (Figure S4, Supporting Information). The difference was a complete rolling instead of merely a bending on increasing the L/W ratio.

In order to demonstrate that the observed results can indeed be understood properly by a combination of thermal expansion and elastic deformation, we conduct finite element simulations using the Abaqus software package (see Methods for details in Supporting Information). These allow us to predict the equilibrium shape of the bilayer mats after complete swelling/shrinking. The poly(NIPAM) layers are modeled as elastic materials whose swelling/shrinking is accounted for by an effective expansion coefficient. The aligned layer is an anisotropic material with expansion coefficients $\alpha_{along} = -0.3$ and $\alpha_{perp} = 0.2$ in direction along and perpendicular to the fiber orientation, respectively, as obtained from Figure S2 in the Supporting Information and Table 1. The elastic moduli are similarly anisotropic with $E_{along}/E_{perp} = 50$ as measured in Figure S3 in the Supporting Information. The random layer is isotropic with $\alpha_{random} = -0.1$ and $E_{along}/E_{random} = 5/3$.

Figure 1c shows the numerically obtained structures for the mats with fibers aligned at 0°, 45°, and 90° in one of the layers corresponding to the experimental images in Figure 1b. For 0° and 90° we observe rolling in fiber direction and for 45° a helical structure is found in very good agreement with experimental observations. In contrast, considering only anisotropic expansion combined with isotropic elasticity leads to shapes which are in clear disagreement with the experimental observations (Figure S5, Supporting Information). This lends strong support to our hypothesis that the observed actuation is indeed due to a combination of an anisotropic expansion with an equally important anisotropy in the elastic modulus.

In conclusion, we present a rare example of a one-component dual actuator with very fast irreversible actuation (1–3 s) to direction controlled 3D tubular forms and almost instant reversible size actuation with temperature in contact with water. The 3D structures kept their form in water at temperatures 4–40 °C with reversible change in size. The actuator is a porous fibrous poly(NIPAM) membrane in which asymmetry in swelling/shrinkage required for irreversible actuation in form is created along the membrane thickness by fiber alignment and direction dependent E modulus. The actuation in size of 3D tubular forms is due to thermoresponsive nature of poly(NIPAM). The actuators can be made in any dimensions and validated by numerical simulations. This work opens up new perspectives of formation of 3D structures by external stimuli with reversible actuation in size without destroying the form useful for creating externally controlled 3D structures, scaffolds for tissue engineering, complex patterns for multi-cell culture, for example.

Supporting Information

Supporting Information is available from the Wiley Online Library or from the author.

Acknowledgements

The authors would like to acknowledge financial support from Deutsche Forschungsgemeinschaft (DFG; SFB 840). L.L. thanks China Scholarship Council for awarding fellowship for carrying out PhD in Germany in the lab of Prof. Seema Agarwal. SG and AG thank the Volkswagen Foundation for financial support.

Received: July 12, 2016
Revised: August 19, 2016
Published online:

[1] B. Li, T. Du, B. Yu, J. van der Gucht, F. Zhou, *Small* **2015**, *11*, 3494.
[2] L. Zhang, S. Chizhik, Y. Wen, P. Naumov, *Adv. Funct. Mater.* **2016**, *26*, 1040.

Materials Views
www.MaterialsViews.com

ADVANCED MATERIALS
www.advmat.de

[3] B. Xu, H. Jiang, H. Li, G. Zhang, Q. Zhang, *RSC Adv.* **2015**, *5*, 13167.
[4] D. Kim, H. Lee, J. Yoon, *Sci. Rep.* **2016**, *6*, 20921.
[5] J. Robertson, A. Torbati, E. Rodriguez, Y. Mao, R. Baker, H. Qi, P. Mather, *Soft Matter* **2015**, *11*, 5754.
[6] L. Zhang, I. Desta, P. Naumov, *Chem. Commun.* **2016**, *52*, 5920.
[7] D. V. Opdenbosch, G. Fritz-Popovski, W. Wagermaier, O. Paris, C. Zollfrank, *Adv. Mater.* **2016**, *28*, 5235.
[8] M. Ji, N. Jiang, J. Chang, J. Sun, *Adv. Funct. Mater.* **2014**, *24*, 5412.
[9] X. Zhang, Z. Yu, C. Wang, D. Zarrouk, J. Seo, J. Cheng, A. Buchan, K. Takei, Y. Zhao, J. Ager, J. Zhang, M. Hettick, M. Hersam, A. Pisano, R. Fearing, A. Javey, *Nat. Commun.* **2014**, *5*, 2983.
[10] E. Wang, M. Desai, S. Lee, *Nano Lett.* **2013**, *13*, 2826.
[11] Y. Kim, M. Liu, Y. Ishida, Y. Ebina, M. Osada, T. Sasaki, T. Hikima, M. Takata, T. Aida, *Nat. Mater.* **2015**, *14*, 1002.
[12] M. Dai, O. T. Picot, J. M. N. Verjans, L.-T. de Haan, A. P. H. Schenning, T. Peijs, C. W. M. Bastiaansen, *ACS Appl. Mater Interfaces* **2013**, *5*, 4945.
[13] X. Xie, L. Qu, C. Zhou, Y. Li, J. Zhu, H. Bai, G. Shi, L. Dai, *ACS Nano* **2010**, *4*, 6050.
[14] S. Taccola, F. Greco, E. Sinibaldi, A. Mondini, B. Mazzolai, V. Mattoli, *Adv. Mater.* **2015**, *27*, 1668.
[15] J. Kim, S. Chung, S. Choi, H. Lee, J. Kim, S. Kwon, *Nat. Mater.* **2011**, *10*, 747.
[16] Y. Haldorai, J. Shim, *New J. Chem.* **2014**, *38*, 2653.
[17] M. Islam, M. Serpe, *RSC Adv.* **2014**, *4*, 31937.
[18] Y. Yamamoto, K. Kanao, T. Arie, S. Akita, K. Takei, *ACS Appl. Mater. Interfaces* **2015**, *7*, 11002.
[19] X. Zhang, C. Pint, M. Lee, B. Schubert, A. Jamshidi, K. Takei, H. Ko, A. Gillies, R. Bardhan, J. Urban, M. Wu, R. Fearing, A. Javey, *Nano Lett.* **2011**, *11*, 3239.
[20] L. Ionov, *e-Polymers* **2014**, *14*, 109.
[21] S. Jiang, F. Liu, A. Lerch, L. Ionov, S. Agarwal, *Adv. Mater.* **2015**, *27*, 4865.
[22] L. Liu, S. Jiang, Y. Sun, S. Agarwal, *Adv. Funct. Mater.* **2016**, *26*, 1021.
[23] A. Yarin, S. Agarwal, *Polymer* **2016**, *97*, 604.
[24] S. Douezan, M. Wyart, F. Brochard-Wyart, D. Cuvelier, *Soft Matter* **2011**, *7*, 1506.
[25] R. Erb, J. Sander, R. Grisch, A. Studart, *Nat. Commun.* **2013**, *4*, 1712.
[26] J. Mu, C. Hou, B. Zhu, H. Wang, Y. Li, Q. Zhang, *Sci. Rep.* **2015**, *5*, 9503.
[27] K. Baek, J. Jeong, A. Shkumatov, R. Bashir, H. Kong, *Adv. Mater.* **2013**, *25*, 5568.
[28] L. Liu, N. Wang, Y. Han, Y. Li, W. Liu, *Macromol. Rapid Commun.* **2014**, *35*, 344.
[29] T. Asoh, M. Matsusaki, T. Kaneko, M. Akashi, *Adv. Mater.* **2008**, *20*, 2080.
[30] R. Namani, M. Wood, S. Sakiyama-Elbert, P. Bayly, *J. Biomech.* **2009**, *42*, 2047.
[31] S. Timoshenko, *J. Opt. Soc. Am.* **1925**, *11*, 233.

ADVANCED MATERIALS

Supporting Information

for *Adv. Mater.*, DOI: 10.1002/adma.201603677

One-Component Dual Actuation: Poly(NIPAM) Can Actuate to Stable 3D Forms with Reversible Size Change

*Li Liu, Ali Ghaemi, Stephan Gekle, and Seema Agarwal**

WILEY-VCH

Supporting Information

for Adv. Mater., DOI: 10.1002/adma.201603677

One-component dual actuation: Poly(NIPAM) can actuate to stable 3D forms with reversible size change

Li Liu[1], Ali Ghaemi[2], Stephan Gekle[2], Seema Agarwal[1]*

Experimental Section

Materials: Photo cross-linker 4-acryloylbenzophenone (ABP) was used and P(NIPAM-ABP) ($M_n = 7.0 \times 10^4$ g/mol, $M_w = 2.0 \times 10^5$ g/mol) was made as described in ref 1.[1]

Preparation of fibrous mats: All fibrous mats were made by electrospinning of P(NIPAM-ABP) using DMF as solvent. The electrospinning conditions were presented in **Table S1**. For obtaining the color contrast in the bilayer fibrous mat, with respect to the weight of P(NIPAM-ABP), an amount of 0.4 wt% of methylene blue (MB) and Rhodamine B (RB) were added into the solutions to get the aligned and random fibrous mats, respectively. The fibers collected by a horizontally rotating disc of diameter 13 cm at 30 rpm formed the random fibrous mat and that collected by a vertically rotating disc of diameter 20 cm and a disc rim of 4 cm with a rotating speed of 800 rpm formed the aligned fibrous mat. After that, the random and aligned fibrous mats were pressed together under 300 bars for 20min, at room temperature, followed by photo cross-linking under UV-lamp (Honle UVAHAND 250 GS) for 4 hour.

Finite element simulations. Bilayer mats are simulated using ABAQUS version 6.14. The mats are meshed using three dimensional, general purpose brick elements, C3D8R, for linearly elastic (but anisotropic) materials. This method solves the elastic equations such that the equilibrium shape is obtained. The layers are tied to each other with a no slip boundary

condition at their interface. No further restrictions are imposed on the free movements of the mats.

Our goal here is to model the irreversible rolling when the fibrous mats are taken from the dry state into the 40°C water. The water influx into the porous medium follows a very complicated time dynamics. Luckily, however, it is not necessary to model this influx in full detail in order to obtain an understanding of the final rolled shape. Therefore, the explicit time dynamics of water influx is not included. Instead, we model the swelling/shrinkage of the material by using ABAQUS' possibility of modeling material expansion. The total length change of each layer was anisotropic with swelling/shrinkage ratios α whose values are given in the main text. Including expansion also in the vertical direction does not lead to significant changes. The shape change is achieved by going from the dry to the 40°C wet state in small increments the number of which is determined automatically so as to ensure numerical convergence.

ABAQUS is capable of treating anisotropic materials whose elastic E moduli differ in different directions (the values are given in the main text). The shear modulus is always isotropic with $E_{random}/G = 3$ and Poisson's ratios are $\nu_{along,perp}=\nu_{along,z}= \nu_{perp,z} =0.3$ for the aligned layer and $\nu_{random}=0.3$ for the random layer. Varying both quantities does not lead to appreciable differences in the results.

In the simulation, the thickness of both mats is 30 μm. To obtain a clear illustration of the bending effects without interpenetration of the mats, the sizes of the mats are chosen as 1600 × 500 μm for the 0°, 2000 × 500 μm for the 45° and 2000 × 1000 μm for the 90° mat.

Characterization: Gel permeation chromatography (GPC) was used to determine the molecular weight of P(NIPAM-ABP) by using DMF as the eluent at a flow rate of 0.5 mL/min at 25 °C. A scanning electron microscope (SEM) (Phenom Pro, Phenomworld) was used to study the diameter and morphology of fibers. The quantified analysis of dimension

change was carried out by a software of Image J. A software named Video Remaker was chosen to capture photos.

And according to the previous literatures, the alignment degree was based on the following formula: [2]

$$d_{Fa} = \frac{3cos^2\theta - 1}{2} \qquad (1)$$

where θ is the angle between the individual fiber and the rotating direction of the collector. The given values are based on an average of 100 fibers.

The porosity (P) of the random and aligned fibrous mats were calculated by the equations of (2), (3) and (4):

$$\rho_{mat} = \frac{mass_{mat}}{area_{mat} \times thickness_{mat}} \qquad (2)$$

$$\rho_{film} = \frac{mass_{film}}{area_{film} \times thickness_{film}} \qquad (3)$$

$$P = \left(1 - \frac{\rho_{mat}}{\rho_{film}}\right) \times 100\% \qquad (4)$$

where ρ_{film} = film density and ρ_{mat} = density of cross-linked electrospun mats, respectively.

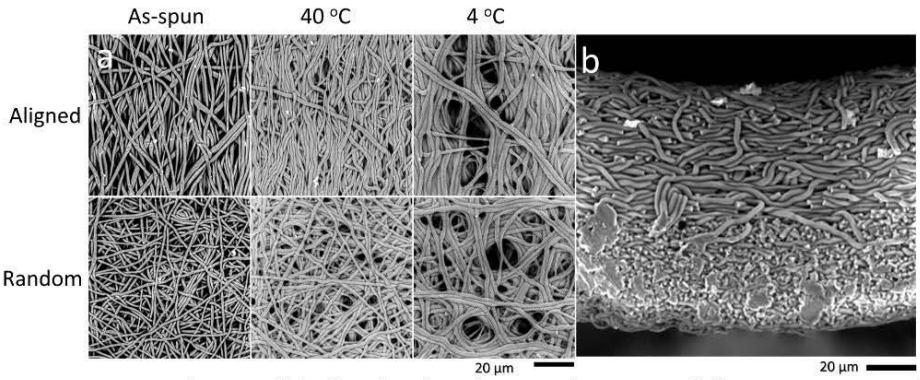

Figure S1. SEM images of a) aligned and random mats in water at different temperatures, b) the cross-section of the Bi-PNIPAM-0° mat in water at 40 °C after drying shows a strong

interface between aligned (upper side) and random (bottom side) fibrous layers. Scale bar = 20 μm.

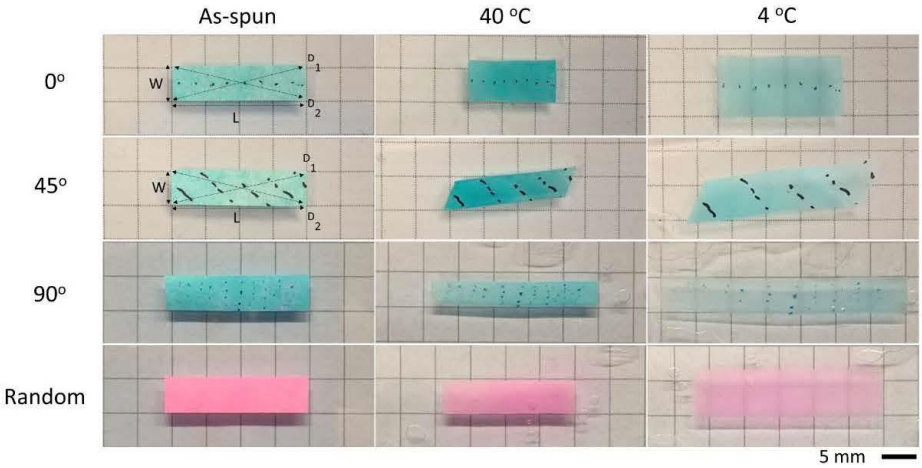

Figure S2. The size change of aligned and random cross-linked fibrous mats (original size: 2.0 cm × 0.5 cm) in water at different temperatures. The similar experiment was done previously in reference 22 (main text) for making bicomponent actuators.

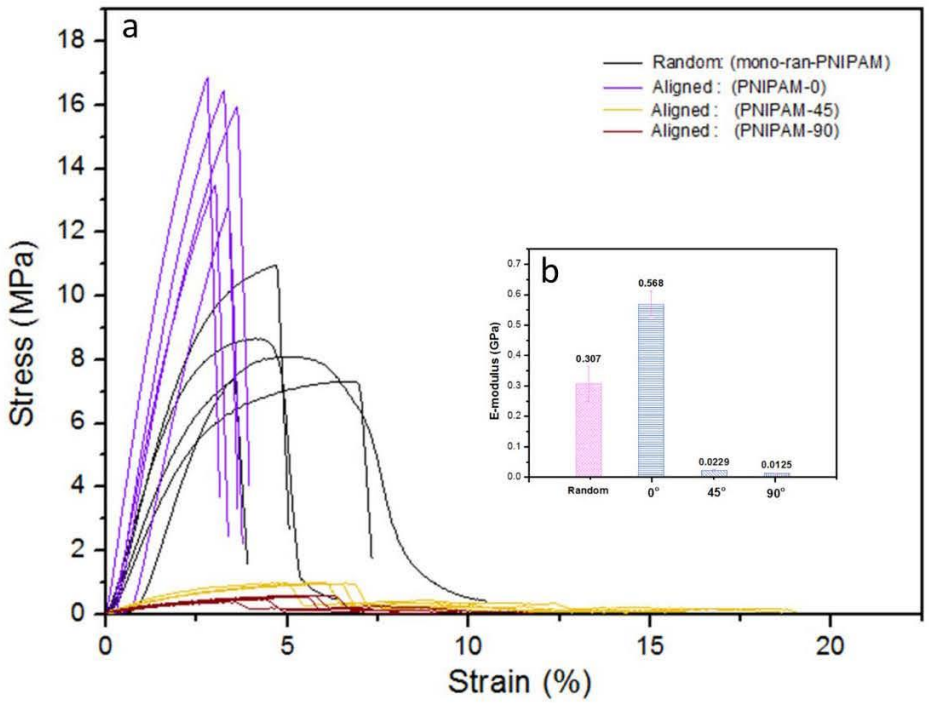

Figure S3. a) strain-stress curve and b) E-modulus of pressed cross-linked one-component Bi-PNIPAM-0°, 45°, 90° samples.

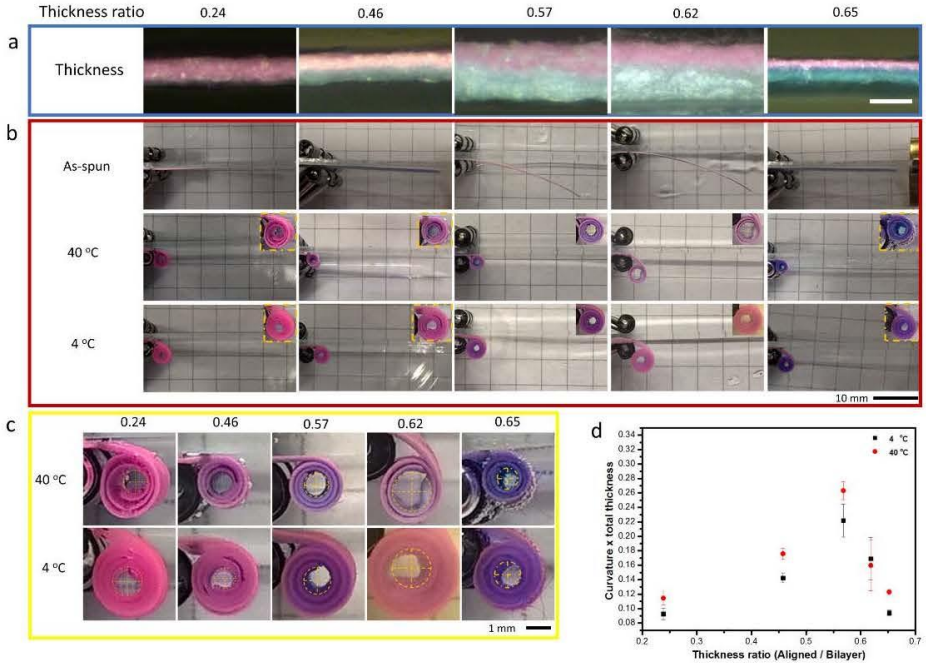

Figure S4. Effect of thickness ratio (aligned / bilayer) on "curvature × bilayer total thickness" of Bi-PNIPAM-0° mats (20 mm × 5 mm) in water at different temperatures. a) Cross-section of Bi-PNIPAM-0° samples with different thickness ratio (blue side is aligned layer; scale bar = 100 μm); b) In water with different temperatures (scale bar = 10 mm); c) radius (r) determination (scale bar = 1 mm); d) Curve of "curvature × bilayer total thickness" against thickness ratio of Aligned / Bilayer. The curvature is taken as 1/r.

6

Figure S5. Equilibrium shapes of the 0°, 45° and 90° bilayer mats from finite element simulations analogous to **Figure 1**c of the main text, but with the oversimplifying assumption of an isotropic elastic modulus in both layers. Comparison with Figure 1 of the main text clearly demonstrates that this simple model is not able to reproduce the experimentally observed shapes. The size of the mats is 1600×500μm for the 0° and 45° and 800×500μm for 90° mat.

Table S1. The electrospinning parameters used for making fibrous membranes. DMF was used as solvent.

	Solution concentration 00- [wt %]	Voltage [KV]	Flow rate [ml/h]	Spinning volume [ml]	Needle diameter [mm]	Collecting distance [cm]
Aligned Mat	40	-2.4 - 17.0	1.3	2.5	0.6	15
Random Mat	40	0.0 - 16.0	1.3	1.0	0.6	20

[1] G. Stoychev, N. Puretskiy, L. Ionov, *Soft Matter* **2011**, *7*, 3277.

[2] R. Dersch, T. Liu, A. Schaper, A. Greiner, J. Wendorff, *J. Polym. Sci. A Polym. Chem.* **2003**, *41*, 545.

5.3 Publication 3: Composite Polymeric Membranes with Directionally Embedded Fibers for Controlled Dual Actuation

Li Liu, Hadi Bakhshi, Shaohua Jiang, Holger Schmalz and Seema Agarwal*, "Composite Polymeric Membranes with Directionally Embedded Fibers for Controlled Dual Actuation", *Macromolecular rapid communications*, 2018, 1800082.

COMMUNICATION
Soft Actuators

Macromolecular Rapid Communication
www.mrc-journal.d

Composite Polymeric Membranes with Directionally Embedded Fibers for Controlled Dual Actuation

*Li Liu, Hadi Bakhshi, Shaohua Jiang, Holger Schmalz, and Seema Agarwal**

In this paper, preparation method and actuation properties of an innovative composite membrane composed of thermo- and pH-responsive poly(*N*-isopropylacrylamide-*co*-acrylic acid) fibers (average diameter ≈ 905 nm) embedded within a passive thermoplastic polyurethane (TPU) matrix at different angles with degree of alignment as high as 98% are presented. The composite membrane has a gradient of TPU along the thickness. It has the capability of temperature- and pH-dependent direction-, and size-controlled actuation in few minutes. The stresses generated at the responsive fiber and nonresponsive matrix provide actuation, whereas the angle at which fibers are embedded in the matrix controls the actuation direction and size. The temperature has no effect on actuation and actuated forms at pH 7 and above, whereas the size of the actuated forms can be controlled by the temperature at lower pH. The membranes are strong enough to reversibly lift and release ≈426 times weight of their own mass (2.47 g metal ring is lifted by a 5.8 mg membrane). Soft actuators are of interest as smart scaffolds, robotics, catalysis, drug release, energy storage, electrodes, and metamaterials.

1. Introduction

Soft actuators made of materials able to change their shape or properties in response to environmental stimuli have attracted much interest in various applications such as sensors, optical and microfluidic devices, walkers and swimmers, and encapsulating/releasing systems.[1,2] Actuation triggered by temperature,[3,4] pH,[5,6] light,[6,7] electric,[8] magnetic[5] fields, and certain chemicals[9] are well-studied. Lately, multistimuli-sensitive soft actuators have attracted more attention from applications' point of view. The combination of various stimuli-responses for an actuator will expand the controllability for the intended applications. Some multistimuli are included but not limited to pH/electro,[10] pH/salt,[11] pH/thermos,[12–14] pH/thermo/salt.[15] Along these lines, actuators that respond to pH and temperature are more interesting, having a higher potential for biomedical applications.[12]

Generally, hydrogel actuators respond very slowly to stimuli, since their swelling/shrinkage behaviors are associated with the diffusion in/out of water or ions. However, the response rate can be improved via modifying the chemical structure, e.g., comb-type grafting,[14] or altering the morphological construction, e.g., macroporous[16,17] and nanodimensional[18,19] structures. Electrospun responsive fibers showed shorter response-time comparing to hydrogel films because of their higher more specific surface area and porosity that increases the rate of diffusion through the polymeric matrix.[20,21]

Soft actuators with bilayer structure have been previously reported.[11,22,23] Their actuation relies on the stimuli-induced anisotropic size change of two attached layers. Li et al.[23] have prepared bilayer actuators based on a semi-interpenetrating network of poly(*N*-isopropylacrylamide) (PNIPAm) and poly(diallyldimethylammonium) on a passive layer of polydimethylsiloxane, which can undergo reversible bidirectional bending to grip an object in response to temperature and pH stimuli. Cheng et al.[22] have fabricated a four-arm gripper based on two layers of PNIPAm and poly(2-(dimethylamino) ethyl methacrylate), which rapidly responses to both temperature and pH. Bassik et al.[11] have presented bilayer actuators made of NIPAm and acrylic acid (AA) hydrogel on a passive polyethylene oxide diacrylate layer, which undergo reversible open and close behavior by varying the pH and ionic strength of the aqueous medium. Nakagawa et al.[24] fabricated a nanofibrous bilayer actuator based on a copolymer of AA and butyl methacrylate by using different flow rate to construct an anisotropic internal structure during the electrospinning process. Most of these actuators are based on PNIPAm as a widely investigated thermoresponsive polymer showing a volume change in water below and beyond the lower critical solution temperature (LCST, 32 °C).[14,23] Since its LCST is in the range of body temperature, it has been widely considered for tissue engineering application.[25,26] Poly(acrylic acid) (PAA) is a pH-responsive polymer, which swells and shrinks in pH values above and below its pK_a (pH 4.25–4.75), respectively.[14,27] It has been used for drug delivery to the regions of local acidosis

L. Liu, Dr. H. Bakhshi, Dr. H. Schmalz, Prof. S. Agarwal
Macromolecular Chemistry II and Bayreuth Center for Colloids and Interfaces
Universität Bayreuth
Universitätsstraße 30, 95440 Bayreuth, Germany
E-mail: agarwal@uni-bayreuth.de
Prof. S. Jiang
College of Materials Science and Engineering
Nanjing Forestry University
Nanjing 210037, China
Dr. H. Schmalz
Bavarian Polymer Institute
University of Bayreuth
Universitätsstraße 30, 95440 Bayreuth, Germany
The ORCID identification number(s) for the author(s) of this article can be found under https://doi.org/10.1002/marc.201800082.

DOI: 10.1002/marc.201800082

ADVANCED SCIENCE NEWS
www.advancedsciencenews.com

Macromolecular Rapid Communications
www.mrc-journal.de

as found in ischemic myocardium (pH 6–7), gastrointestinal tract, and tumor areas (4.5–6.0).[5,12,28,29] The combination of PNIPAm with PAA within a hydrogel provides dual thermo- and pH-responsivity.[11,12,14]

Most of the soft actuators undergo only one directional deformation, reversible bending or opening/closing. Recently, we have developed direction-controlled bilayer actuators which ultrafast response to temperature.[30,31] Multiresponsive actuators with controlled directional movements and size-changes are still desired. Herein, we show 1) a simple method of making composite polymeric membranes with directionally embedded dual-responsive fibers in thermoplastic polyurethane matrix for controlled actuation. The composite has a concentration gradient of the nonresponsive matrix polymer along the thickness; 2) pH- and temperature-dependent fast reversible direction- and size-controlled coiling, rolling, bending, and twisting deformations by controlling the direction of dual responsive fibers alignment in thermoplastic polyurethane (TPU) matrix; 3) formation of irreversible actuated forms at pH 7 and above not affected by temperature.

2. Results and Discussion

2.1. Crosslinkable Poly(NIPAm-AA)s

In this study, copolymers of NIPAm and AA (50:50 molar ratio) containing 2–6 mol% of UV-crosslinkable 4-acryloylbenzophenone (ABP) were synthesized via free radical solution polymerization at 70 °C (**Figure 1**; Table S1, Supporting Information). The chemical structures of the polymers were completely confirmed by nuclear magnetic resonance (NMR) and fourier-transform infrared (FTIR) spectroscopy (Figures S1–S3, Supporting Information). Primary studies showed that the electrospun mat based on poly(*N*-isopropylacrylamide-*co*-acrylic acid) (poly(NIPAm-AA)) with 2 mol% of ABS cannot be crosslinked sufficiently, where polymer leached out in water. Although increasing the ABP content within polymers improved their crosslinkability resulting in stable mats, it reduced their pH and especially thermoresponsivity. Thus, poly(NIPAm-AA) containing 4 mol% of ABP (sample P4 in Table S1 in the Supporting Information) was chosen in this work as the appropriate polymer for the fabrication of soft actuators. Its LCST and pK_a values were determined as 12.0 °C and 6.2, respectively (Figures S4 and S5, Supporting Information).

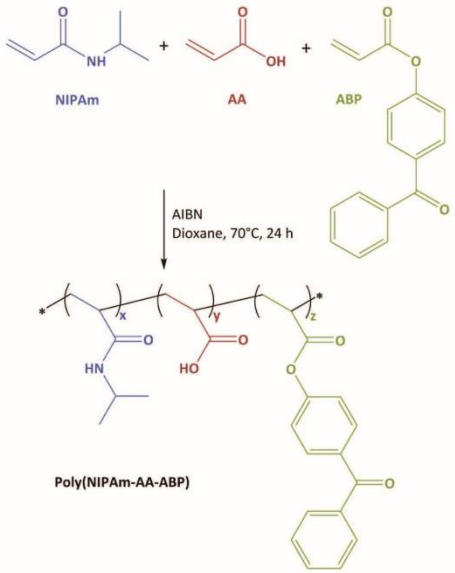

Figure 1. Synthesis of UV-crosslinkable poly(NIPAm-AA).

2.2. Electrospun Aligned Fibrous Mats

The poly(NIPAm-AA) aligned fibrous mats were prepared by electrospinning from a dimethylformamide (DMF) solution (40 wt%). The membranes were pressed under 300 bar at room temperature and crosslinked under UV light for 3.5 h for each side. The scanning electron microscopy (SEM) images showed smooth aligned fibers with an average diameter of 905 nm and degree of alignment of 98% (**Figure 2**a,b).

The crosslinked poly(NIPAm-AA) aligned fibrous membrane showed an interesting size change in buffer solutions (pH 3, 7, and 10) at different temperatures (Figure 2c; Table S2, Supporting Information). In pH 3 and at 6 °C (below LCST) after 10 min, fibrous mat shrunk in length (along fibre axis) by 29%, but increased in width (perpendicular to fibers' axis) by 28%, whereas at 40 °C (above LCST), it shrunk in length by 41% and increased in width by 6%. At both temperatures, the mat shrank significantly in the direction of fibers' alignment and swell in the perpendicular direction. Since pH 3 is lower than the pK_a of the copolymer (6.2; Figure S5, Supporting Information), the carboxylic acid groups of AA moieties in the polymer backbone remain protonated and hence in the hydrophobic state.[23,27] Therefore, the change in dimensions is mainly controlled by the conformational changes of NIPAm moieties of the copolymer. Although PNIPAm membranes should swell in both directions at low temperatures, the mat shrank in the length due to the relaxation of polymer chains within fibers. In fact, during the electrospinning process, the fibers were stretched by the electric force and deposited on the high-speed rotating collector in an unstable high energy stretched state due to a very fast evaporation of the solvent.[32,33] In the course of immersing in water, the polymer chains relaxed to the lower-energy coiled conformation. This behavior has been observed in our previous studies regarding thermoresponsive actuators.[30,31,34] At 6 °C, which is below the LCST of poly(NIPAm-AA) (Figure S6a, Supporting Information), the shrinkage in length was much less than at 40 °C due to the compensation of two counteracting effects: swelling of thermoresponsive PNIPAm moieties and shrinkage during polymer chains' relaxation.

ADVANCED SCIENCE NEWS
www.advancedsciencenews.com

Macromolecular Rapid Communications
www.mrc-journal.de

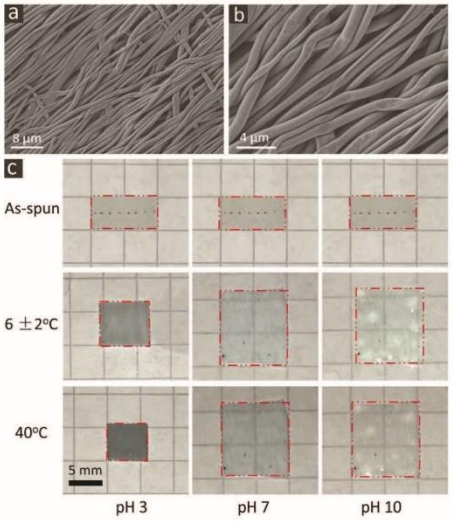

Figure 2. a,b) SEM images of crosslinked poly(NIPAm-AA) aligned fibrous mat. Sample P4 in Table S1 in the Supporting Information. c) Planar state of crosslinked poly(NIPAm-AA) aligned fibrous mat after immersing into buffer solutions with different pH at different temperatures for 10 min.

In pH 7 and 10, an interesting phenomenon was observed; the fibrous mat showed an asymmetric swelling by size-changing only in the perpendicular direction at both 6 and 40 °C (Figure 2c). In fact, the carboxylic acid units start playing their role in deformation of mats. In pH 7 and 10, the majority of carboxylic acid units are deprotonated and highly hydrophilic. The swelling arisen from the carboxylate units overweighed the temperature-dependent swelling/shrinkage of PNIPAm moieties. Therefore, no LCST was detected in pH 7 and 10 (Figure S6b, Supporting Information). Previous reports about dual thermo- and pH-responsive hydrogels also mentioned the reduction or even elimination of the thermosensitivity at a high level of hydrophilicity.[14,35] The swelling of carboxylate groups was strong enough to stop the shrinkage of mat in the direction of fiber's alignment due to the polymer chains' relaxation (Figure 2c).

2.3. Gradient Composite Membrane

The aligned fibers were embedded in a TPU matrix to generate a composite membrane with gradient TPU content along the thickness. The composite membrane was generated by dropping a TPU solution on one side of poly(NIPAm-AA) mat (**Figure 3a**). In general, bilayer electrospun membranes for the actuation purpose are made by the sequential spinning of two polymer solutions[30,34] or one polymer solution with different alignments,[31] and in situ hydrogel formation in the presence of fibers,[36] which all consist of complex and time-consuming processes. The method presented in this study is simple, fast, and reproducible.

The gradient structure of the composite membrane was studied via Raman atomic force microscopy (AFM) imaging (Figure 3b–d). To get a closer insight into the spatial distribution of poly(NIPAm-AA) and TPU over the composite membrane a Raman x/z cross-section (Figure 3c) was performed at the position indicated by a red line in Figure 3b. To this end, the Raman spectra of the neat components (Figure 3d) were used as references for true component analysis. The Raman cross-section nicely confirmed the presence of a gradient composite structure with a dense and homogenous TPU top layer (colored in yellow) on the underlying poly(NIPAm-AA) fibers (colored in green), where the amount of TPU significantly decreased near the fibrous mat (Figure 3c).

The morphology of the composite membrane was also investigated by SEM (Figure 3e–h). SEM images (Figure 3g; Figure S7, Supporting Information) showed a dense TPU top layer (thickness of 16 μm) on a porous poly(NIPAm-AA) layer reinforced with aligned fibers (thickness of 35 μm). A strong interface between the fibers and TPU was obvious from SEM images (Figure 3h).

TPU layer does not show any size-change in buffer solutions, whereas swelling/shrinking of the poly(NIPAm-AA) mat is expected to generate the internal-stress leading to directional bending in the composite membranes. On putting the composite membrane (10 mm × 5 mm, fibers aligned along the long axis) in a buffer solution with pH 3 at 40 °C (above LCST), it made a multiwalled tube by rolling sideways along the direction of fibers' alignment with TPU on the outside and poly(NIPAm-AA) making the inside layer (**Figure 4a,b**). The shrinkage of poly(NIPAm-AA) mat in the direction of fiber's alignment (Figure 2c) generated differential stresses across the composite membrane leading to rolling sideways. In this case, although composite membrane always rolls along the fiber's alignment with TPU film outside, however, the rolling direction and the final morphed shape depends on the angle of fiber's alignment with respect to the long axis. By changing the angles, short tube rolling side-ways (0°), helix tube (45°), and long tube rolling in perpendicular direction (90°) could be obtained (Figure 4a,b). Decreasing the temperature to 6 °C (below LCST) led to swelling of poly(NIPAm-AA) mat and hence opening of the tubes (Figure 4c).

On transferring the composite membrane from pH 3 to pH 7 or 10 (higher than pK_a) at 40 °C, a process of tube opening and rerolling in the direction perpendicular to fiber orientation with poly(NIPAm-AA) mat outside was observed. This means that a change in pH not only altered the size of tube but also exchanged its inner and outer surfaces, i.e., poly(NIPAm-AA) and TPU. This is explained by asymmetric swelling of poly(NAPAm-AA) mat in pH 7 or 10. The fibrous mat swells to its original length of as-spun in the direction along the fiber alignment and nearly doubles in the perpendicular direction (Figure 2c), which results in opening and rerolling behaviors of the composite membrane. This process is reproducible for multiple cycles (at least three cycles).

A composite membrane (10 mm × 5 mm, fibers aligned along the long axis) formed a tube in pH 7 or 10 with a curvature of 6.2 mm^{-1}. The tubes were stable and not affected by

ADVANCED SCIENCE NEWS
www.advancedsciencenews.com

Macromolecular Rapid Communications
www.mrc-journal.de

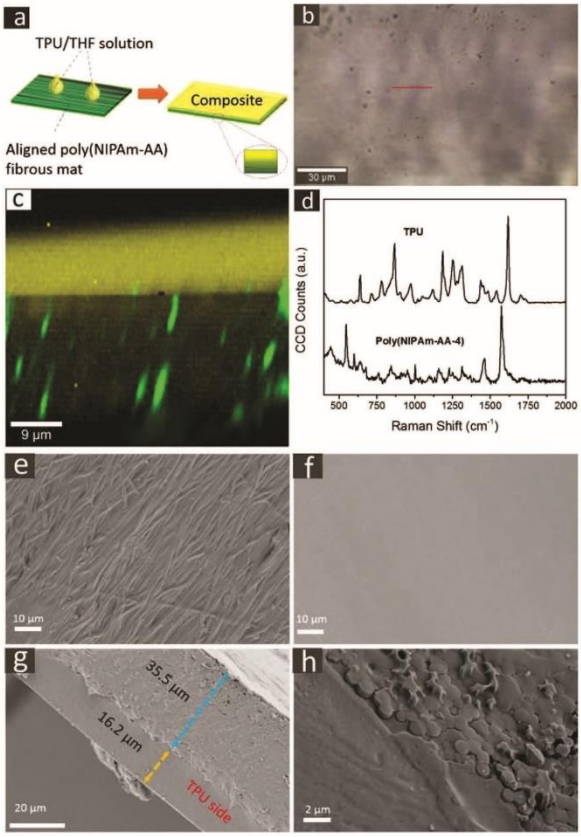

Figure 3. a) Schematic fabrication of the composite membrane. Raman-AFM imaging of the composite membrane; b) optical microscope image with position of Raman cross-section (red line), c) Raman cross-section with domains rich in TPU colored in yellow and those rich in poly(NIPAm-AA) in green, and d) Raman spectra of neat components, i.e., TPU and poly(NIPAm-AA). SEM images of the composite membrane; e) poly(NIPAm-AA) aligned fibrous mat side, f) TPU side, g) cross-section, and h) interface between aligned poly(NIPAm-AA) fibers and TPU.

the change in temperature. Compared with other pH-responsive actuators, our composite system finished the whole rolling process for forming stable tubes within 10 min, which is three times faster than the previous pH-responsive actuator.[33] This is attributed to the high specific surface area and porosity of fibrous structure of the poly(NIPAm-AA) mat, which could provide faster diffusion of water for the porous fibrous membrane compared with the film.

On the other hand, in pH 3, the change in the temperature affected the curvature of the tube (**Figure 5**a). The curvature increased with increasing the temperature with an obvious jump around 12 °C, which is the LCST of the poly(NIPAm-AA) mat (Figures S4 and S6a, Supporting Information).

Interestingly, a piece of composite membrane (20 mm × 5 mm, fibers aligned along the long axis) generates a force of 2.4 mN in pH 3 at room temperature (Figure 5b). It can also lift a 426 times heavier weight (2471 mg metal ring is lifted by a 5.8 mg composite membrane) in pH 3 and release that in pH 10 (Figure 5c). This is because of a self-locking mechanism during the lifting process.

3. Conclusion

We have demonstrated a simple method of making soft actuator for fast and direction controlled dual actuation. Our fast dual-responsive composite membrane composed of poly(NIPAm-AA) aligned fibers embedded within a passive thermoplastic polyurethane exhibited fast pH- and thermoresponsive properties with the capability of direction-, and size-controlled movements. At lower pH 3 composite membrane always rolls sideways with poly(NIPAm-AA) aligned fibrous mat along fiber orientation inside the rolls and the rolling direction is dependent on the bias angle in the mat between fibers and long axis. By changing the angles, short (0°), helix (45°), and long (90°) tubes can be obtained. Second, in pH 7 and 10, it always rolls side-ways with poly(NIPAm-AA) aligned fibrous mat outside the rolls in the direction perpendicular to the fiber orientation. Third, the actuated shape and form is stable in pH 7 and 10 even the temperature changed and besides the pH-triggered actuation, its rolling size can be adjusted by controlling the temperature in pH 3. Also, a piece of composite membrane can generate 2.4 mN in pH 3 buffer solution, it can lift at least a 426 times heavier weight (2471.3 mg metal ring by 5.8 mg of membrane) in pH 3 at 25 °C and the ring was released in pH 10. Based on these features, this kind of multiresponsive actuators has great potential in sensors, artificial muscles, and other biomedical applications.

4. Experimental Section

4.1. Materials

NIPAm (TCI), AA (Sigma-Aldrich), TPU (Desmopan DP 2950, Bayer Materials Science), Indigo and Dispersion Red dye were used as received. ABP was synthesized according to the previously reported procedure.[4]

ADVANCED SCIENCE NEWS
www.advancedsciencenews.com

Macromolecular Rapid Communications
www.mrc-journal.de

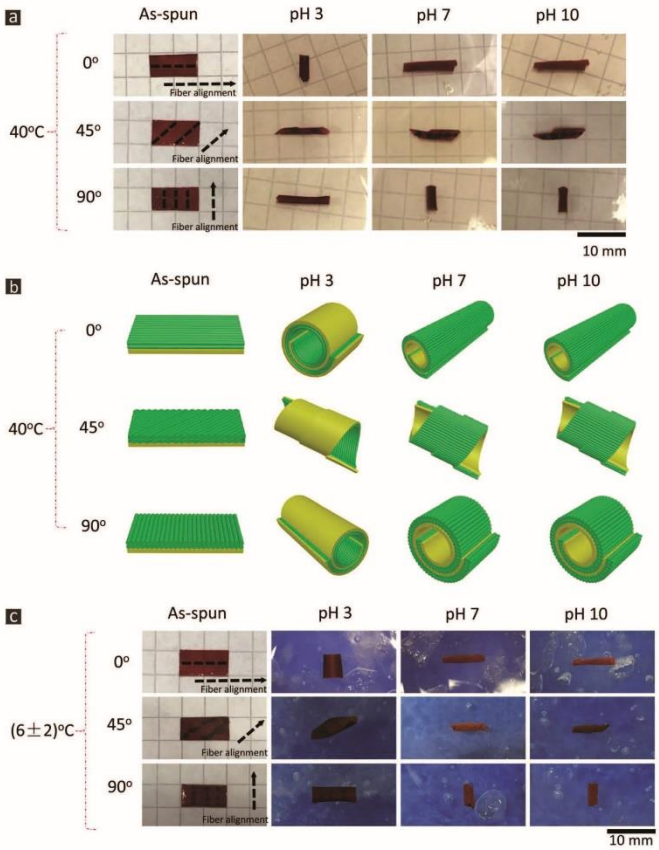

Figure 4. a) Actuation of the composite membrane in buffer solution with different pHs at 40 °C. b) The corresponding schematics for the actuation of composite membrane at 40 °C. Poly(NIPAm-AA) is colored in green and TPU in yellow. c) Actuation of the composite membrane in buffer solution with different pHs at 6 ± 2 °C.

4.2. Synthesis of Poly(NIPAm-AA-ABP)s

As a general procedure, a two-neck round bottom flask was charged with NIPAm (47–49 mmol), AA (47–49 mmol), ABP (2–6 mmol), AIBN (3 mmol), and 100 mL of dioxane. The reaction mixture was bubbled with Ar for 10 min to remove the dissolved oxygen, and then stirred at 70 °C under Ar atmosphere in a dark condition overnight. In the next day, high amount of white powder appeared in the reaction flask. Dioxane was removed by a rotary vacuum evaporator at 45 °C and the residue was immersed in Et_2O. The product was separated by a Büchner funnel, washed again with Et_2O, and dried in a vacuum oven at room temperature in dark condition for 2 d. The formulations of synthesized polymers are listed in Table S1 in the Supporting Information.

4.3. Electrospinning of Fibrous Mats

Poly(NIPAm-AA-ABP) and Indigo (0.4 wt% of polymer) were completely dissolved in DMF (40 wt%). The solution was injected from a syringe with a needle diameter of 0.9 mm and a flow rate of 0.66 mL h^{-1} at negative and positive voltages of −2.7 and 14.3 kV, respectively. To obtain aligned fibers, a vertically rotating disc (1200 rpm) with a diameter of 10 cm and a disc rim of 2.5 cm was used as collector at distance of 8 cm. The obtained aligned fibrous mats were pressed under 300 bars at room temperature for 20 min before irradiating by a UV lamp (Honle UV-F 400F, wavelength of 320–400 nm, intensity of 21–60 mW cm^{-2}) for 3.5 h (for each side) to be crosslinked.

ADVANCED SCIENCE NEWS
www.advancedsciencenews.com

Macromolecular Rapid Communications
www.mrc-journal.de

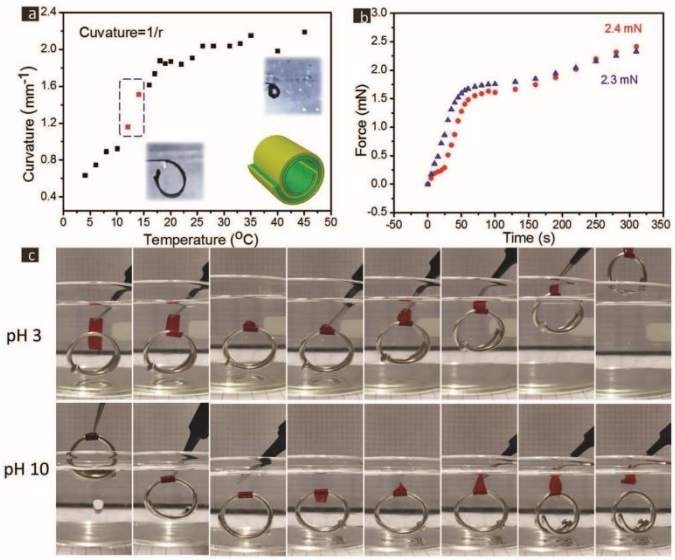

Figure 5. a) Effect of temperature on the curvature of rolled composite membrane in pH 3. b) The generated force during the bending of composite membrane (20 × 5 mm^2) against time in pH 3 at room temperature. c) A piece of composite membrane (20 × 5 mm^2, 5.8 mg) can lift a silver ring (2471.3 mg) in pH 3 and release it in pH 10 at room temperature.

4.4. Preparation of Gradient Composite Membrane

The gradient composite membrane was fabricated by dropping a dilute solution of TPU and dispersion red (0.4 wt% of polymer) in tetrahydrofuran (THF) (7 wt%) on the crosslinked poly(NIPAm-AA) electrospun mats. For this purpose, one side of the crosslinked mat (25 mm × 25 mm) was prewetted by THF and then, TPU solution (0.375 mL) was homogeneously dropped on it. After 3 min, the wet surface was covered with a piece of glass and the sample was dried in an oven at 70 °C for 4 min.

4.5. Instruments

A Bruker spectrometer (model Avance 300) was used to record ^{1}H-NMR and ^{13}C-NMR spectra at room temperature using DMSO-d_6 as solvent. FTIR spectra were obtained using a Digilab spectrometer (model Excalibur FTS-3000 series) equipped with an attenuated total reflection (ATR) unit. The molecular weight distribution of polymers was obtained by gel permeation chromatography (GPC) using a styrene-divinylbenzene (SDV) precolumn (8 mm × 50 mm) and a SDV column (linear XL, 5 µm, 8 mm × 300 mm) from polymer standards service (PSS) GmbH in DMF with a flow rate of 0.5 mL min^{-1} at 40 °C. The data were evaluated by Win GPC Unity software (build 6807) using polystyrene as the standards.

A Netzsch thermogravimetric analyzer (model TG 209 F1 Libra) operating at a heating rate of 10 °C min^{-1} under N_2 atmosphere was used to study the thermal degradation of samples. Glass transition temperature (T_g) and melting point (T_m) of samples were obtained from differential scanning calorimetry (DSC, Mettler Toledo, model DSC 821e) at a heating rate of 10 °C min^{-1} under N_2 atmosphere. A Setaram Micro-DSC III operating at a heating rate of 0.25 °C min^{-1} was used to measure the LCST of samples in water (1 wt%).

The tensile properties of samples were evaluated on a Zwick/Roell testing machine (model Z0.5) equipped with a load cell of 200 N and pneumatic grips at 21 °C and a relative humidity of 20%. Samples were stamped-cut into dog-bone shaped specimens having a width of 2 mm and a length of 20 mm. A digital micrometer was used to accurately measure the width and thickness of specimens. The crosshead speed was set at 100 mm min^{-1}. Data were evaluated by testXpert II software. The reported values are an average of at least three specimens for each sample.

Field emission scanning electron microscopy was done by a Zeiss instrument (model LEO 1530 Gemini). Standard holders were used for mounting samples using conductive adhesion graphite-pad (Plano) and vapor-coated with platinum using a Balzers Union coater (model MED 010).

For chemical imaging, a combined Raman-AFM instrument (WITec, model alpha 300 RA+) equipped with a ultrahigh throughput spectrometer (UHTS, model 400 VIS-NIR) and an infrared-optimized deep depletion charge-coupled device (CCD) camera (Andor, model DU401 BR-DD) was used. The Raman spectra for the Raman x/z cross-section (50 × 50 µm^2) were acquired using an excitation wavelength of λ = 785 nm and an integration time of 0.7 s pixel 1 (50× LWD objective, NA = 0.55, step size 250 nm in x-direction and 500 nm in z-direction, software WITec Control FOUR 4.1). All spectra were subjected to a cosmic ray removal routine and baseline correction. The spatial distributions of poly(NIPAm-AA) and TPU in the composite fiber mat were determined by using the Raman spectra of the neat components as references for true component analysis (software WITec Project Five).

4.6. Methods

pK_a of poly(NIPAm-AA-ABP)s was determined via back titration method using an auto-titrator (Metrohm, model 809 Titrando) at 20 °C. Briefly, sample (0.1687 g) was dissolved in NaOH solution (0.0094 M, 150 mL) and back titrated against HCl solution (0.01 M, 2 mL min^{-1}) in the presence of a pH electrode. Meanwhile, in order to ensure the smooth progress of titration, precipitation of the sample was monitored by measuring the turbidity via a UV electrode.

Fiber alignment degree (d_{Fa}) for the aligned fibrous mat was determined by the following equation[37]

$$d_{Fa} = \frac{3\cos^2\theta - 1}{2} \quad (1)$$

where θ is the angle between the alignment of individual fiber and the collector's rotational direction. The values are an average of 50 fibers.

Curvature change of gradient composite membrane in buffer solution (pH 3) was carried out at a temperature range of 4–45 °C controlled by a refrigerating circulator chiller (Lauda–Brinkmann, model RC6). At the same time, a thermometer was put inside to read the real temperature. Video Remaker software was used to capture pictures from the recorded videos. The quantified analysis of curvature and dimension change was calculated by Image J software.

The force generated by the actuators (20 mm × 5 mm) in buffer solution (pH 3) at room temperature was measured according to a method developed in the laboratory (Figure S8, Supporting Information). The big iron and fixed iron bar were fixed together. The top of the sample was fixed, when the bottom side started bending, a force was generated from the sample which would lift the weight from the balance.

Supporting Information

Supporting Information is available from the Wiley Online Library or from the author.

Acknowledgements

L.L. and H.B. contributed equally to this work. The authors would like to acknowledge financial support from Deutsche Forschungsgemeinschaft (DFG; SFB 840). L.L. thanks China Scholarship Council for awarding PhD fellowship. H.B. acknowledges Alexander von Humboldt Foundation for financial support during this research. The authors thank Tingting Chen for drawing the actuation schematic, Florian Käfer and Mahsa Mafi for their assistance in titration.

Conflict of Interest

The authors declare no conflict of interest.

Keywords

controlled directional movement, electrospinning, oriented fibers, surface switching

Received: January 29, 2018
Revised: March 11, 2018
Published online:

[1] S. J. Jeon, A. W. Hauser, R. C. Hayward, *Acc. Chem. Res.* **2017**, *50*, 161.
[2] L. Ionov, *Mater. Today* **2014**, *17*, 494.
[3] G. Stoychev, N. Puretskiy, L. Ionov, *Soft Matter* **2011**, *7*, 3277.
[4] S. Zakharchenko, N. Puretskiy, G. Stoychev, M. Stamm, L. Ionov, *Soft Matter* **2010**, *6*, 2633.
[5] H. Li, G. Go, S. Y. Ko, J.-O. Park, S. Park, *Smart Mater. Struct.* **2016**, *25*, 027001.
[6] P. Techawanitchai, M. Ebara, N. Idota, T.-A. Asoh, A. Kikuchi, T. Aoyagi, *Soft Matter* **2012**, *8*, 2844.
[7] P. Yuan, J. M. McCracken, D. E. Gross, P. V. Braun, J. S. Moore, R. G. Nuzzo, *Soft Matter* **2017**, *13*, 7312.
[8] M. L. O'Grady, P. L. Kuo, K. K. Parker, *ACS Appl. Mater. Interfaces* **2010**, *2*, 343.
[9] B. Xu, H. Jiang, H. Li, G. Zhang, Q. Zhang, *RSC Adv.* **2015**, *5*, 13167.
[10] X. Shi, Y. Zheng, G. Wang, Q. Lin, J. Fan, *RSC Adv.* **2014**, *4*, 47056.
[11] N. Bassik, B. T. Abebe, K. E. Laflin, D. H. Gracias, *Polymer* **2010**, *51*, 6093.
[12] J. C. Garbern, E. Minami, P. S. Stayton, C. E. Murry, *Biomaterials* **2011**, *32*, 2407.
[13] D. P. Huynh, M. K. Nguyen, B. S. Kim, D. S. Lee, *Polymer* **2009**, *50*, 2565.
[14] J. Zhang, L.-Y. Chu, Y.-K. Li, Y. M. Lee, *Polymer* **2007**, *48*, 1718.
[15] Y. Zhao, H. Su, L. Fang, T. Tan, *Polymer* **2005**, *46*, 5368.
[16] X.-Z. Zhang, Y.-Y. Yang, F.-J. Wang, T.-S. Chung, *Langmuir* **2002**, *18*, 2013.
[17] X.-Z. Zhang, Y.-Y. Yang, T.-S. Chung, K.-X. Ma, *Langmuir* **2001**, *17*, 6094.
[18] X. Jin, Y.-L. Hsieh, *Polymer* **2005**, *46*, 5149.
[19] T. Sakai, R. Yoshida, *Langmuir* **2004**, *20*, 1036.
[20] L. Wang, P. D. Topham, O. O. Mykhaylyk, J. R. Howse, W. Bras, R. A. L. Jones, A. J. Ryan, *Adv. Mater.* **2007**, *19*, 3544.
[21] H. Chen, Y.-L. Hsieh, *J. Polym. Sci., Part A: Polym. Chem.* **2004**, *42*, 6331.
[22] Y. Cheng, K. Ren, D. Yang, J. Wei, *Sens. Actuators, B* **2018**, *255*, 3117.
[23] X. Li, X. Cai, Y. Gao, M. J. Serpe, *J. Mater. Chem. B.* **2017**, *5*, 2804.
[24] H. Nakagawa, Y. Hara, S. Maeda, S. Hasimoto, *Polymers* **2011**, *3*, 405.
[25] E. L. Lee, H. A. von Recum, *J. Biomed. Mater. Res., Part A* **2010**, *93A*, 411.
[26] H. Von Recum, A. Kikuchi, M. Okuhara, Y. Sakurai, T. Okano, K. Sung Wan, *J. Biomater. Sci., Polym. Ed.* **1998**, *9*, 1241.
[27] G. Kocak, C. Tuncer, V. Bütün, *Polym. Chem.* **2017**, *8*, 144.
[28] H. Du, M. Liu, X. Yang, G. Zhai, *Drug Discovery Today* **2015**, *20*, 1004.
[29] F. Meng, Y. Zhong, R. Cheng, C. Deng, Z. Zhong, *Nanomedicine* **2014**, *9*, 487.
[30] L. Liu, S. Jiang, Y. Sun, S. Agarwal, *Adv. Funct. Mater.* **2016**, *26*, 1021.
[31] L. Liu, A. Ghaemi, S. Gekle, S. Agarwal, *Adv Mater.* **2016**, *28*, 9792.
[32] R. Xiao, J. Guo, D. L. Safranski, T. D. Nguyen, *Soft Matter* **2015**, *11*, 3977.
[33] C. Yu, P. Yuan, E. M. Erickson, C. M. Daly, J. A. Rogers, R. G. Nuzzo, *Soft Matter* **2015**, *11*, 7953.
[34] S. Jiang, F. Liu, A. Lerch, L. Ionov, S. Agarwal, *Adv Mater.* **2015**, *27*, 4865.
[35] G. Funduenanu, M. Constantin, S. Bucatariu, P. Ascenzi, *Polymer* **2017**, *110*, 177.
[36] Q. Zhao, L. Ning, Y. Liang, Z. Zhang, L. Ren, *Polymers* **2017**, *9*, 270.
[37] R. Dersch, T. Liu, A. K. Schaper, A. Greiner, J. H. Wendorff, *J. Polym. Sci., Part A: Polym. Chem.* **2003**, *41*, 545.

Supporting Information

for *Macromol. Rapid Commun.*, DOI: 10.1002/marc.201800082

Composite Polymeric Membranes with Directionally Embedded Fibers for Controlled Dual Actuation

Li Liu, Hadi Bakhshi, Shaohua Jiang, Holger Schmalz, and Seema Agarwal*

WILEY-VCH

Supporting Information

Composite Polymeric Membranes with Directionally Embedded Fibers for Controlled Dual Actuation

Li Liu,[§1] Hadi Bakhshi,[§1] Shaohua Jiang[2], Holger Schmalz[1,3] and Seema Agarwal[1]*

[1]Macromolecular Chemistry II and Bayreuth Center for Colloids and Interfaces, Universität Bayreuth, Universitätsstraße 30, 95440 Bayreuth, Germany
E-mail: (agarwal@uni-bayreuth.de)

[2] College of Materials Science and Engineering, Nanjing Forestry University, Nanjing 210037, China
[3] Bavarian Polymer Institute, University of Bayreuth, Universitätsstraße 30, 95440, Bayreuth, Germany

[§]L. Liu and H. Bakhshi contributed equally to this work.

1.1. Synthesis of UV-curable poly(NIPAm-AA)s

NMR and FTIR spectroscopy confirmed the chemical structure of synthesized polymers (**Figures S2-S4**). The polymers had a molecular weight (M_w) in the range of 10900-20000 with molar mass distribution (Đ) of 1.48-1.88 (**Table S1**). They showed a glass transition temperature (T_g) in the range of 134-152°C without any exothermic melting peak. Increasing the ABP content within the formulation of the polymers decreased their lower critical solution temperature (LCST) from 18°C to 12°C due to the hydrophobicity of ABP moieties.

Table S1. Formulation and characterization of synthesized poly(NIPAm-AA-ABP).

Sample	NIPAm/AA/ABP (mol ratio)	M_w	Đ	T_g (°C)	LCST (°C)	Crosslinkability	Thermo-responsivity
P2	0.49/0.49/0.02	20000	1.87	152	18	bad	yes
P4	0.48/0.48/0.04	10900	1.48	152	12	good	yes
P6	0.47/0.47/0.06	13100	1.88	134	12	good	no

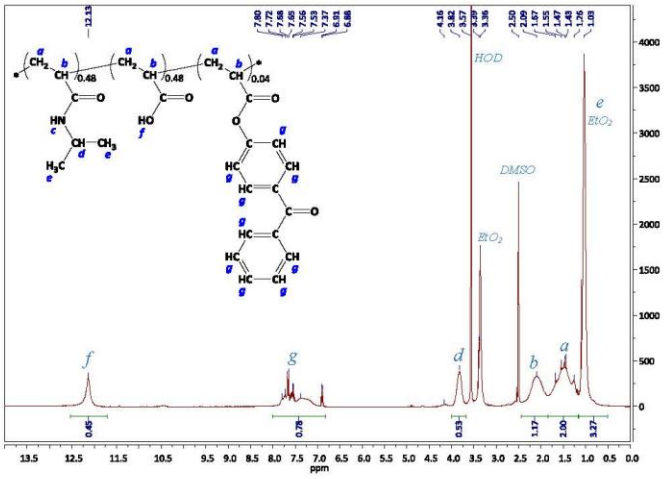

Figure S1. ^{1}H-NMR spectrum of sample P4 in DMSO-d_6.

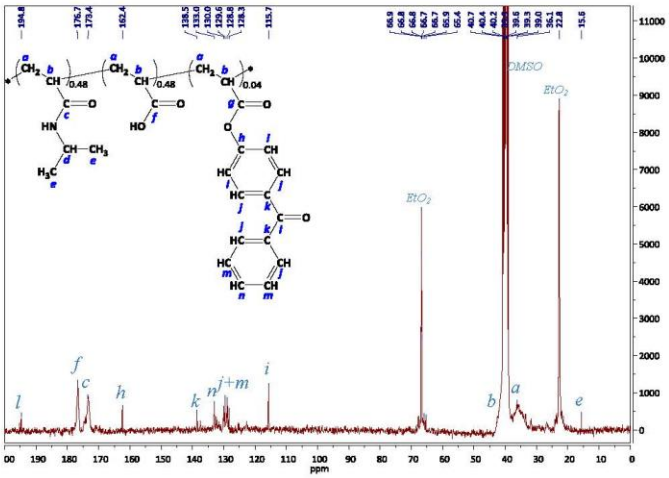

Figure S2. ^{13}C-NMR spectrum of sample P4 in DMSO-d_6.

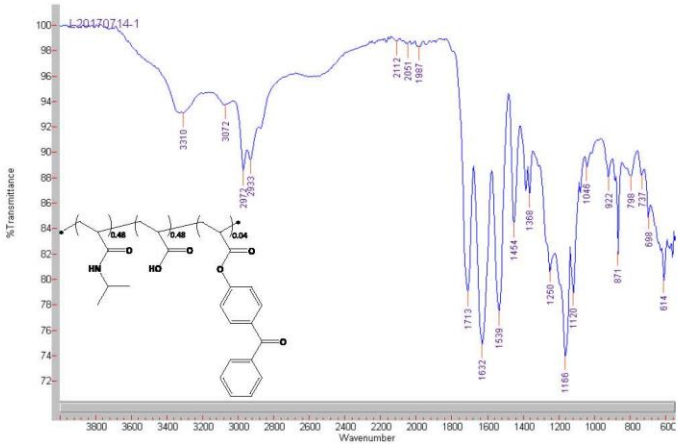

Figure S3. FTIR spectrum of sample P4. $1/\lambda$ (cm^{-1}): 3310 (N–H, ν and O–H, ν), 2972 and 2933 (C–H, ν), 1802 (CC=OC, ν) 1713 (C=OOH, ν), 1632 (C=O, amide I, ν), 1539 (N–H, amide II, δ), 1454 (CH3–, δ and –CH2–, δ) and 1368 (CH3–, δ).

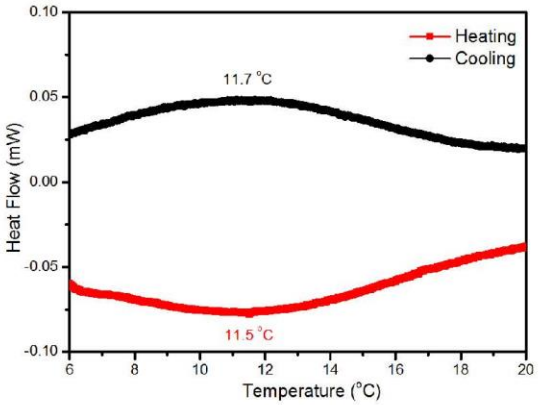

Figure S4. Micro-DSC curve for poly(NIPAm-AA) (sample P4).

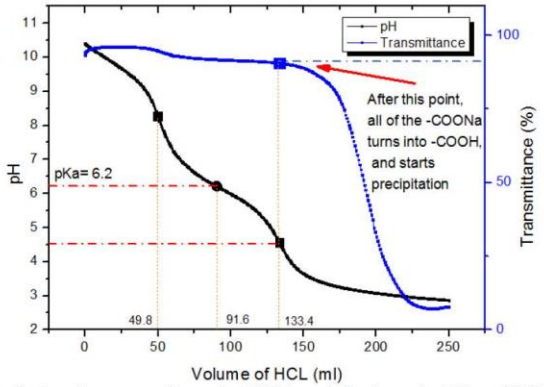

Figure S5. Back titration curve for poly(NIPAm-AA) (sample P4) at 20 °C against HCl solution (0.01 M, 2 mL/min).

1.2. Poly(NIPAm-AA) aligned fibrous mat

Table S2. Size change of crosslinked poly(NIPAm-AA) (sample P4) aligned fibrous mat in various buffer solution.

	pH 3			pH 7			pH 10		
	as-spun	6±2°C	40°C	as-spun	6±2°C	40°C	as-spun	6±2°C	40°C
L (cm)	10.1	7.2	6.0	9.8	9.8	9.8	9.8	9.8	9.8
W (cm)	5.1	6.6	5.4	4.9	11.9	11.7	4.9	12.0	11.6

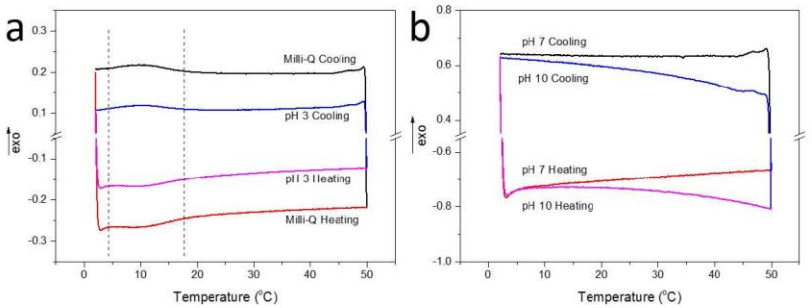

Figure S6. DSC curves for crosslinked poly(NIPAm-AA) (sample P4) aligned fibrous mat in different buffer solution.

1.3. Gradient Composite Membrane

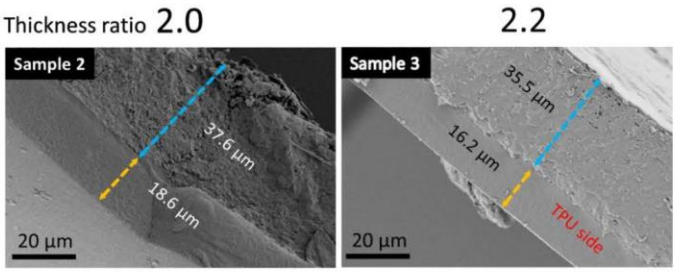

Figure S7. SEM images for cross-sections of the gradient composite membrane.

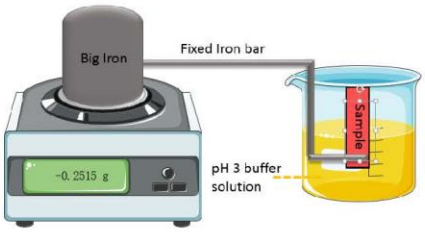

Figure S8. Schematic of measuring the force generated by the composite membrane.

6. List of publications

[1] **L. Liu**, S. Jiang, Y. Sun, S. Agarwal*, "Giving Direction to Motion and Surface with Ultra-Fast Speed Using Oriented Hydrogel Fibers", *Advanced Functional Materials*, 26(7) (2016) 1021-1027.

[2] **L. Liu**, A. Ghaemi, S. Gekle, S. Agarwal*, "One-Component Dual Actuation: Poly(NIPAM) Can Actuate to Stable 3D Forms with Reversible Size Change", *Advanced Materials*, 28(44) (2016) 9792-9796.

[3] **Li Liu**, Hadi Bakhshi, Shaohua Jiang, Holger Schmalz and Seema Agarwal*, "Composite Polymeric Membranes with Directionally Embedded Fibers for Controlled Dual Actuation", *Macromolecular rapid communications*, 2018, 1800082.

(Eidesstattliche) Versicherungen und Erklärungen

(§ 9 Satz 2 Nr. 3 PromO BayNAT)

Hiermit versichere ich eidesstattlich, dass ich die Arbeit selbstständig verfasst und keine anderen als die von mir angegebenen Quellen und Hilfsmittel benutzt habe (vgl. Art. 64 Abs. 1 Satz 6 BayHSchG).

(§ 9 Satz 2 Nr. 3 PromO BayNAT)

Hiermit erkläre ich, dass ich die Dissertation nicht bereits zur Erlangung eines akademischen Grades eingereicht habe und dass ich nicht bereits diese oder eine gleichartige Doktorprüfung endgültig nicht bestanden habe.

(§ 9 Satz 2 Nr. 4 PromO BayNAT)

Hiermit erkläre ich, dass ich Hilfe von gewerblichen Promotionsberatern bzw. -vermittlern oder ähnlichen Dienstleistern weder bisher in Anspruch genommen habe noch künftig in Anspruch nehmen werde.

(§ 9 Satz 2 Nr. 7 PromO BayNAT)

Hiermit erkläre ich mein Einverständnis, dass die elektronische Fassung meiner Dissertation unter Wahrung meiner Urheberrechte und des Datenschutzes einer gesonderten Überprüfung unterzogen werden kann.

(§ 9 Satz 2 Nr. 8 PromO BayNAT)

Hiermit erkläre ich mein Einverständnis, dass bei Verdacht wissenschaftlichen Fehlverhaltens Ermittlungen durch universitätsinterne Organe der wissenschaftlichen Selbstkontrolle stattfinden können.

…….
Ort, Datum, Unterschrift